INFORMATION TO USERS

This manuscript has been reproduced from the microfilm master. UMI films the text directly from the original or copy submitted. Thus, some thesis and dissertation copies are in typewriter face, while others may be from any type of computer printer.

The quality of this reproduction is dependent upon the quality of the copy submitted. Broken or indistinct print, colored or poor quality illustrations and photographs, print bleedthrough, substandard margins, and improper alignment can adversely affect reproduction.

In the unlikely event that the author did not send UMI a complete manuscript and there are missing pages, these will be noted. Also, if unauthorized copyright material had to be removed, a note will indicate the deletion.

Oversize materials (e.g., maps, drawings, charts) are reproduced by sectioning the original, beginning at the upper left-hand corner and continuing from left to right in equal sections with small overlaps.

Photographs included in the original manuscript have been reproduced xerographically in this copy. Higher quality 6" x 9" black and white photographic prints are available for any photographs or illustrations appearing in this copy for an additional charge. Contact UMI directly to order.

Bell & Howell Information and Learning
300 North Zeeb Road, Ann Arbor, MI 48106-1346 USA

UMI®
800-521-0600

DEVELOPMENT OF MAGNETIC CARRIERS FOR METAL ION REMOVAL

Joachim Broomberg

Department of Mining and Metallurgical Engineering

McGill University, Montréal

March 1998

A Thesis submitted to the
Faculty of Graduate Studies and Research
in partial fulfillment of the requirements of the degree of
Master of Engineering

To a great country, Canada,
and a wonderful Province, Québec,
where I have spent three of the
richest and fullest years of my life...

Abstract

A novel method has been developed to prepare magnetic carriers for metal ion removal from dilute solutions. In this work, magnetic carriers were prepared by coating an organic surfactant on magnetic particles. The coating was deposited by molecular self-assembly. Two coatings were tested, using two similar bolaamphiphiles* of different chain lengths, HS-$(CH_2)_{11}$-COOH and HS-$(CH_2)_{15}$-COOH. The magnetic particles were nanosized maghemite (γ-Fe_2O_3).

The surfactants were synthesized and characterized. Magnetic carriers were prepared, characterized, and tested for metal ion loading. Molecular orientation, density, and stability of the surfactant coatings were characterized by diffuse reflectance infrared Fourier-transform spectroscopy (DRIFTS), x-ray photoelectron spectroscopy (XPS), wetting tests, and leaching tests. The coatings, resulting from the chemisorption of the surfactants on maghemite through carboxylate bonding, were found to be dense, well-packed, and resistant to acid and base attack.

The potential use of coated particles for metal ion removal was assessed with Cu and Ag solutions. The metal ion uptake by the carriers was characterized by atomic adsorption and XPS. The influence of pH and metal concentration on adsorption was studied. Metal ion uptake was found to be dependent on pH, and was not significantly different for both types of coated carriers and for bare maghemite. The maximum loading capacity was low, at approximately 6 mg Cu/ g particles for Cu. The similarity in loading for coated and bare particles needs further clarification.

* Bolaamphiphiles are surfactants with a functional group at each end.

Résumé

Une nouvelle méthode a été développée pour préparer des porteurs magnétiques, dans le but de les utiliser pour éliminer les ions métalliques dissous dans des solutions diluées. Dans cette étude, les porteurs magnétiques ont été préparés en déposant une monocouche de tensioactifs à la surface de particules magnétiques par auto-assemblage moléculaire. Deux types de porteurs magnétiques ont été synthétisés, par auto-assemblage de deux tensioactifs similaires, mais de longueur différentes, $HS(CH_2)_{11}COOH$ et $HS(CH_2)_{15}COOH$. Les particules magnétiques utilisées étaient des nanoparticules de γ-Fe_2O_3.

Les tensioactifs ont été synthétisés et analysés. Les porteurs magnétiques ont été préparés, analysés, et testés pour leur capacité à adsorber des ions métalliques. L'orientation des tensioactifs à la surface des particules, la densité de la couche déposée, ainsi que la résistance de la monocouche dans des milieux fortement acides ou basiques ont été étudié par spectroscopie infrarouge à transformée de Fourier par réflexion diffuse (DRIFTS), spectroscopie photo-électrique à rayons-X (XPS), flottation, et par étude de dissolution. Il a été trouvé que le film de tensioactif à la surface des particules s'est formé grâce à la réaction chimique entre le groupe carboxylique du tensioactif et l'oxide de fer à la surface des particules. Ce film est dense, bien ordonné, et résiste au contact de solutions acides et basiques.

La capacité d'adsorber des ions métalliques de ces porteurs a été testé avec des solutions ioniques de cuivre et d'argent. L'adsorption des ions a été caractérisée directement par XPS, et indirectement par spectroscopie d'absorption atomique. L'effet du pH sur l'adsorption des ions a aussi été étudié. Il a été montré que le pH a une influence sur l'adsorption des ions métalliques sur les porteurs, et que cette adsorption a quasiment la même valeur pour les particules recouvertes des deux types de tensioactifs et pour les particules de γ-Fe_2O_3 non recouvertes. La capacité maximale d'adsorption des ions par les porteurs est faible, à environ 6 mg Cu/ g de particules dans le cas du cuivre.

Acknowledgments

As I am finishing writing up my thesis, I realize how many people have been involved, closely or remotely, in helping me to get here. I want to thank my parents, for their long and patient work to raise and educate me, and their constant support throughout these years. I am also indebted to the Ecole des Mines de Saint-Etienne that gave me the opportunity to come and study in Canada, as well as the Région Rhônes-Alpes that granted me a fellowship for my first 8 months here. I am very grateful to the McGill Mining and Metallurgical Engineering department that hosted me for over three years. The professors and staff have always been there to help and support. A special mention to Purnima, our graduate secretary (and to Cynthia, after her), who was always kind and joyful. Thanks to Charles and Claudine who housed me in their stress-free home for the last month.

A special thank to professor Zhenghe Xu and doctor Qingxia Liu who initiated that project, got me started, and guided me during the first year of my thesis. Qingxia passed onto me a lot of his knowledge on this topic and Zhenghe helped me to keep going when needed. Thanks to Antonella Badia, Louis, Tara, and Emmanuelle, from doctor Lennox's chemistry laboratory at McGill for their kind help in synthesizing the surfactants. Thanks to Monique Riendeau for her assistance with the atomic adsorption spectroscopy. Thanks to Ram Rao for his help in the laboratory. Thanks to the members of the mineral processing group, their family spirit, and valuable contributions in meetings. Thanks to Sidney, Colin, Gunther, Tony, and Stéphanie, whose friendship made my life sunnier when everything else was hard. I reserve a special thanks to Andrew Vreugdenhil whose help has been invaluable whether it was to de-bug my computer, to assist me with IR and XPS spectra interpretations, or to correct my manuscript.

Finally, I want to express my deep and sincere gratitude to my supervisor, professor Jim Finch. I thank him for allowing this mineral processing group to exist, be so lively, and make it be a joy working there. I thank him for working out the grants and fellowships so we can be paid. I thank him for his patience, his guidance, and for the amazing work he did to correct this thesis. A special thank for the ski week-ends.

Table of Contents

List of Figures

List of Tables

Chapter 1

Introduction

1. Introduction

1.1. The Canadian mining industry and the environment

The mining industry in Canada is a $20 billion industry which generates over 80,000 direct employment in mines, mills and smelters, over 300,000 additional jobs in downstream and support industries, and roughly 16% of the nation's export revenues (Standing Committee on Natural Resources, 1996). The Canadian mining sector is a "huge wealthcreator and job generator" (Wasny, 1997). Canada ranks first in potash, uranium, and zinc, second in sulfur, asbestos, nickel and cadmium, and third in the production of titanium, primary aluminum, gypsum, and platinum (Wasny, 1997).

Unfortunately, the mining industry also poses major threats to the environment. The largest environmental liability facing the mining industry, worldwide, is acid mine drainage (AMD) (Feasby et al., 1997, Harries, 1997). Most base metal, gold, uranium, and coal deposits contain sulfide minerals. When the sulfide minerals are exposed to oxygen and water, they oxidize, and run-off water becomes acidic if acid neutralizing material is not present. The acidic water can in turn dissolve toxic metals from the waste rocks or tailings, and may end up carrying toxic concentrations of metals and dissolved salts. The resulting contaminated water is known as AMD. Rainfall and snow-melt flush the toxic AMD from the waste sites into the environment. If acidic drainage is left uncollected and untreated, it could contaminate groundwater and local water courses, damaging the health of plants, wildlife, and fish. In Canada, it was estimated that the collective liability for the sulfide-containing mine wastes is between $2 and $5 billion (Feasby et al., 1997). In the US, because of the numerous abandoned mine sites, the liability was estimated to be as high as $70 billion (Herbert et al., 1997). AMD has also raised major concerns in Australia, Norway, Sweden, Germany, Chile, Costa Rica, Venezuela, Brazil, and Peru.

Another related issue is the sludges produced in treating AMD. Sludges generated by lime treatment of effluents from many mine sites contain significant metal values. Over the years, sludges have accumulated ever more metals, and increased in total value. A sludge from Brunswick Mining, for example, was found to contain 19.6 % Zn. Millions of

tons of such sludges are dormant, and could be a potential source of metals, in particular, zinc, nickel, and to a lesser extent, copper. These sludges, are both a potential source of renewed AMD and of recoverable metal values. From both environmental and economic points of view, a key issue for the mining industry is to develop technologies to remove and/ or recover metal from effluents and sludges.

1.2. Conventional technologies for metal ion removal

Precipitation: Precipitation, usually as hydroxide but sometimes as carbonate or sulfide, is the most widespread metal ion removal technique. It is a simple and effective process, for removal of large quantities of metals from contaminated water. Some of the problems associated with this technique are: difficult solid-liquid separation, disposal of voluminous sludge, and secondary contamination (i.e., subsequent leaching of sludges disposed inappropriately).

Adsorption: This technique relates to adsorption on a solid adsorbent such as, activated carbon, sandstone, fly ash, natural minerals (clay). Some of the issues complicating the use of this method are the need for prefiltration to remove finely divided solids that may clog the adsorbent (especially if used in packed columns), the need to regenerate the adsorbent, and the costs for adsorbent replacement.

Ion Exchange: Ion exchange resins are typically styrene or acrylic porous resins that contain either cationic (e.g., sodium or hydrogen) or anionic (e.g., chloride) that can be exchanged with ionic contaminants. The resin loads ionic contaminants until its exchange capacity is exhausted, then it needs to be regenerated. This process allows for the removal of dissolved ions to very low residual concentrations. The main drawbacks are the potential poinsening, the need for regeneration, possible clogging, and the need for prefiltration.

Many technologies have been developed for metal ion removal from effluents. From the technologies described, each has its specific range of application and its own limitations. High capacity methods such as precipitation have the drawback of high residual metal concentration, whereas adsorption is efficient only for low concentrations

systems. Several of the methods are prone to either clogging or fouling due to suspended solids. One of the primary objectives in developing magnetic carrier technologies was to circumvent this problem of clogging by designing a dispersed, specific-adsorbing material that could easily be separated and collected.

1.3. Magnetic carrier technology

Magnetic carrier technology, or more generically 'magnetic support' technology (Moffat et al., 1994) was introduced to allow magnetic separation to be applied to materials that are not naturally magnetic. Magnetic supports are materials aimed at selectively enhancing the magnetic properties of the non-magnetic material (the target) that needs to be separated. They can be particles (usually called 'carriers') or liquids such as oils (hence the wider term of 'supports'). Magnetic support materials should fulfill two functions (Moffat et al., 1994): First, provide highly selective attachment to the target species through appropriate surface properties; and second, confer magnetic properties to those targets to be separated.

Magnetic support materials are of interest in areas as diverse as mineral processing, biology, water treatment, and the food industry. They are of particular interest for the separation of fine particles, colloids, and organics, which are slow and difficult to separate by classical methods. In the case of the food industry, Dixon (1980) showed that conventional methods were not appropriate to separate impurities of low molecular weight from a stream containing both larger product molecules and suspended solids. There were two requirements: i) specific adsorption of the impurity, and ii) separation of the loaded adsorbent from aqueous suspension. Dixon showed that magnetic polymer beads were suitable for such a separation (Dixon 1980). Another advantage of magnetic support technology is that it can remove impurities down to very low concentrations; an increase in the amount of magnetic adsorbent will increase the target uptake, and removal to trace levels will be possible (Chen et al., 1991). Figure 1-1 illustrates the principle of magnetic carrier separation. Some magnetic supports are added to the mixture containing target species and other species. The magnetic supports selectively bind to the target, and

magnetic separation allows the separation of the targets from the undesired species. This method can be used either to recover valuable species, or to remove undesired species from a stream.

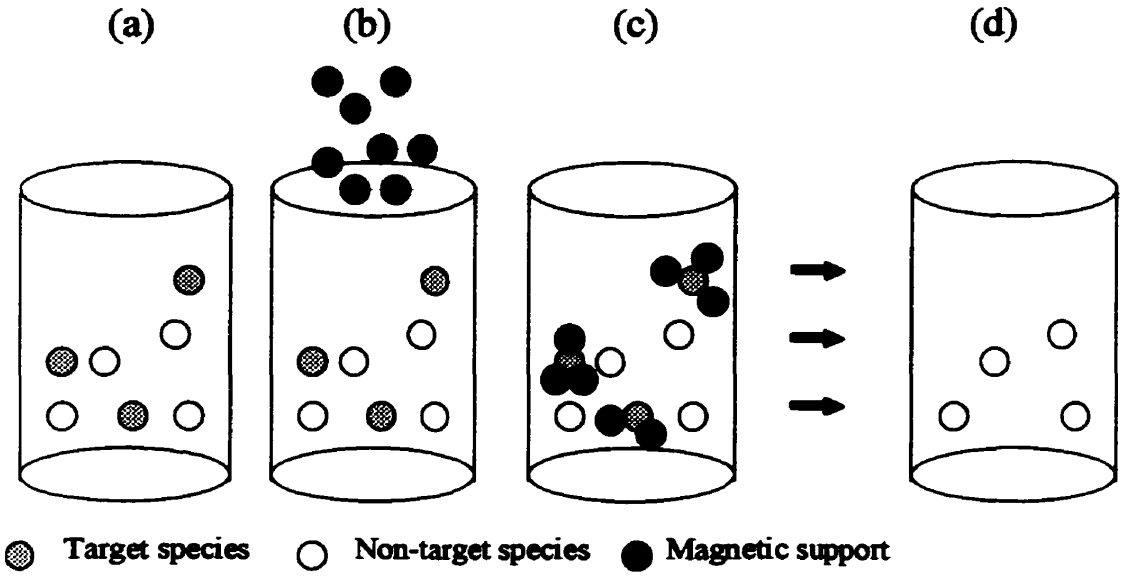

Figure 1-1: Principle of magnetic carrier separation. A mixture to be treated contains target and non target species (a). Magnetic support material is added to the mixture (b). The magnetic carriers selectively bind to the target species (c). After magnetic separation, the system is purified by removing the target species (d).

The purpose of the present thesis was to develop a specific type of magnetic carrier and to investigate its potential for metal ion removal from solution. Chapter 2 is a review of the theoretical principles underlying this research and a review of existing magnetic carrier technologies. Chapter 3 explains the magnetic carrier design for this study, and states the objectives of the work. Chapter 4 summarizes the experimental set up and the procedures. Chapter 5 presents the results along with discussion. Chapter 6 offers some conclusions and suggestions for future work.

Chapter 2

Background

2. Background

2.1. General principles

2.1.1. Magnetic carriers and magnetic tags

Moffat et al. (1994) classify magnetic support materials in two groups, magnetic carriers and magnetic tags. Magnetic carriers are usually 10 to 1000 times larger than the target species. The principle is to vary the surface characteristics (of the carrier), to achieve selective recovery of colloidal and macromolecular (or ionic) species by attaching them onto the surface, or entrapping them within, a magnetic carrier particle (Moffat et al., 1994). Figure 2-1 shows the case where the target coats the surface of the magnetic carrier (i), and the targets are entrapped within a porous magnetic carrier (ii).

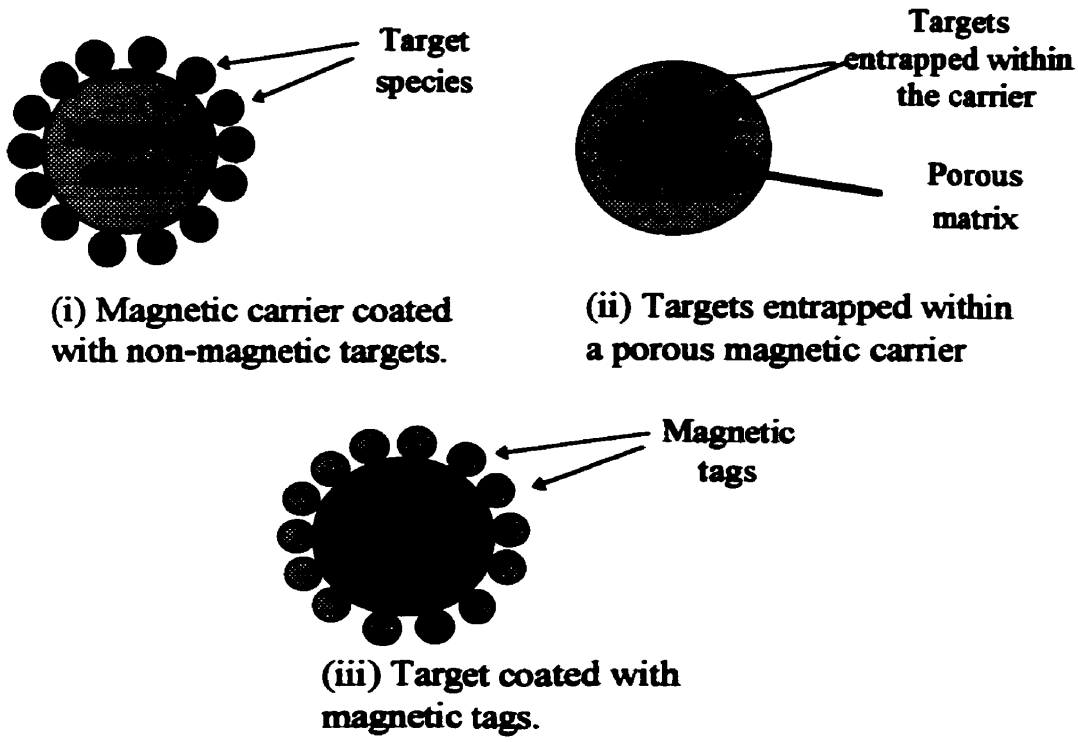

Figure 2-1: Schematic representation of magnetic carrier ((i) and (ii)), and magnetic tagging principles (iii) (adapted from Moffat et al., 1994).

A related technology is magnetic tagging. The tags are usually smaller than the particles to be separated. Tags can be either ions (e.g., Y^{3+}) or fine magnetic particles (e.g., Fe_3O_4) that coat or cluster around non-magnetic species in order to allow them to be manipulated using external magnetic fields (Moffat et al., 1994). The mechanism of tagging can be through very specific coupling mechanisms (e.g., an antibody-antigen interaction), or through electrostatic adsorption. Figure 2-1 (iii) is an illustration of the tagging mechanism.

2.1.2. Magnetic properties of materials

2.1.2.1.Magnetic susceptibility

The magnetizability of a material is characterized by its magnetic susceptibility χ. The unit used for χ is either a non-dimensional SI unit for volume magnetic susceptibility, or $cm^{-3}g^{-1}$ for mass or specific magnetic susceptibility. Magnetic susceptibilities vary greatly from one material to the other, allowing them to be separated according to their differential magnetic properties (Kopp, 1991). For discussion purposes, strong magnetic materials are those with $\chi \geq 4 \times 10^{-3}$ $cm^{-3}g^{-1}$, which can be separated by weak magnetic induction, up to 0.15 T. Weak magnetic materials are those in the range 8×10^{-6} $cm^{-3}g^{-1} \leq \chi \leq 4 \times 10^{-3}$ $cm^{-3}g^{-1}$ and can be separated by magnetic induction up to 0.8 T. Materials with $\chi \leq 8 \times 10^{-6}$ $cm^{-3}g^{-1}$ are classified as non-magnetic. Another classification characterizes the materials according to their intrinsic physical properties and divides them into ferromagnetic (e.g., iron), paramagnetic (e.g., hematite and ilmenite), diamagnetic, anti-ferromagnetic, ferrimagnetic (e.g., magnetite), and super-paramagnetic. Ferro- and ferrimagnetic materials are strong magnetic materials that are readily magnetized under even low magnetic flux densities. However, their magnetization usually (depending on geometry) saturates for flux densities above 0.2 T. Paramagnetic materials, on the other hand, are weak magnetic materials, and their magnetization increases linearly with flux density which allows them to be strongly magnetized at high magnetic flux density.

2.1.2.2. Ferromagnetism, ferrimagnetism, paramagnetism and superparamagnetism

The magnetic properties of some materials have been known and used for centuries, long before any physical explanation of the phenomena involved were discovered (Svoboda, 1987). Different materials respond differently to an applied magnetic field according to the magnetic field of the atoms that constitute that material.

In ferromagnetic materials, the interaction between neighboring atoms is stronger than the force of thermal motion and the magnetic moments of all atoms are aligned parallel to each other, forming so-called Weiss domains (Svoboda, 1987). Depending on the fields to which the material has been exposed, the different Weiss domains are mutually oriented so that the total magnetization may have any value between zero and saturation. After ferromagnetic materials have been placed in a magnetic field, they can remain magnetized because of remanent polarization. Iron is ferromagnetic.

In ferrimagnetic materials atomic magnetic moments are ordered in an antiparallel sense, but more moments are pointing in one direction, resulting in a non-zero magnetization. The properties of ferrimagnetic material are similar to those of ferromagnetic materials. Magnetite is the best known example of a ferrimagnetic material.

Paramagnetic materials do not retain their magnetization when removed from a magnetic field. Under thermal agitation, the intrinsic magnetic moments are randomly oriented and the overall magnetic moment is zero. In the presence of a magnetic field, the magnetic moments tend to orient along the direction of that field, resulting in an overall magnetization.

Superparamagnetic materials have characteristics similar to those of paramagnetic material, but they have much larger magnetic moments which result in a much higher susceptibility. They have no remanent polarization. Superparamagnetism arises when the size of the material becomes so small that it is similar to the magnetic domain size of that material. The material then has a single domain structure and becomes superparamagnetic. That is why maghemite (γ-Fe_2O_3) that is naturally ferrimagnetic, becomes superparamagnetic when it is nanosized. The advantage of superparamagnetic

materials is that their high susceptibilities allow high magnetization under a magnetic field while they have no remanent magnetization, which allows them to be easily redispersed.

2.1.3. Magnetic separation

2.1.3.1.Magnetic force

The magnetic force exerted on a magnetizable particle of volume V, and volume magnetic susceptibility χ in a magnetic field of strength H is given by:

$$F_m = \mu_0 \chi V.H.dH/dx \qquad (1)$$

where $\mu_0 = 4\pi \times 10^{-7}$ T.m/A.

From equation (1) it can be seen that several factors influence the magnitude of the force. First, it can be noted that not only the field strength, H, but also the field gradient, dH/dx, directly influences the force. A force is generated on the particle because of the presence of a gradient. The product H.dH/dx is the determining parameter in a separator and is called the force factor. Technological improvements have sought to increase both field strength and field gradient. The magnetizability and size of the particle also play a key role.

The action of magnetic support particles is to enhance the magnetic properties of a non-magnetic material so that its magnetization under a given magnetic flux equals the magnetization of the same volume of a typical paramagnetic material (i.e., enough to make it separable with an industrial magnetic separator). To achieve that, only a small amount of strongly magnetic material is needed. Ferro or ferrimagnetic materials such as ferrosilicon and magnetite have susceptibilities orders of magnitude greater than typical paramagnetic materials. A volume fraction of magnetic support material in the range of 0.1 to 1 % is usually enough to achieve suitable magnetization of a non-magnetic material. Table 2-1 below shows the magnetization of different paramagnetic materials under given flux densities, and the corresponding amounts of magnetite to be added to a non-magnetic material for equivalent magnetization (from Parsonage 1992).

Table 2-1: Variation of magnetization M, with flux density, B, for paramagnetic materials, and magnetite content of non-magnetic particle for equivalent magnetization (from Parsonage, 1992).

Volume susceptibility of paramagnetic mineral, χ (SI units)	Magnetic flux density, B (T)	Magnetization M ($A\ m^{-1}$)	Magnetite content of non-magnetic particle to give equal magnetization (volume %)
5×10^{-3}	0.2	7.96×10^{2}	0.17
	1	3.98×10^{3}	0.83
	2	7.96×10^{3}	1.66
10^{-3}	0.2	1.59×10^{2}	0.03
	1	7.96×10^{2}	0.17
	2	1.59×10^{3}	0.33

2.1.3.2.Magnetic separators

Since the early 1900s, many magnetic separation devices have been developed and used. Many different ways of generating magnetic fields and gradients are available. Two factors have motivated the development of magnetic equipment: high field strength, to magnetize weakly magnetic material, and high field gradients to create a strong magnetic force (Mathieu, 1988). Magnetic separators are classified in terms of low intensity (for strong magnetic materials) versus high intensity high gradient devices (for weak magnetic materials), and as dry versus wet processes. Typically, dry processes are not suited for particles finer than 75 μm, and wet high gradient high intensity separators are required for these applications. Magnetic separators are still under development. For the magnetic separation of very fine particles (below 100 μm), Ahn et al. have developed a fully integrated micromachined magnetic particle separator on a silicon wafer (Ahn et al., 1996). This type of device may be of interest for high precision magnetic separation, for instance in biological cell separation.

Progress has led to: high gradient magnetic separators (HGMS) (Svoboda, 1987; Mathieu, 1988), superconducting magnetic separators (Kopp, 1991), and synthetic permanent magnets (Wells et al., 1992). Improved technology allows for the separation of finer and finer particles at faster and faster rates.

2.1.4. Adsorption mechanisms

When using magnetic carriers, the selectivity of magnetic separation is controlled by the selectivity of the binding between the magnetic support and the desired target. Mechanisms controlling the binding of the magnetic support with the target material are the same as those in other mineral processes, such as flotation or coagulation (Liu et al., 1994). In the magnetic separator, clearly, the binding forces between the particles to be removed and the carrier must exceed the hydrodynamic forces that are exerted on the particle by the fluid (van Velsen et al., 1991).

Various interaction mechanisms, broadly known as surface forces, contribute to the total energy of interaction, some of which, such as hydrophobic or hydration forces, are not yet well understood. The interparticle forces that control the attachment of the magnetic support with the target were discussed by Parsonage (1992). The interaction energy from each source is summed, to provide a total energy of interaction, V_T. The variation of V_T with distance between the two particles is the potential function. Maxima and minima act as barriers and wells, tending to aid either repulsion or adhesion of the particles. Adhesion occurs when the energy barrier is insufficient to prevent the particles approaching to the position of the primary potential well (Parsonage, 1992).

Chemical reagents can be used to modify most of these interactions by altering the surface properties of the particles. Those reagents are either molecules that bind at the surface of the particle, or ionic species that modify their surface charge. In practical applications, the most useful reagents are hydrocarbon based surfactants, water soluble polymeric flocculants, and pH regulators (Parsonage, 1992). How some of those reagents are used to control the selectivity of the separation processes will be discussed for specific examples in section 2.2.

2.1.5. Electrical properties at mineral-water interface

2.1.5.1.Surface charge

When a mineral is in water, it develops a charge at the solid-water interface. Depending on the mineral, the charge develops on the surface through different

mechanisms. The charge can be created by either of the two following ways (Israelachvili, 1991): (i) ionization or dissociation of surface groups (for instance, -COOH => $-COO^-$ + H^+, which gives a negatively charged surface), or (ii) adsorption (binding) of ions from solution to a previously uncharged surface (for example, the binding of Ca^{++} ions on the switterionic headgroups of lipid bilayer surfaces, giving a positively charged surface). The surface charge is the net charge resulting from the presence on the surface of negative and positive sites. The expression of the surface charge for a univalent salt is given by equation (2) (Kelly and Spottiswood, 1982):

$$\sigma_s = F(\Gamma_+ - \Gamma_-) \qquad (2)$$

where Γ_+ and Γ_- represent the density of positive and negative sites, respectively, and F is the Faraday constant (σ_s is in ion/m^2).

In order to maintain the electroneutrality of the system, there is some transfer of counter ions from the solution towards the mineral surface, to compensate for this surface charge. These counterions are of charge opposite to that of the surface charge. If σ_s is negative, for instance, cations will be attracted to the surface, while anions will be repelled. A concentration gradient is established next to the solid, until a steady state is reached at equilibrium, when σ_s is balanced by an equal but opposite space charge in the solution, referred to as the diffuse layer of charge σ_d (de Bruyn and Agar, 1962). This charge distribution is known as the electrical double layer.

2.1.5.2.Surface potential - Zeta potential

The electrical double layer may be represented by a parallel plate condenser, with a variable distance ($1/\kappa$) between the two charged plates (de Bruyn and Agar, 1962). For this hypothetical condenser, the potential drop between the two plates will be equal to ψ_0 and the surface charge σ_s will follow the relationship (3):

$$\sigma_s = \frac{\varepsilon}{4\pi(1/\kappa)}\Psi_0 \qquad (3)$$

where ψ_0 is the surface potential, i.e. the total potential of the double layer, and $1/\kappa$

represents the distance from the solid surface to the center of gravity of the electrical charge in the diffuse layer, and is referred to as the diffuse layer thickness.

Some counterions are anchored to the surface, and form the so-called Stren layer. When there is motion of the solution relative to the mineral surface, shear occurs at a plane close to the boundary of the Stern layer (Kelly and Spottiswood, 1982). This means that the ions of the Stern layer are "anchored" to the surface, while the ions in the diffuse layer are carried with the solution. At this plane of shear the potential is termed zeta potential (ξ). Zeta potential measurements usually involve the measurement of a particle's velocity under an applied electric field. The unit used is the velocity (m/s) per unit of potential gradient (V/m), or electrophoretic mobility (base unit (m/s)/(V/m). This mobility can be converted to zeta-potential, in mV. When the potential determining ions are H^+ and OH^-, the activity is simply the pH. Figure 2-2 shows a typical example of the influence of pH on the surface potential and the zeta potential at a mineral-solution interface (Kelly and Spottiswood, 1982). The activity of the potential determining ions at which the surface charge is zero is called the point of zero charge (pzc).

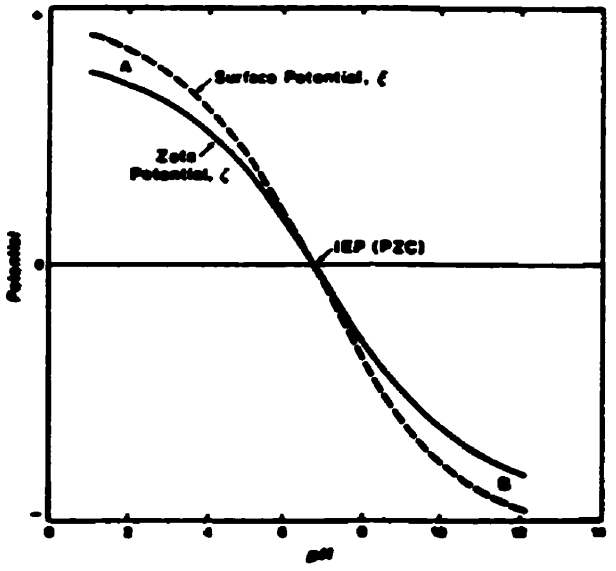

Figure 2-2: Representation of the effect of the activity of the potential determining ions on the surface potential and zeta potential at a mineral-solution interface (from Kelly and Spottiswood, 1982).

2.1.6. Molecular self-assembly

Molecular self-assembly relates to the spontaneous adsorption of surfactants dispersed in solution onto a surface. The monolayer formed this way is called a self-assembled monolayer (SAM). The term self-assembly has been used to distinguish from the Langmuir-Blodgett technique of monolayer formation. The Langmuir-Blodgett technique requires that the surfactants be well ordered and packed at the surface of a liquid prior to contact with the solid surface to be coated. This technique is not useful for depositing monolayers onto finely dispersed particles. In molecular self-assembly, the surfactant is simply dispersed in a solvent, and it is the intrinsic properties of the surfactant that account for the formation of a well ordered, densely packed monolayer on a surface. Figure 2-3 gives a schematic representation of molecular self-assembly. A surfactant must fulfill two functions to allow for molecular self-assembly: one headgroup must have a strong affinity for the surface to be coated, and its hydrocarbon chain must be long enough so that a significant strong interaction exists. Spontaneous adsorption is due to the strong affinity, and close-packing results from the strong attractive hydrocarbon chain interaction.

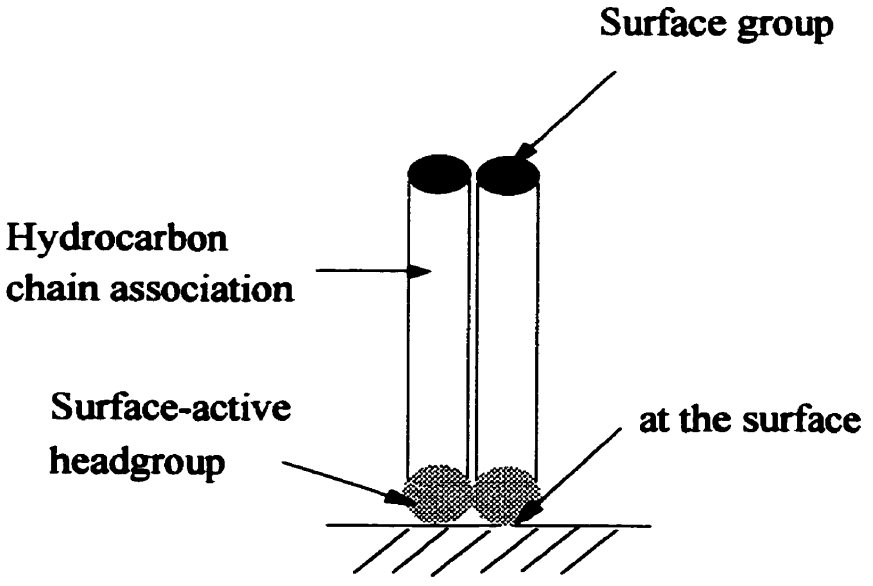

Figure 2-3: Schematic representation of molecular self-assembly (from Liu, 1996, p. 40)

Previous studies have shown that *n*-alkanethiols can form SAMs on the surface of gold (Bain et al., 1989), and *n*-alkanoic acids on the surface of oxidized aluminum substrates (Allara and Nuzzo, 1985a and 1985b). Other studies showed that thio groups chemisorbed strongly on Cu, Au, and Ag surfaces (Laibinis et al., 1991), while carboxylic acid groups were successfully used to bind on aluminum oxide surfaces (Allara and Nuzzo, 1985a and 1985b). It was also found that a carbon chain longer than approximately 12 carbons favored SAM formation (Allara and Nuzzo, 1985a).

Liu (1996) investigated the coating of nanosized magnetic iron oxide (maghemite) particles with 16-mercaptohexadecanoic acid (MHA: $HS-(CH_2)_{15}-COOH$). He showed that the carboxylic group anchored onto the maghemite surface while the thiol was oriented outwards, ready for reaction with various adsorbates. Figure 2-4 shows a schematic representation of the maghemite surface coated with a well-ordered monolayer of MHA.

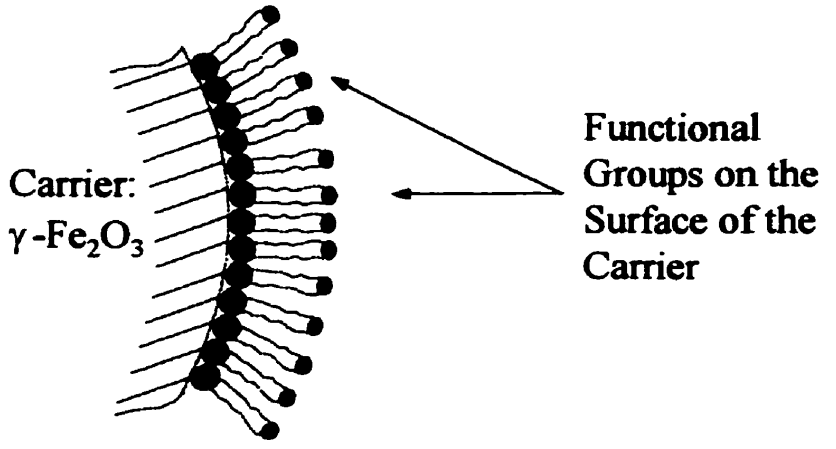

Figure 2-4: Self-assembled monolayer of $HS-(CH_2)_{15}-COOH$ at the surface of meghamite ($\gamma-Fe_2O_3$). (adapted from Liu, 1996)

2.2. Review of magnetic carrier technologies

Magnetic carrier technology originated in the early 1940s, when magnetite was used to remove organic impurities from waste water streams using electrostatic adsorption (Urbain et al., 1941). Since the early 1970s, many efforts have been made to develop magnetic support technologies in fields as diverse as biological cell separation, drug delivery, effluent treatment, and mineral separation. The present review puts more emphasis on effluent treatment and mineral processing.

2.2.1. Biological and pharmaceutical applications

There is an abundant literature on biological and pharmaceutical applications of magnetic carriers, and it is out of the scope of this thesis to review them in detail. For a review, and for references, see Moffat et al. (1994). In the present section, only the principles of different methods will be outlined, based on the review by Moffat et al..

The key concept of biological cell separation is based on affinity separation. Affinity separation refers to the very specific interaction between the magnetic carrier and the target. For instance, highly selective separations can be achieved by exploiting reversible complex formation between two or more interacting biological species. The principle is so-called *key-lock*: the magnetic carriers are made so that they contain a functional group (e.g., an antibody) that will react only with one specific target (e.g., an antigen). The tags developed in that way are sometimes called magnetic bio-affinity materials (Moffat et al., 1994).

Another area of application is drug or reagent delivery. By incorporating drugs in a magnetic microsphere, they can be delivered to a specific site in the body. After injection, a bipolar magnetic field is placed around the targeted area in the body and an appropriate magnetic field is applied to hold the drug in the capillaries through which the blood flows (Moffat et al., 1994).

2.2.2. Effluent processing and metal ion removal

2.2.2.1. Bare Magnetite Carriers

Some of the pioneer work on the use of magnetite for the removal of metal ions (and suspended solids) from a solution was performed by de Latour (1976). He studied the precipitation of Al (III), Fe (III), and Cu (II) and their co-precipitates after addition of magnetite seed. The main finding was the correlation between the zeta-potential of the different species and the removal of those species from solution. Maximum removal occurred around the point of zero charge of the precipitate species. De Latour's work showed that in the case of magnetite, the main interaction to be considered is the electrostatic adsorption of the species. De Latour's study also demonstrated that the way to alter adsorption on magnetite was to vary the pH, to add coagulants, or to compress the double layer by increasing the electrolyte concentration.

Selective magnetic coating for mineral separation was studied by Parsonage (1984). To distinguish, the colloidal, chemically precipitated magnetite in de Latour's work was used as a carrier, whereas in Parsonage's work it was used as a tag. Parsonage also studied the stability of the magnetite colloid. He demonstrated that stability was dependent on pH and on the addition of surfactants (oleate, and dodecylamine). The point of zero charge (pzc) of magnetite alone was found to be pH 6.5. The presence of the anionic oleate surfactant resulted in a shift of pzc to pH 4.5. With a cationic amine surfactant the zeta-potential was positive over the pH range 3-11. The stability of the magnetite colloid was well correlated with the pzc of the suspensions. The interest in controlling the surface charge of the colloid is twofold. First, a well-dispersed colloid is required so that the reactive surface area available is maximized. Second, controlling the surface charge of the colloid is necessary to control the selectivity of electrostatic adsorption by the species to be removed. Parsonage demonstrated selective magnetic coating on calcite and not on apatite at pH 11, resulting in effective and selective magnetic separation of the two minerals.

Work by Terashima et al. (1986) on the removal of dissolved heavy metals by chemical coagulation, magnetic seeding, and high gradient magnetic separation corroborated the results of both de Latour and Parsonage. They showed that in the case of dissolved heavy metals, it is effective to form magnetic agglomerates by coagulating precipitates with magnetic seeds through adjustment of the chemistry. They also found that the coupling (or binding) of the magnetic seeds with the targets was primarily due to surface charge (through electrostatic interactions), and the capture of particles in the mesh structure of precipitated $Fe(OH)_3$.

To summarize, the main factor controlling the selectivity of magnetite attachment to target species is electrostatic interaction. Selectivity was therefore mainly controlled by particle surface charge through the addition of appropriate pH modifiers. The second issue was that of obtaining a suitable dispersion, or the opposite, coagulation (to produce entrapment), again involving pH modifiers and surfactants.

2.2.2.2. Gel coated magnetite

The incentive to use gel-coated magnetite was to increase the carrier specific surface area hence to increase its adsorption capacity. Commercial magnetite tends to have a small specific surface area, and is therefore not a very good adsorbent by itself, whereas amorphous Fe oxide gels are much better (Chen et al., 1991). Ferrihydrite was chosen by Chen et al. because it was amorphous and had well-known characteristics. Chen et al. (1991) report that surface binding site density was 1.33×10^{-3} mol/g for ferrihydrite whereas it was only 2.0×10^{-5} mol/g for 2 μm-sized magnetite (that is more than 50 times lower).

Chen et al. (1991) studied the removal of Cr (VI) and Zn using a composite adsorbent prepared by precipitating ferrihydrite onto magnetite. It was found that metal removal and recovery were good after one adsorption and desorption cycle, but decreased in subsequent cycles. During the first cycle, the coated particles were able to adsorb twice as much metal as the non-coated magnetite. This application was found to have two main drawbacks. First, a decline in adsorbent performance was observed, due to the accumulation of adsorbate on the solids. After 10 cycles, the adsorbent had lost 90 % of

its capacity. Second, the composite adsorbent was found to lose its coating during desorption.

A similar study was carried out by Anderson et al. (1982). Ferric hydroxide gel (of non-defined structure) was deposited on fine magnetic particles, and tested for the removal of color and turbidity from wastewater. The study pointed to the amphoteric behavior of ferric oxide, meaning that its surface can be either acidic (i.e., positive) or basic (i.e., negative) depending on pH. The surface species involved are:

$$Fe\text{-}OH + H^+ \Leftrightarrow FeOH_2^+$$

$$Fe\text{-}OH + OH^- \Leftrightarrow FeO^- + H_2O$$

In this work the pzc for ferric oxide was about pH 8. Negatively charged colloids were adsorbed at pH below 8, and particles were regenerated at pH above 8. The main drawback of this method, as in the previous, was the poor integrity (i.e., long term stability) of the gel coating. Substantial gel loss occurred after each regeneration, and in some cases all the gel was gone after as little as 6 cycles. More information on the amphoteric nature of the ferric oxide surface, and adsorption phenomena on oxide surfaces can be found in a study by Benjamin et al. (1982).

2.2.2.3.Magnetic polymer resins

Work on magnetic polymeric beads, also called magnetic resins, was initiated by Bolto et al (1979) in Australia, in the division of chemical technology of the CSIRO. The initial idea was that of a continuous ion exchange process. Conventional ion exchange resins are faced with several problems. First, in compact bed systems, the operation is not truly continuous, is relatively complex, and attrition of the resin can be significant. On the other hand, the use of conventional ion exchangers in a fluidized bed suffers from low density differences between the resins and the water phase, resulting in reduced contacting and stage efficiency. Magnetic ion exchangers were designed to increase sedimentation velocity (by exploiting magnetic flocculation), without decreasing reactivity so that they could be used in continuous fluidized bed systems. Such ion exchangers are characterized

by fast reaction rates (small particle size, large reactive surface area) and fast sedimentation rates (magnetic flocculation) (Bolto et al., 1979).

Two principal types of magnetic resins have been developed. First, homogenous resins, consisting either of a magnetic material uniformly distributed within the cross-linked ion-exchange resin, or of magnetic material and micro ion exchangers (e.g., activated carbon), uniformly distributed within an inert cross-linked polymer (Bolto, 1980). In this latter type, selectivity is controlled by allowing the permeability of the resin to vary by the nature and degree of cross-linking of the polymer backbone, in order to limit the size of the molecules able to penetrate the resin matrix (Dixon, 1980). Lab and pilot plant studies were carried out to test the use of these magnetic resins in the dealkilization of water, and showed the technical viability of such applications (Bolto et al., 1979, and Anderson et al., 1979). However, the regeneration of the resins was not easy, and if it required a strong acid or base, the magnetic oxide could degrade (Dixon, 1980).

The second type of resins developed are called heterogeneous, or whisker type resins. They consist of active polymeric chains grafted onto a core of magnetic polymer of the former homogenous type (Bolto, 1980). The advantage of the heterogeneous type is the following: "grafting of a precursor monomer followed by chemical modification enables a wider range of exchange resins to be produced" (Bolto et al., 1978). For these heterogeneous resins, the selectivity can be tailored by choosing the appropriate type of active polymer to be grafted on the surface. This capacity to tailor the selectivity of the carrier by choosing the functional group of the graft is referred to as functionalization.

Anderson et al. (1980) tested different types of homogenous and heterogeneous magnetic resins for the removal of color and turbidity from wastewater, and found two main problems. First, the polymer grafted resins could become irreversibly fouled, and second the cost of the particles was prohibitive (Anderson et al., 1980). Research on these kinds of magnetic resins was consequently discontinued.

2.2.2.4. SIROFLOC process

From the same CSIRO research group, tests were made on the direct use of magnetite particles (Kolarik, 1983). The magnetite particles were activated at pH 4-6, resulting in protonated surfaces following a mechanism similar to that discussed in section 2.2.2.1 for ferric oxide. Protonated surfaces provide good adsorption sites for negatively charged colloids or suspended solids. The study showed that alkali-treated magnetite was an effective reusable coagulant-adsorbent. Adsorption was performed at pH 4 to 6, and regeneration was achieved in a weak (0.1 M) NaOH solution. It was also shown that for highly turbid and colored waters, an alternative preferable to adding more magnetite was to add small amounts of coagulant or flocculant. This work also investigated the effect of magnetite particle size, pH, and stirring speed. Very poor coagulation was obtained for particles above 6 μm, due to their low specific surface area. For particles below 1 μm, on the other hand, settling rates were detrimentally slow. The operating size was consequently chosen in the range 1-5 μm. Removal was effective only below pH 5, due to a more protonated surface, and to the compression of the double layer. Too low a stirring speed resulted in too little particle-particle contact and low removal efficiency, while too high a rate of stirring resulted in excessive shear forces and agglomerate disruption. Stirring speed of 160 rpm was selected for the mixing stage. Regeneration was performed in 0.1 M NaOH, and 'no significant deterioration in the adsorption efficiency over prolonged reuse' was observed. This work from Kolarik was the starting point for the development of a very successful process for wastewater treatment, the SIROFLOC™ process. Process development, pilot plant studies, and full-scale applications will be presented in section 2.2.3.

Subsequent research on the SIROFLOC process investigated the role of different polyelectrolytes in water clarification, which led to a better understanding of the process (Anderson et al., 1987). The proposed mechanism is the following: at pH 6, magnetite has a positive surface charge and upon contact with water it rapidly adsorbs color in the form of soluble organic anions and some of the negatively charged turbidity particles. The loaded magnetite then has a negative surface charge. The addition of cationic

polyelectrolytes causes the remaining negatively charged impurities to be bound to the loaded magnetite, with the polymer acting as a bridge. A more recent study showed that traces of cationic polymer can become attached to the negatively charged oxide under alkaline regeneration conditions. It was concluded that an ideal polymeric agent would be one that is cationic under acidic condition and neutral or preferably anionic in alkali solution (Anderson et al., 1993). Such polymers are called amphoteric polymers. A trade off must be found between the anionic character of the polymer, which improves regeneration, and the cationic character, which allows for high removal efficiency (Anderson et al., 1993).

2.2.2.5.Surfactant functionalized magnetic carriers

Functionalization of magnetic carriers was mentioned in section 2.2.2.3 concerning the whisker-type heterogeneous resins created by Bolto et al. The goal was to graft active polymeric chains on a core magnetic resin in order to tailor the active function group responsible for adsorption. The development of a novel method along this line is credited to Hwang (1989; 1990). It consists of two layers of surfactants directly attached on colloidal (nanosized) magnetite. The inner layer has an affinity with the magnetite surface, while the functional group of the outer layer can be tailored to have an affinity with the desired target mineral. The two layers are bound through hydrophobic interaction.

Another development in this direction was initiated by Liu and Xu (1995; 1996). They investigated the functionalization of nanosized maghemite (γ-Fe_2O_3) particles by coating them with a monolayer of bolaamphiphile surfactants. A bolaamphiphile surfactant is the one with two different headgroups, in this case with one group intended to bind to the magnetic particle and the other designed to attach to the target. The bolaamphiphile used was HS-$(CH_2)_{15}$-COOH (16-mercaptohexadecanoic acid). It was demonstrated that the surfactant is anchored to the magnetic particle by chemisorption of the carboxylic (COOH) group on the surface oxide, and that the adsorbed layer is dense and resistant to acid or base leaching (Liu and Xu, 1995). Further tests showed that the thio groups are reactive for the adsorption of metal ions such as silver or copper (Liu and Xu, 1996). It was also demonstrated that the loaded metal ion could be removed by acid

stripping, but that the loading performance tended to decrease upon subsequent reuse (Liu, 1996). More systematic work remains to be done to assess selectivity and the performance of such functionalized particles upon prolonged reuse.

2.2.2.6. Other techniques

In his review on magnetic coating and magnetic carrier technologies, Parsonage reports magnetic oil and chemical coating applications (Parsonage, 1992). The principle of magnetic oil is that oil droplets will readily attach to, or spread over, the surfaces of particles that have been made hydrophobic or oleophilic. If the oil contains a finely dispersed magnetic phase, then a magnetic coating is formed. So called chemical coating methods consist in the conversion of the surface layer of a non-magnetic or weakly magnetic mineral to a more magnetic phase. These methods include roasting, oxidative alkaline pressure leaching, or surface decomposition of a gas phase (Parsonage, 1992).

2.2.3. Process development and industrial applications

Results from Kolarik (1983) on the SIROFLOC process (see section 2.2.2.4) were followed up by studies on process development and pilot plant operation (Anderson and Priestley, 1983; Anderson et al., 1983). The process development study showed that magnetite had to be demagnetized before contact with the water, in order to be fully dispersed and to present its full surface area to the water (Anderson and Priestley, 1983). Figure 2-5 shows the process block diagram proposed by Anderson and Priestley and Figure 2-6 shows the corresponding process flow diagram. Figure 2-7 is a schematic representation of the pilot plant flowsheet with the equipment specifications.

The patented SIROFLOC™ process has been successfully demonstrated on a 0.2 megalitre per day pilot plant at Malabar sewage treatment plant, Australia, and has been successfully scaled-up to 5 megalitre per day (Booker et al., 1994). The plant in Malabar was efficient in removing floating, suspended, and colloidal solids, as well as oil, grease, color, phosphates, and coliforms (Booker et al., 1994).

The first SIROFLOC™ process outside Australia was commissioned in 1988 by Yorkshire Water at Redmires, England. Pilot plant studies and process development were

carried out at Morehall Water Treatment Works, Yorkshire, in a 0.45 megalitre per day plant (Gregory et al., 1988). It was demonstrated that the process can produce water which complies with EC Drinking Water Directive (Gregory et al., 1988). Another study analyzed the first four months of operation at the full-scale 20 megalitre per day Redmires water treatment plant and showed that highly colored waters were efficiently treated (Home et al., 1992). The unit cost for potable water was lower or at least equivalent to that of other modern treatment works (Home et al., 1992). The process avoided the use of primary coagulants and eliminated the problems arising with the carry-over of residual coagulant. Finally, the process enhanced the robustness of the plant in adapting to major changes in raw water quality (Home et al., 1992).

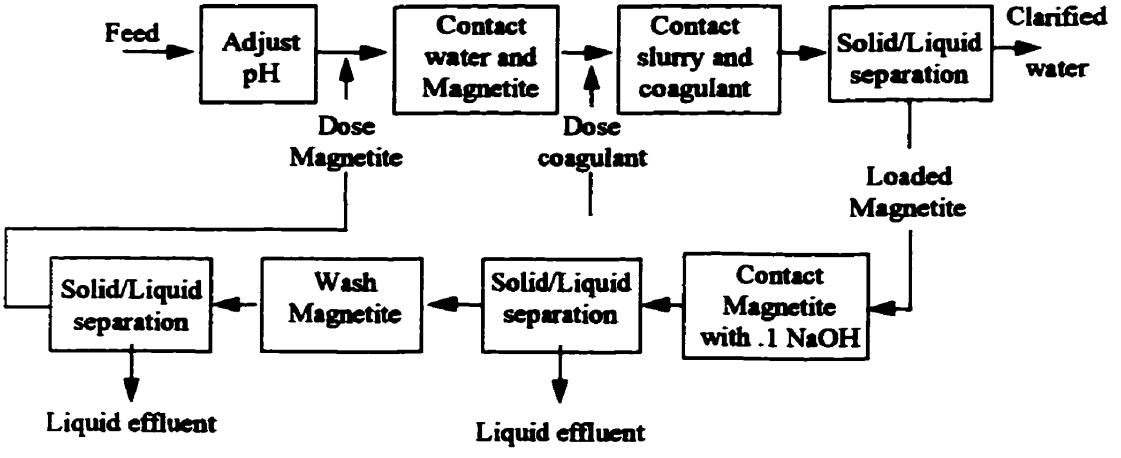

Figure 2-5: Process block diagram for color and turbidity removal with reusable magnetite particles (Reprinted from Water Research, Vol. 17, N. J. Anderson and A. J. Priestley, "Colour and turbidity removal with reusable magnetite particles - V," p. 1228, Copyright 1983, with permission from Elsevier Science)

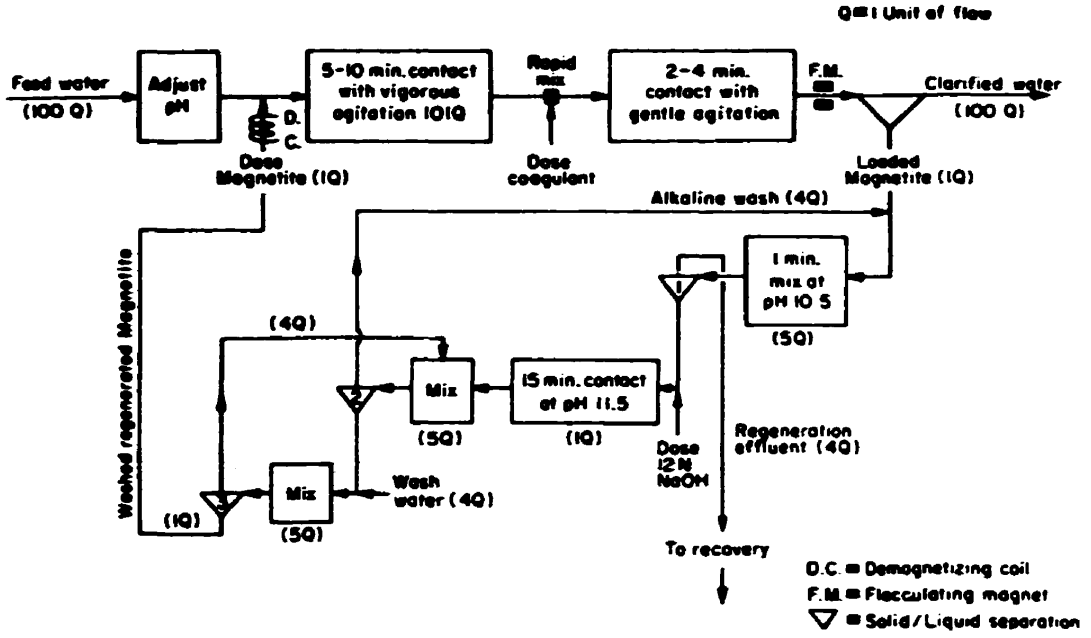

Figure 2-6: Process Flow Diagram (Reprinted from Water Research, Vol. 17, N. J. Anderson and A. J. Priestley, "Colour and turbidity removal with reusable magnetite particles - V," p. 1231, Copyright 1983, with permission from Elsevier Science).

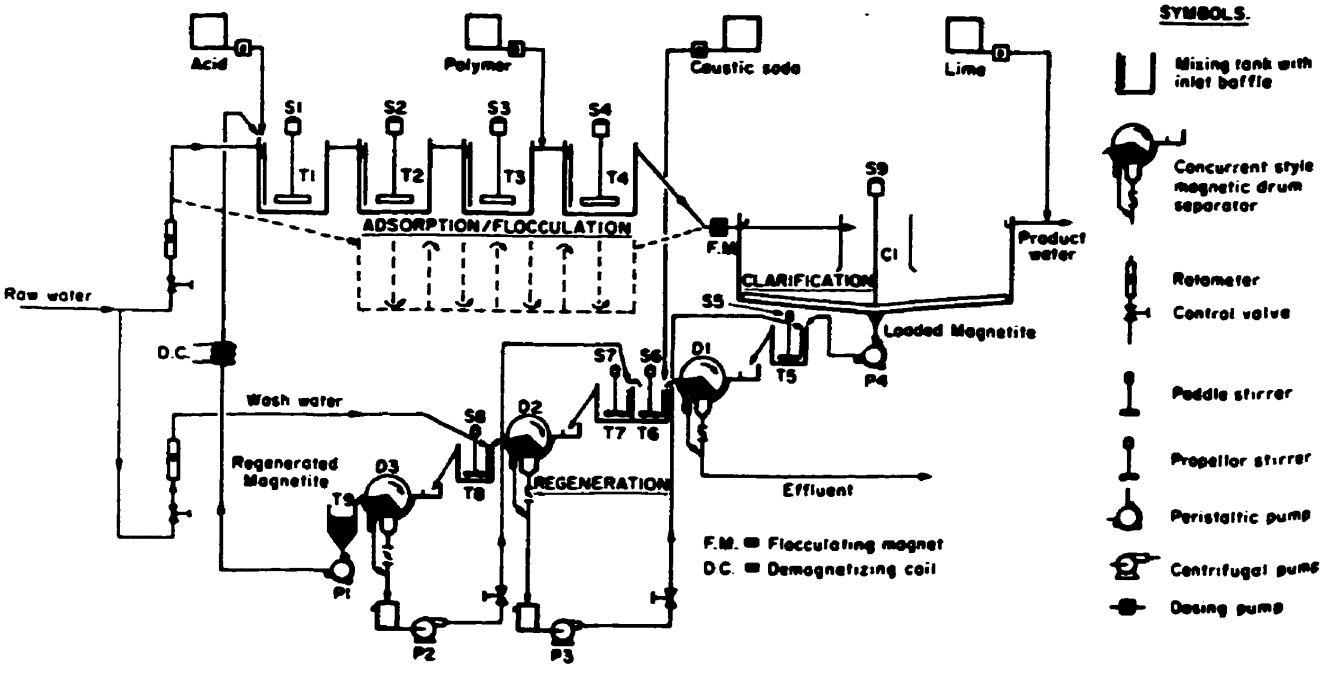

Figure 2-7: Pilot Plant Flowsheet and Equipment Specification (Reprinted from Water Research, Vol. 17, N. J. Anderson and A. J. Priestley, "Colour and turbidity removal with reusable magnetite particles - V," p. 1232, Copyright 1983, with permission from Elsevier Science).

2.2.4. Summary

From this review of existing magnetic carrier technologies, it is possible to derive some general characteristics for the preparation and use of magnetic carriers. The following address the issues of selectivity, removal (or absorption) capacity, potential for prolonged reuse, process parameters, and costs.

2.2.4.1.Selectivity

Two principal ways by which selectivity is achieved are electrostatic adsorption and functionalization. For magnetite based carriers, electrostatic adsorption is the main interaction mechanism affecting selectivity. Electrostatic adsorption occurs either by hetero-coagulation of species of opposite surface charge or by double layer compression. Selectivity can be monitored by controlling the zeta-potential of the species, and is usually achieved by adjusting pH, ionic strength, or by surfactant addition. It was established that the amphoteric character of iron oxide species allows the reversible adsorption and desorption of target species by setting the pH below or above the pzc.

Functionalization relates to specific coupling mechanisms between the surface species of the carrier and the surface species of the target. Highly selective carriers can be designed this way, based on the key-lock principle. The selectivity in this case depends primarily on the ability to prepare functionalized particles. Surfactant coated magnetic particles and graft polymerized magnetic polymer beads were developed for this purpose.

2.2.4.2.Removal capacity

Removal, or adsorption capacity depends mainly on the available reactive surface area, or the surface binding site density of the magnetic carriers. Particle size is crucial with respect to reactive surface area. For example: 16 μm particles have a surface area of 2 m^2/g while 30 nm sized particles have a surface area of 40 to 50 m^2/g. In the case of functionalized carriers, the corresponding parameter would be functional group density.

Another key point is to maintain the colloid in a dispersed form, to present maximum available surface area. Therefore, the colloidal stability of the carrier suspension is a

factor to monitor. The parameters affecting colloidal stability are mainly surfactant addition, and pH.

The order of magnitude of the removal capacities achievable with magnetic carriers can be derived from the example of bare magnetite. For 2 m^2/g, 16 μm-sized magnetite the surface binding site density is 2.0×10^{-5} mol/g. If Cu ions were to be loaded on this magnetite, and assuming uniform adsorption, up to 1.3 mg Cu/g magnetite would be the maximum capacity.

2.2.4.3.Potential for prolonged reuse

Some problems seem to arise with "composite" carriers (e.g., gel-coated or functionalized) upon prolonged use. The two issues at stake are: coating deterioration, and irreversible adsorption of the species.

The first issue relates to the robustness of coatings: i.e., the resistance to acid and base attack during regeneration, as well as the resistance to shear and other mechanical shocks during use must be assessed. Composite materials are obviously the ones prone to these kinds of problems.

The other problem is associated with desorption of adsorbed species: how reversible is the adsorption of the species to be removed? No problems occurred with bare magnetite particles, but some arose with magnetic polymer beads and gel coated magnetite. A related issue is the kinetics of desorption, which should also be assessed.

2.2.4.4.Process parameters

One of the principal advantages of magnetic carrier technology is that it can be easily used industrially. Magnetic carriers allow for truly continuous processes. They can be used in fluidized beds. Appropriately designed magnetic carriers can allow fast reaction rates, high separation efficiency, and selective separation.

One of the key parameters in the adsorption processes is the stirring speed. This has to be optimized so to allow high contacting rates while avoiding excessive shear. Some other parameters related to the dispersion of the colloid, include demagnetization and pH control.

2.2.4.5. Cost considerations

Some full-scale applications have shown that a careful design of a magnetic carrier based process can be economical. Some of the costs incurred for materials such as magnetic carriers and reagents can be offset by the improved process efficiency and by the reuse of the carriers and the recycling of the separated species.

2.2.5. Conclusions

Magnetic carrier principles and some of the technologies developed so far have been described. It was demonstrated that magnetic carriers can provide an innovative and efficient way to apply magnetic separation to non-magnetic species. Many advantages over conventional methods (e.g., filtration, precipitation, ion exchange resin, or ion flotation) have been outlined. Magnetic carriers have been designed and developed in order to combine the advantages of "adsorption" technologies (such as ion exchange resins or activated carbon), namely removal to very low concentrations, specific adsorption of target species and fast reaction rates, with the advantages of magnetic separation, that is of high separation efficiency and fast continuous processing.

A wide variety of processes have been presented, ranging from the less specific, more industrial oriented SIROFLOC™ process, to the very specific laboratory scale affinity separation carriers used in biological cell separation. Two main kinds of carriers have been introduced, bare carriers where adsorption occurs directly on the surface of the magnetic material, and composite carriers where adsorption is controlled by an absorbing material bound to the magnetic particles. Composite carriers were developed for two purposes: i) to increase the loading capacity of the carrier (e.g., gel-coated magnetite), and ii) to be able to increase the selectivity of the carrier by tailoring the functional group responsible for absorption (e.g., whisker-type resins). The two types of carriers that have been successfully used so far are, on one end of the spectrum, the non-specific large scale bare magnetite SIROFLOC™ process, and, at the other end, the small-scale very specific biological cell separation and drug delivery processes.

The key parameters characterizing magnetic carriers that need to be taken into account in magnetic carrier design are summarized below:

I. *Removal capacity*: Related to surface binding site density through

- Specific surface area for bare carriers, and
- Functional group density for functionalized carriers.

II. *Specificity*: Related to the ability to attach specifically to the target species, and

- Controlled by process parameters (pH, ionic strength) for bare carriers, and
- Tailored by the functional group in functionalized carriers.

III. *Robustness*: Reffered mainly to composite carriers.

- Dependent on the strength of the binding between the magnetic material and the "functional" adsorbent, and
- Critical for reusability of the particles.

IV. *Reaction rate*: Dependent on two main factors:

- The state of dispersion of the carriers, and
- The adsorption and desorption kinetics.

V. *Magnetic separability*: This depends on two main factors:

- The magnetic susceptibility, or magnetizability, and
- The size of the particles to be separated (ideally should be above 10 μm, to be separable by magnetic separators).

Many challenges remain, in particular in the area of composite magnetic carriers. There are two main issues. First, to be able to "graft" appropriate function groups on a magnetic core and make sure the function group is left "free" for further adsorption. Second, to get a stable and robust composite that will not degrade upon regeneration and reuse. One of the only large-scale applications so far is the SIROFLOC™ process, where magnetite is used as an indifferent adsorbent to remove various kinds of contaminants in municipal waters. The purpose of my research, which pursues the work initiated by Liu and Xu (Liu and Xu, 1995, Liu, 1996), is to develop a magnetic carrier that would possess both the high selectivity found in biological applications and the potential for industrial application similar to that of the SIROFLOC™ process.

Chapter 3

Choice of Materials and Objectives

3. Choice of materials and objectives

3.1. Preliminary remark

This thesis continues the research initiated by Liu and Xu on functionalized magnetic particles (Liu and Xu, 1995, Liu, 1996). The review on magnetic carriers showed that bare magnetic carriers were easy to use and did not degrade upon reuse, but yielded low selectivity between different contaminants. On the other hand, active polymer grafted magnetic resins could be made very selective but were expensive to make, prone to degradation, and to irreversible adsorption. There was clearly a need to develop magnetic carriers that would combine the robustness and ease of use of bare magnetite with the specificity (or selectivity) of polymer grafted resins. This motivated Liu and Xu to prepare magnetic carriers by molecular self-assembly of bolaamphiphiles on nanosized maghemite particles. They showed that molecular self-assembly could successfully coat HS-$(CH_2)_{15}$-COOH on the surface of maghemite particles to produce a layer that was dense and resistant to acid and base attacks. They also showed that these coated particles were able to load some Ag and Cu ions dissolved in water.

3.2. Choice of materials

3.2.1. Nanosized γ-Fe_2O_3 particles

Nanosized γ-Fe_2O_3 particles were chosen because they exhibit several advantages over typical micron-sized Fe_3O_4 particles. First, γ-Fe_2O_3 particles are reddish brown which allows them to be analyzed using DRIFTS whereas Fe_3O_4 particles are black and absorb too much light to yield a detectable signal using DRIFTS (Liu, 1996, p. 23). Second, γ-Fe_2O_3 particles are superparamagnetic when they are nanosized (see section 2.1.2.2), which makes them ideal for magnetic carrier applications. They have high susceptibilities, thus can be magnetized strongly, but have no remanent magnetization when the magnetic field is removed, which makes them easily dispersible. Finally, because of their small size, they have a high specific surface area. This latter characteristic implies that such particles should have a large removal (or adsorption) capacity.

3.2.2. Bolaamphiphiles: HS-$(CH_2)_{11}$-COOH and HS-$(CH_2)_{15}$-COOH

In section 2.1.6 the principles of molecular self-assembly, and the characteristics of the surfactant required were described. For this study, two bolaamphiphile surfactants, of similar structure but different chain length, HS-$(CH_2)_{11}$-COOH and HS-$(CH_2)_{15}$-COOH, were chosen. In this thesis, the abbreviation C_{12} will be used for HS-$(CH_2)_{11}$-COOH, and C_{16} for HS-$(CH_2)_{15}$-COOH. Three main reasons motivated the choice of C_{12} and C_{16}:

- The carboxylic functionality tends to chemisorb at the surface of γ-Fe_2O_3,
- Chain lengths greater than 12 are preferable to achieve good SAM, because they favor chain-chain attraction, and hence contribute to better packing,
- The thio (SH) group was chosen for its affinity to Cu and Ag ions.

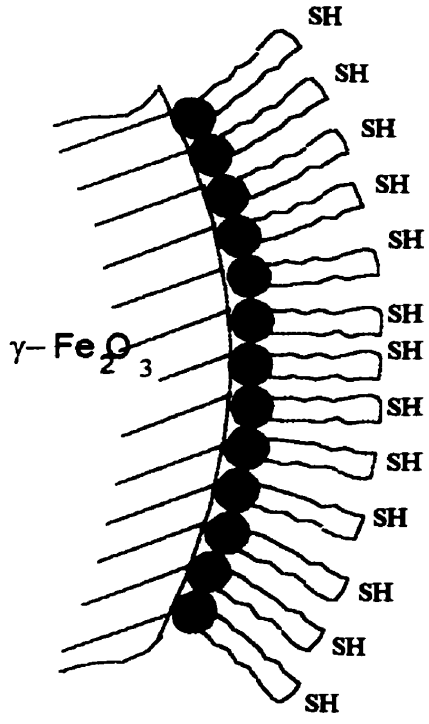

Surfactants:

$C_{12} = HS(CH_2)_{11}COOH$

$C_{16} = HS(CH_2)_{15}COOH$

- COOH: to bind with maghemite
- SH: affinity for Cu, Ag, AU
  can be modified to SO_4^-
- CH_2 chain: for chain-chain interaction (> 12)

Nanosized maghemite:

- Superparamagnetic properties
- High specific surface area (49 m^2/g)

Figure 3-1: Schematic representation of the surface of a functionalized magnetic carrier, and description of the material used.

3.2.3. Target metal ions: Cu and Ag

Copper and Ag were chosen as the metal ion targets. Copper was chosen as a typical metal found in contaminated effluents, and that needs to be removed. Silver was chosen as an example of a high value metal that industry may wish to recover for re-use.

3.3. Objectives

The current study has the following objectives:

1. To coat the surface of nanosized maghemite particles with two similar bolaamphiphiles of different chain lengths, HS-$(CH_2)_{15}$-COOH and HS-$(CH_2)_{11}$-COOH.

2. To characterize the coatings produced by self assembly of the surfactant.

3. To compare the behavior of the two types of carriers with regard to metal ion loading.

4. To understand further the mechanisms controlling metal ion adsorption on the carriers.

Chapter 4

Experimental Procedures

4. Experimental procedures

4.1. Materials

Materials: The particles used were γ-Fe_2O_3 powder from Alfa Chemicals with the following characteristics: 99% γ-Fe_2O_3, average size around 30 nm, and surface area of 49 m^2/g. Fisher volumetric standard $CuSO_4$ were used for copper solutions (1 mL = 0.198 mg Cu). Silver solutions were prepared from Fisher volumetric standard $AgNO_2$ (1 mM).

Both C_{12} and C_{16} were synthesized in the Chemistry Department at McGill University. The starting materials for the synthesis were, respectively, $Br(CH_2)_{11}COOH$ and $OH(CH_2)_{15}COOH$ from Aldrich. The reactions and procedures for surfactant synthesis are summarized in Appendix 1 to 3. The surfactants prepared were pure, as seen from the NMR spectra (see Appendices 4 and 5).

Glassware: Forty mL cylindrical glass vials with threaded plastic caps were used as reactors for the preparation of magnetic carriers. Forty mL conical plastic tubes were used as reactors for the loading of metal ions on the magnetic carriers. These tubes were specially bought to fit in the centrifuge used in the experiments. All glassware (beakers, graduated cylinders, pipettes, vials, tubes) was cleaned with a solution of 10 % ethanol in 2 M sodium hydroxide (25 g NaOH + 50 mL EtOH 100 % + 425 mL distilled H_2O). Water used was distilled with a Corning Mega-Pure equipment. All other chemicals (EtOH, chloroform, hexanes) were reagent grade.

4.2. Analytical techniques

4.2.1. Diffuse Reflectance Infrared Fourier-Transformed Spectroscopy (DRIFTS)

DRIFTS is one of several infrared spectroscopy techniques. Infrared (IR) spectroscopy is a widely used method for the characterization of the chemical structure of organic species. IR techniques are based on the following principle: infrared radiation is absorbed by molecules and that causes changes in the vibrational and rotational energy states of the molecules. The frequency of radiation at which adsorption occurs is

characteristic of the chemical species. Various IR techniques have been developed to determine the IR absorption characteristics of species in qualitative and quantitative ways. IR techniques are very useful, due to their versatility which allows the study of samples as gases, liquids, and, with appropriate procedures, solids (Fuller and Griffiths, 1978). Some of the pioneer work on DRIFTS was performed by Fuller and Griffiths (1978). They showed that almost any type of powder samples can be studied, even at submicrogram quantities, that good quantitative analysis could be obtained, and that the technique allowed the kinetics of heterogeneous reactions of gases with powdered solids to be studied (Fuller and Griffiths, 1978).

In DRIFTS, an IR beam, focused on a sample by an ellipsoidal or hemiellipsoidal reflector (Ferraro and Rein, 1985), is partially reflected by the sample, collected back by the reflector, and sent onto the detector. The optical diagram for a specific DRIFTS accessory is shown in Figure 4-2 i) (left) (from Fuller, Nicolet FT-IR Tecnical Note, TN-0933). Figure 4-2 ii) (right) shows the three types of reflectance that occur when a powdered sample interacts with an IR beam. The ray labeled *true specular (Rs1)*, is a simple reflection from a crystal surface. It emerges at an angle equal to the incident angle, and has not been absorbed by the sample. The ray *diffuse specular (Rs2)* has undergone multiple 'mirror like' reflection and has not been absorbed either. The "true" reflectance ray is the *Rv* ray reflected within the sample after penetrated through the sample. This ray contains information about the matter it has penetrated. It is this ray that the DRIFTS technique singles out, collects, and measures. The other two parasitic rays introduce spectral distortions, but their effect can be reduced by diluting the sample with a powdered alkali halide such as KBr. The other limitation of this method is the low level of reflected energy, but this can be overcome by using more sensitive detectors such as the cooled mercury cadmium telluride (MCT) detector.

The effect of sample dilution and particle size/morphology can be found in a study by Olinger and Griffiths (1993). Another valuable contribution is the study by Ferraro and Rein (1985) on the application of DRIFTS in the far IR region.

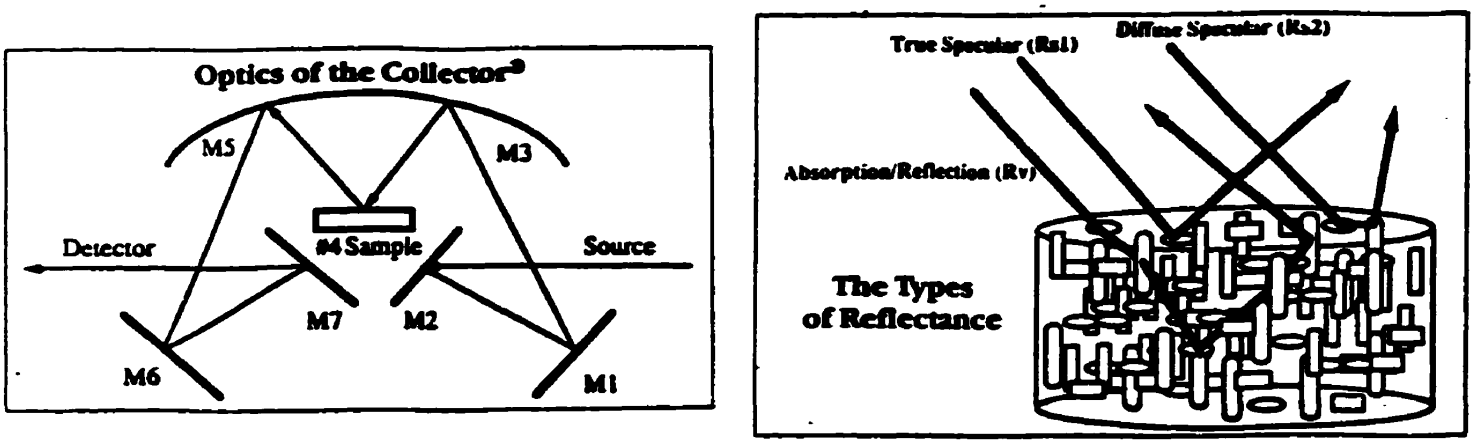

Figure 4-2: i) The optical diagram of the Spectra-Tech Collector® diffuse reflectance accessory (left) , and ii) the three types of reflectance that occur from a powdered sample (right). (from Fuller, Nicolet FT-IR Technical Note, TN-9033)

4.2.2. X-ray Photoelectron Spectroscopy (XPS)

The principle of XPS is the following (Ulman and Elman, 1995). During an XPS measurement, a sample is probed by X-rays. The X-rays react with the inner shell electrons of the sample atoms. If E_0 is the energy of the incident X-ray and E_j that of the inner shell electron (s, p, d etc.) in the atom, an electron (called *photoelectron*), will be ejected with the energy $E_0 - E_j$. Since E_j is characteristic of a particular electron in a particular atom (it is its signature), measuring E_j provides atomic identification. Furthermore, as the numbers of electrons ejected is proportional to the number of atoms present in the sample, the composition can be determined quantitatively. XPS can also provide information on the chemical state of different atoms because it can detect chemical shifts. Photoelectrons are emitted only from a small depth, and that allows the contribution of atoms from different depths to be emphasized in a process known as depth profiling. For more information on XPS, an extensive review of XPS instrumentation and applications for thin film analysis can be found in a book edited by Briggs and Seah (1994).

4.2.3. Thin Film Flotation

Thin film flotation is a fast and easy way to estimate the critical surface tension of wetting, the complete wetting surface tension, and the non-wetting surface tension (Fuerstenau and Williams, 1987). The critical surface tension is defined as the surface tension resulting in a 50 % lyophobic fraction, the non-wetting surface tension is defined for 0 % lyophilic fraction, and the complete wetting surface tension is that for 100 % lyophilic. The critical surface tension gives an indication of the coverage of the particles by the surfactant. The difference between wetting and non-wetting values is a function of surface heterogeneity in the case of SAMs (Liu and Xu, 1995). Information on the packing density can thus be inferred from these measurements.

The principle of this method is the following: First, the surface tension of the liquid is adjusted to the desired value. In this thesis, water methanol solutions were used. The surface tension of a water-methanol mixture can be calculated from referenced values (see section 4.3.1.3). Second, a known amount of particles is spread uniformly on the surface of the liquid. The particles should be spread to present only one layer of particles on the surface. Third, the lyophobic fraction is scooped out and weighed, and the fraction of lyophobic particles is determined. The results are plotted as the fraction of lyophilic particles (in %) versus the surface tension of the liquid (in mN/m). A typical thin film flotation curve is shown in Figure 4-3.

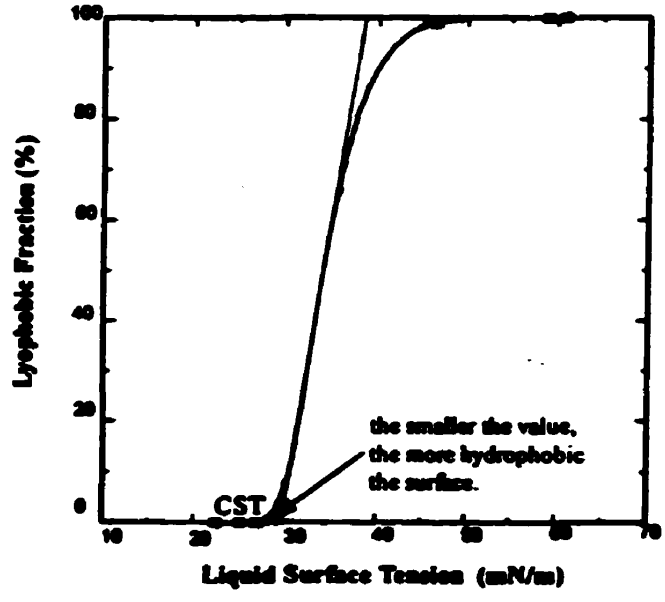

Figure 4-3: A typical thin film flotation curve (from Liu, 1996)

4.3. Procedures

The research activity was carried out in 5 steps. In step I there were two objectives: i) to follow the procedures used by Liu and Xu in order to become familiar with the techniques and to test the reproducibility of their results; ii) to compare the characteristics of the coatings obtained using C_{12} or C_{16} surfactants. Step II experiments were preliminary loading tests aimed at becoming familiar with the procedures as well as allowing a comparison between the loading of Ag and Cu and between the loading on C_{12} and C_{16} carriers. Step III went further, to characterize the reproducibility of Cu adsorption on C_{12} particles, and the effect of Cu concentration on adsorption. In step IV, systematic experiments were carried out to investigate Cu loading on C_{16} carriers. Comparisons of Cu loading on bare and C_{16} coated particles, and zeta potential measurements were performed to try to understand the loading mechanism. Finally, in step V, some of step IV experiments were repeated in a more controlled and systematic way to test the validity of those results.

4.3.1. Step I: Preparation and characterization of C_{12} and C_{16} coated particles

4.3.1.1. Coating procedure

The γ-Fe_2O_3 powder was first dried overnight in a vacuum oven (40°C, 12 psi), to remove any physisorbed water (Liu and Xu, 1995). The surfactant solutions prepared were 3 mM, to exceed critical micelle concentration, in order to favor SAM formation (Liu and Xu, 1995). Particles and surfactant solutions were mixed in a 40 mL vial, shaken by hand for up to one minute. Next, they were sonicated for 2-3 minutes to ensure mixing and dispersion of the particles, and then shaken for 24 h in a laboratory shaker (New Brunswick Scientific, Inc., USA). The amounts used for solution preparation and particle coating are summarized in Table 4-1.

Table 4-1: Quantities used for C_{12} and C_{16} coated particles preparation.

	For 100 mL of 3 mM solution	For 50 mg coated particles
C_{12} surfactant	C_{12} solution: 70 mg C_{12} + 100 mL EtOH	C_{12}-coated particles: 50 mg γ-Fe_2O_3 particles in 25 mL C_{12} solution
C_{16} surfactant	C_{16} solution: 87 mg C_{16} + 100 mL EtOH	C_{12}-coated particles: 50 mg γ-Fe_2O_3 particles in 25 mL C_{16} solution

After shaking, the vials were centrifuged for 5 minutes in a Dynac Centrifuge (at speed 85 on the scale), and the liquid decanted. The remaining particles were washed three times in EtOH. Each washing consisted of filling the vial with EtOH, hand shaking for one minute, centrifuging at 85 for 5 minutes, and pouring the liquid out. Partidles were then dried in vacuum oven and stored for further characterization.

4.3.1.2.DRIFTS analysis

DRIFTS was performed on a Bruker IFS 66 FTIR spectrometer equipped with a narrow-band MCT detector, using a Nicolet advanced diffuse reflectance accessory. KBr (Aldrich, dried overnight at 400°C in oven) was used for the background measurement and was mixed with every sample analyzed. The sample preparation for DRIFTS was the following: a small amount of sample (between 5 and 20 mg) was mixed with a large excess of KBr (between 50 and 100 mg) and ground together in a small mortar.

For each series of DRIFTS measurements, a background measurement was performed on some of the ground KBr used for sample dilution. Prior to each measurement, 5 to 10 minutes were needed to purge the sample cell from ambient air, to reduce the absorption by H_2O and CO_2.

4.3.1.3.Wetting test

The experimental setup used for thin film flotation is shown in Figure 4-4. The starting liquid was 10 mL distilled water. The surface tension was modified by adding controlled amount of methanol (reagent grade) with the graduated syringe. The curve representing the variation of surface tension relative to the percentage of methanol added,

derived from the literature, is given in Appendix 6. In this experiment, the amount of particles floated (15 mg) was too low to be accurately weighed. Therefore, the method used was to successively add controlled amounts of methanol with the syringe in a funnel equipped with a valve. After each injection, the fraction that sank relative to that still floating was estimated. While a qualitative method, it allows one to observe in a sufficiently reliable way the evolution of floatability with surface tension.

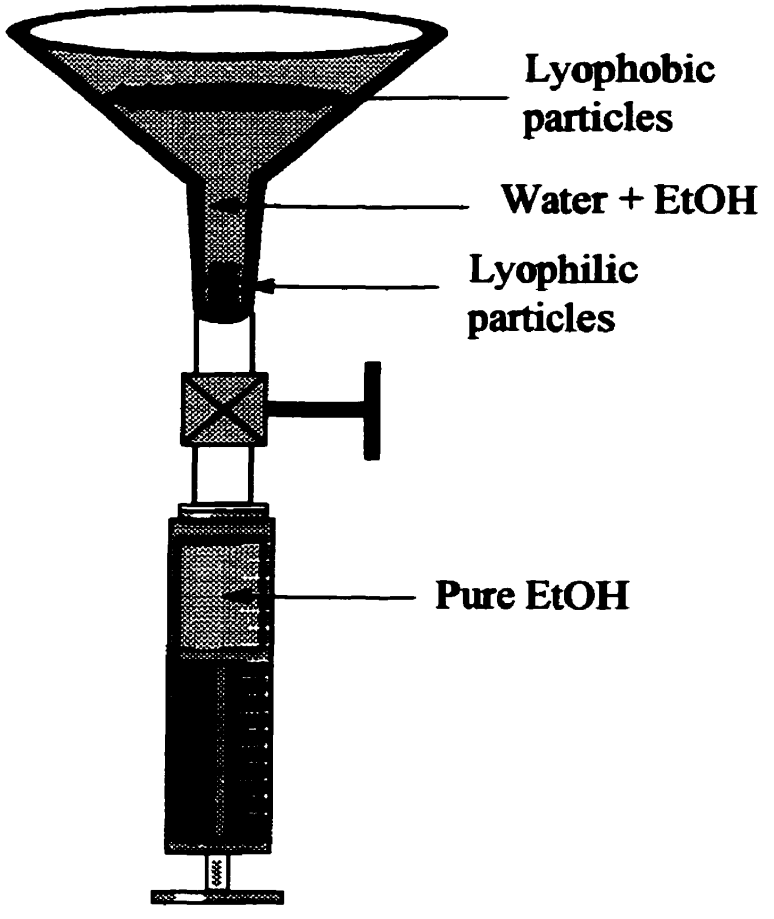

Figure 4-4: Experimental setup for thin film flotation.

4.3.1.4.Leaching test

Leaching tests were performed to assess the stability (robustness) of the SAMs. When the chains are well packed and well ordered, they stretch outward from the surface and protect the γ-Fe_2O_3 surface. In that case, chemicals cannot reach the γ-Fe_2O_3, and cannot break the bonds between surfactant and surface. Such a packed and ordered monolayer should ensure that neither the monolayer, nor the particle itself will degrade. The leaching tests can thus yield information on the relative packing density of the SAMs and on the ordering of the chains.

Six samples were prepared. For each of the three types of particles (γ-Fe_2O_3 particles, C_{12} coated particles, and C_{16} coated particles), two leaching tests (at pH 2.8 and 10.55) were performed. For each of the six samples, 15 mg of particles were added to 25 mL of the pH solution, shaken, and let stand for 7 days. Leachates were filtered and were analyzed for total iron ions with atomic absorption spectrometry (AA). The AA instrument was a Perkin Elmer model 3110 and was calibrated with Fe standards of 1, 3, and 5 ppm. The detection limit under these conditions was 0.5 ppm.

4.3.1.5.Elemental analysis

Some elemental analysis (EA) was conducted with a FISIONS EA 1108 elemental analyzer. Two samples of 5 mg of the C_{12} and C_{16} coated particles were analyzed for S, C, and H content. The EA device gives the weight percentage of a given element relative to the total mass of the sample. This method provides a means to measure quantitatively the mass of surfactant present on the surface of the particles. Standards are required to perform quantitative EA. The standard used contained 93.56 % C, 5.62 % H, 0.176 % N, and 0.38 % S. The detection limit of the analyzer was 5 μg.

4.3.1.6.XPS analysis

XPS was performed on an EscaLab 220-IXL instrument with an Al K_α anode ($h\nu$ = 1486.6 ev) at a take-off angle normal to the sample (mode used: large area XL source, mono 1 mm). The energy resolution was 1 ev. The samples had to be dry, because XPS operates under a high vacuum. Sample prepararion was to spread a few milligrams of sample evenly on a copper tape. One C_{16} coated sample was analyzed. The spectra were

all corrected for charging by calibrating their C1s peak to 284.9 ev. The spectra were analyzed using the XPS-Peak™ peak processing and peak fitting program. Peak processing and peak fitting were performed with the help and guidance of Andrew Vreugdenhil, from the McGill Mining and Metallurgical Engineering Department.

4.3.2. Step II: Loading of Cu and Ag on C_{12} and C_{16} coated particles

This series of experiments was aimed at comparing the loading capacities of C_{12} and C_{16} coated particles, and to compare the adsorption of Cu with that of Ag for both carriers. The experiments were designed to measure metal ion adsorption by comparing the metal ion concentration of the solution before and after contacting with the carriers. Initial and final metal ion concentrations were measured by atomic absorption spectroscopy (AA). Knowing the volume of solution used, the mass of Cu adsorbed can be calculated from the difference between initial and final concentration. Finally, knowing the mass of particles used, it is possible to calculate an equivalent mass of metal adsrobed per gram of particles. In this first series of loading experiments, the limited amount of carriers meant only a few experiments could be performed. Four loading tests were performed, as described below.

4.3.2.1.Materials

For these loading experiments the C_{12} and C_{16} coated particles were used. The particles had been prepared in batches of 50 mg each and dried overnight at 40 C in a vacuum oven. The particles were kept in the vials where they had been prepared and dried. The vials were purged with nitrogen and sealed with Teflon tape prior to being capped and stored.

Copper and silver solutions were prepared from Fisher volumetric standards. The water used for solution preparation was distilled from a Corning Mega-Pure system. It was decided that only one solution of Cu and one solution of Ag would be prepared and that both carriers would be tested with each solution, for a total of 4 tests.

4.3.2.2.Solution preparation

Considering the results on coating density obtained in step I, theoretical loading capacities were calculated (see calculations in section 5.2.1). The Ag and Cu concentrations were chosen to correspond to half the maximum loading capacity. The characteristics of the solutions are summarized in Table 4-2.

Table 4-2: Cu and Ag solution characteristics.

	Preparation	Theoretical concentration (ppm)	Measured AA concentration (ppm)	pH
Ag	8 mL $AgNO_2$ in 100 mL distilled H_2O	8.6	7.4	5.9
Cu	2 mL $CuSO_4$ in 100 mL distilled H_2O	3.96	3.94	5.7

4.3.2.3.Loading procedure

Four samples were prepared for this experiment:

- #1: 20 mg C_{12} particles + 25 mL Ag solution
- #2: 20 mg C_{16} particles + 25 mL Ag solution
- #3: 20 mg C_{12} particles + 25 mL Cu solution
- #4: 20 mg C_{16} particles + 25 mL Cu solution

For each sample, the following procedure was followed. The coated carrier was weighed (20 mg) and placed in a 40 mL centrifuge tube. As used, after drying, the coated carrier looked like dried clay. It had to be scrapped off the bottom of the vial to yield a few chunks of agglomerated carrier. The coated carriers were very hydrophobic, and could not be easily dispersed in water. Pre-conditioning was thus required, consisting of adding a few drops of EtOH to the carrier, and sonicating the sample for two to three minutes. After that, the carrier particles dispersed.

The next step was the addition of 25 mL of the metal ion solution. After addition, the sample was sonicated for 2 minutes, then the vials were sealed, and shaken overnight in the laboratory shaker.

4.3.2.4.Supernatant extraction and analysis by atomic absorption spectrometry

Soon after shaking, the samples were centrifuged to separate the solids from the solution. The centrifuge used was a Du Pont Instruments Sorvall RC-5B Refrigerated Superspeed Centrifuge. The HB-4 rotor was used, the speed was 12,000 rpm, the time of centrifugation 1/2 h, and it was operated at room temperature. The supernatant was extracted with a pipette and poured into a 15 mL tube.

For AA analysis of the supernatant, it was necessary to use standards. The Cu standards used were pre-prepared by the analytical laboratory technician. Silver standards were prepared from $AgNO_3$ salts. A 50 mg of $AgNO_3$ was carefully weighed and mixed with 100 mL of distilled water in a volumetric flask, to make the stock solution. Next, 1 mL of the stock solution was taken with an Eppendorf micropipette and mixed with distilled water in a 100 mL volumetric flask. This solution was labeled Solution 1. A Solution 2 was also prepared, that used 2 mL of the stock solution in the second step. Finally, two other standard solutions (S3 and S4) were prepared from Solution 1, with the characteristics listed in Table 4-3. Some dilutions were required to analyze the supernatants, so that the concentration would fall in the linear range of the AA calibration. The atomic adsorption spectrometer used was a Perkin Elmer 3110.

Table 4-3: Standards preparation for Ag AA analysis.

	Solution preparation	Theoretical concentration (ppm)	Measured AA (ppm)
Solution 1 (S1)	As described	3.17	3.21
Solution 2 (S2)	2 mL instead of 1 mL in step 2.	6.34 (x 2 Solution 1)	5.83
Solution 3 (S3)	5 mL S1 + 5 mL H_2O	1.58	1.41
Solution 4 (S4)	2 mL S1 + 8 mL H_2O	0.63	1st point = 0.042 Abs.

4.3.2.5.Solids analysis.

After the supernatant had been extracted, the remaining solution was poured out, and the sample that remained at the bottom of the tubes was dried in a vacuum oven (40°C, 12 psi), without prior rinsing. The 4 solid samples were analyzed by DRIFTS and the two Ag loaded samples were also analyzed by XPS.

4.3.3. Step III: Further Cu loading tests

4.3.3.1.Reproducibility

Materials: The particles were C_{16} coated particles. The Cu solution was prepared from Aldrich volumetric standard $CuSO_4$ solution. A 250 mL solution of 10 ppm Cu was prepared by adding 13 mL of $CuSO_4$ solution to 237 mL of Millipore water.

Loading procedure: Four tubes were prepared, each with 20 mg of particles. Next, 25 mL (measured with a pipette) of the stock solution was added, and the suspension was sonicated for 5 minutes, then shaken in a laboratory shaker over the week-end.

AA analysis: The four samples were centrifuged as described above. The supernatant was filtered and put in a 15 mL tube for AA analysis. The AA was calibrated with pre-prepared Cu standards (2, 3, 4, and 5 ppm). The stock solution was diluted 1:3 in Millipore water to fall in the linear range of the AA calibration. The supernatant solutions did not need dilution before measurement.

4.3.3.2.Incremental Cu loading

This series was designed to measure the adsorption of Cu ions on C_{12} coated particles as a function of Cu concentration. Five solutions were prepared, 1.7, 2.6, 4.4, 8.1, and 9 ppm Cu. Another goal of this series was to determine the effect of sonication time on adsorption. The following samples were prepared:

- # 2-1: 20 mg C_{12} carrier in 25 mL 1.7 ppm Cu, sonication: 2 minutes
- # 2-2: 20 mg C_{12} carrier in 25 mL 1.7 ppm Cu, sonication: 6 minutes
- # 3: 20 mg C_{12} carrier in 25 mL 2.6 ppm Cu, sonication: 6 minutes

- # 5-1: 20 mg C_{12} carrier in 25 mL 4.4 ppm Cu, sonication: 1 minutes
- # 5-2: 20 mg C_{12} carrier in 25 mL 4.4 ppm Cu, sonication: 4 minutes
- # 5-3: 20 mg C_{12} carrier in 25 mL 4.4 ppm Cu, sonication: 8 minutes
- # 8: 20 mg C_{12} carrier in 25 mL 8.1 ppm Cu, sonication: 6 minutes
- # 9: 20 mg C_{12} carrier in 25 mL 9 ppm Cu, sonication: 6 minutes

4.3.4. Step IV: Investigation of the mechanisms controlling Cu loading on carriers

4.3.4.1. Batch preparation of carriers

Previously, the coating of maghemite particles had been in small batches of 50 mg. In this step, preparation of a larger amount of particles was attempted: the preparation of 2 g of C_{16} carriers in one batch. The coating procedure was as follows:

- 250 mL of 6×10^{-3} M C_{16} solution was prepared: 0.43 g of C_{16} was added to 250 mL of EtOH and sonicated for 10 minutes under nitrogen bubbling.
- 2 g of maghemite was added to 205 mL of the C_{16} solution in a 250 glass container
- The suspension was stirred (glass stirrer) for 40 minutes under nitrogen bubbling
- The jar was sealed and shaken for 17 hours in a laboratory shaker
- For washing, the following procedure was used: the suspension was placed above a strong electromagnet, forcing the particles to settle at the bottom, and the solution was extracted with a syringe. When almost all of the solution was 'pumped' out, the container was filled anew with EtOH, shaken, and the procedure repeated. The particles were washed 6 times using this procedure.

The C_{16} coated particles obtained were analyzed using DRIFTS which showed traces of unbound surfactant. It was decided to separate the batch of particles in 8 40-mL glass vials, and perform an additional 2 chloroform/2 EtOH washings using the previous

washing procedure (i.e., the one involving centrifugation for solid/liquid separation). The carriers so-prepared are the ones used in all subsequent step IV experiments.

4.3.4.2.Cu loading on bare and C_{16} coated particles vs. pH

This series was aimed at investigating the effect of pH on the loading of Cu on the carriers. The same loading experiments were performed on the bare particles to compare their adsorption behavior with that of the coated carriers.

Three 20-ppm Cu solutions (100 mL) were prepared at pH 3.2, 4.4, and 5.6. For each sample, 25 mg of particles was added to 25 mL of solution, sonicated 5 minutes, and shaken for 16h. The samples were then centrifuged for 10 minutes at 12,000 rpm in the Du Pont centrifuge, and the supernatant filtered and put in tubes for AA analysis. The AA spectrometer was calibrated with pre-prepared standards at 2, 4, and 5 ppm. The solutions were diluted for AA using the Brinkmann Digital dispensette 2-10.

4.3.4.3.Zeta potential measurements

Zeta-potential measurements were used to compare the surface charge of the bare and coated particles and to investigate the effect of Cu loading on surface charge. The zeta potential meter used was a Pen Kem Inc. Laser Zee Meter model 501. For all measurements, the supporting electrolyte was 10^{-3} M KCl (prepared by adding 0.075 g of KCl in 1 L of Millipore water).

The procedure was as follows: a small amount of particles was added to 300 mL KCl electrolyte, and stirred for 5 minutes until the pH stabilized. After 5 minutes, a 30 mL solution sample was taken with a syringe, introduced into the Laser Zee cell, and a measurement was taken. Then, pH was adjusted to the next value by adding NaOH or HCl. Two sets of measurements were required for each type of sample in deriving the zeta potential/ pH relationship. Starting at ca pH 5.5, one set was obtained by decreasing pH (to pH 3) and the other set (with a new batch of particles and KCl) by increasing pH (to pH 10.5). Usually, small amounts of particles (around 15 mg) were used for each set. A difficulty resulted from the need to disperse the coated carrier. It was necessary to add a few drops of EtOH and to sonicate the coated particles prior to zeta-potential

measurements. An experiment done on bare particles showed that adding a few drops of EtOH prior to zeta potential measurement did not affect significantly the resulting curve. Zeta potential measurements were performed on bare maghemite, on C_{16} coated particles, and on bare and C_{16} coated particles that had been used for Cu ion loading.

4.3.4.4.Cu and Ca loading on bare and C_{16} coated particles vs. pH

Adsorption tests were run on solutions containing both Cu and Ca ions to test whether a selective adsorption of one type of ion occured. Four 100-mL solutions of 50 ppm Cu and 50 ppm Ca were prepared at four different pHs (pH 3, 4.5, 6.1, and 8.1). For each solution, two adsorption tests were performed, one on bare particles and one on C_{16} coated carriers. For each adsorption test, the following procedure was used.

- 100 mg of particles were weighed on a microbalance
- the C_{16} carriers were sonicated 9 minutes in a few drops of ethanol
- 25 mL of solution was added to the particles
- the preparation was sonicated for 9 minutes and 30 seconds
- the samples were shaken for 2h at 300 rpm
- the samples were centrifuged in the laboratory Dynac Centrifuge setting at 80 for 5 minutes
- the supernatant was filtered with ashless filter paper and poured in conical tubes

For AA analysis, Ca standards were prepared from Ca volumetric standard (1 mL = 1 mg Ca), at 2, 4, and 5 ppm. Cu standards were the laboratory prepared standards. The AA results, and dilutions used are shown in Appendix .

4.3.5. Step V: Confirmation of Step IV results

The results obtained in step IV were not expected, so it was decided to carefully plan a last series of experiment to determine whether the results found were reproducible or due to an experimental artifact.

4.3.5.1.C_{16} coated carriers preparation

One problem that had arisen was to disperse the coated carriers once they had been dried. A procedure was designed to avoid drying the coated carriers before adsorption. One of the reasons that motivated drying was to be able to weigh the amount of particles used. To solve that problem it was decided that coated carriers would be prepared in individual samples of known amount (50 mg), and that for each adsorption point, whole sample would be used. First, a series of 12 individual samples of C_{16} carriers was prepared in 40 mL conical plastic tubes. A second series of 16 50-mg samples were prepared later for the next series of loading tests. The procedure was as follows:

- a fresh C_{16} solution (3×10^{-3} M) was prepared; 0.3 g of C_{16} surfactant was added to 350 mL of EtOH and sonicated for 20 minutes.
- 50 mg of maghemite was weighed and poured into 40-mL tubes.
- 25 mL of the C_{16} solution was added to the particles using a pipette.
- the samples were sonicated for 10 minutes.
- the samples were shaken overnight.
- the samples were centrifuged in the Dynac centrifuge and washed 4 times with EtOH and then stored for a few days. Traces of unbound surfactant were observed by DRIFTS, so two additional chloroform washings followed by one EtOH washing were performed. The samples were stored in EtOH until the loading tests.

4.3.5.2.Cu loading on bare and C_{16} coated particles

This series was designed to characterize the adsorption of the coated carriers for a wide range of Cu concentration. Eight Cu solutions were used, 2, 5, 7, 10, 15, 20, 30, and 50 ppm. For each solution, three adsorption tests were performed: a blank test, done on an empty tube to test if there was some adsorption by the tube itself, one on bare particles, and one on the C_{16} carriers. The C_{16} carrier samples did not need to be redispersed this time. The bare particle samples were weighed and placed in the tubes. Empty tubes were used for the blank tests. All of the sample went through the following procedure:

- 25 mL of solution was added (pipette), the tube was sealed, and shaken by hand. The pipette was rinsed each time after finishing using one solution, started with 2 ppm samples, and ended with 50 ppm samples to reduce the risk of pipette contamination.

- The samples were sonicated by batches of 12 for 15 minutes.

- The samples were shaken for 21 hours.

- The samples were centrifuged for 10 minutes by batches of 4.

- The supernatant was filtered with ashless filter paper and poured in 15 mL conical tubes.

Pre-prepared standards were used for AA.

4.3.5.3.Cu loading on bare and C_{16} coated particles vs. pH

Sixteen individual C_{16} samples were prepared. The procedure differed a little concerning the washing of the sample. It was decided to wash the particles two times in chloroform, followed by three times with EtOH. DRIFTS showed no traces of unbound surfactant.

For the loading vs. pH test, 6 pHs were selected: 3, 3.5, 4, 4.5, 5, and 6. For each solution, three samples (blank, bare, and C_{16}-coated particles) were used, for a total of 18 samples. For each sample, 25 mL of 20 ppm Cu solution was added and the same procedure as the one used in the previous section was used. For each type of sample, three repeat tests were prepared at pH 3.5, 4, and 5. The supernatants were analyzed with AA.

As the Cu vs. pH test was being run, some repeat tests for Cu loading vs. Cu concentration were also carried out for 7, 15, and 30 ppm Cu solutions. These tests were performed on three types of samples: bare particle samples, C_{16} samples from the section 4.3.5.2 batch, and on samples from the 4.3.5.3 section batch. The procedures used were the same as those used in section 4.3.5.2.

Chapter 5

Results and Discussion

5. Results and Discussion

5.1. Step I: Preparation and Characterization of C_{12} and C_{16} coated particles

5.1.1. Molecular orientation of the surfactants at maghemite surface

5.1.1.1. DRIFTS

Figure 5-1 shows the DRIFTS spectra over a wide frequency range for pure C_{16} (top), and C_{16} coated samples (bottom). Two regions are of interest: a high frequency region between 3000 and 2800 cm^{-1}, characteristic of the C-H stretching of the $(CH_2)_{15}$ chain, and a low frequency region between 1400 and 1750 cm^{-1}, related to the vibrational motion of the carboxylic headgroup. The high frequency region is shown in more detail in Figure 5-2 and the low frequency region in Figure 5-3.

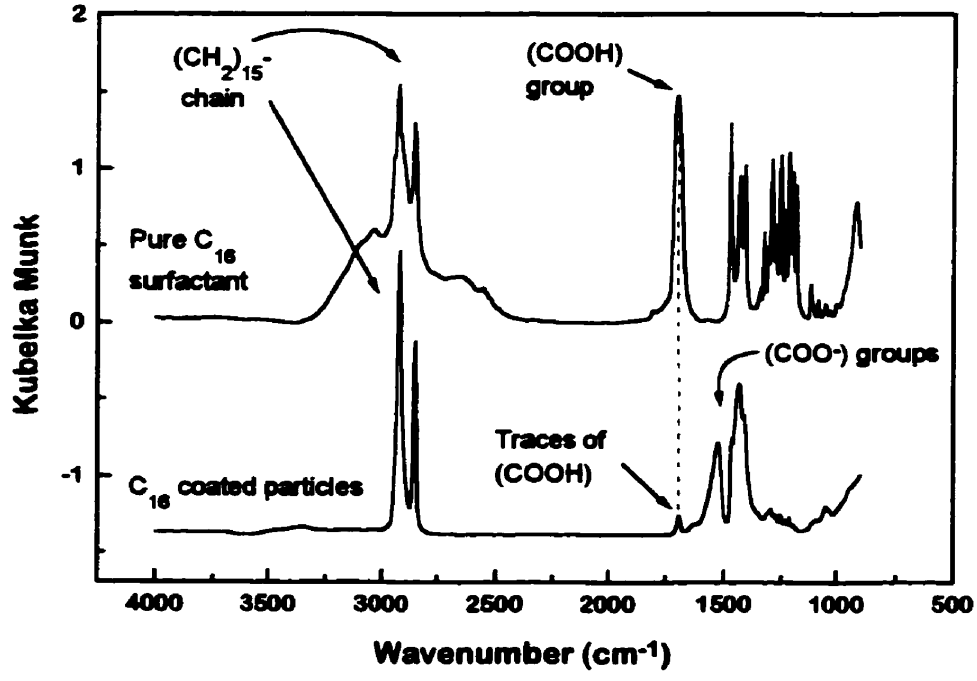

Figure 5-1: DRIFTS spectra of pure C_{16} surfactant (top) and C_{16} coated particles (bottom). The CH_2 region remains unchanged. The COOH function shifted to COO^- for the coated sample.

In the high frequency region, two major peaks are observed, at 2927 and 2853 cm^{-1} (see Figure 5-2 below). Those peaks correspond, respectively, to the antisymmetric (ν_a) and symmetric (ν_s) C-H stretching of the CH_2- groups. They appear at exactly the same position whether the surfactant is unbound or coated on the particle surface.

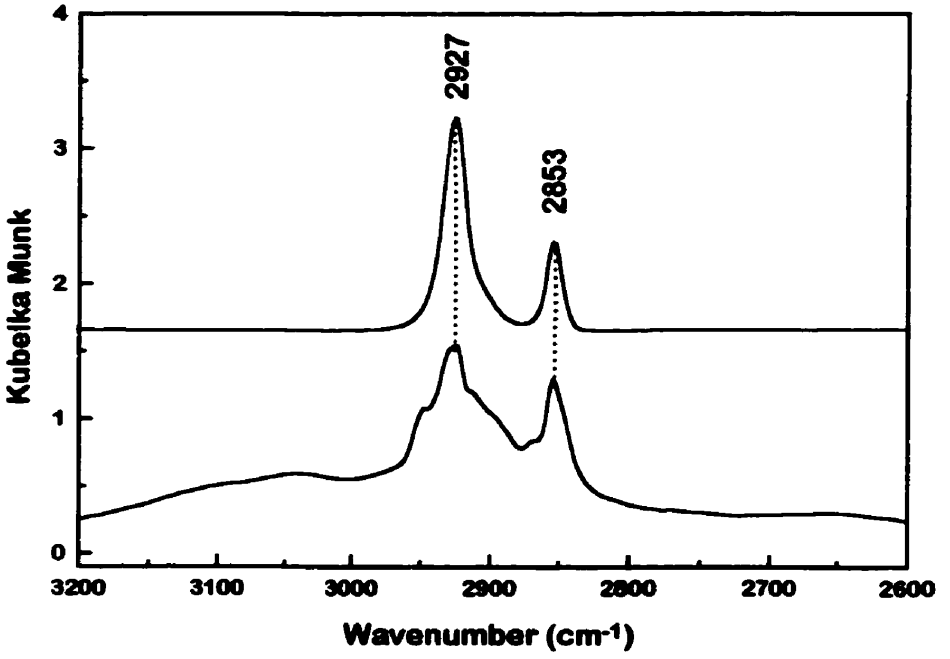

Figure 5-2: DRIFTS spectra of the high frequency region for pure C_{16} surfactant (bottom) and C_{16} coated particles (top). The two peaks, characteristic of the CH_2 stretching have exactly the same positions, at 2927 and 2853 cm^{-1}.

In the low frequency region (Figure 5-3) in contrast, the spectra for unbound and bound surfactant are markedly different. The spectrum for unbound surfactant (top) contains three regions of interest: a single peak at 1703 cm^{-1}, a series of peaks between 1400 and 1500 cm^{-1}, and a series of peaks between 1100 and 1350 cm^{-1}. The spectrum for C_{16} coated particles (bottom) shows only two peaks, at 1526 and 1430 cm^{-1}. The peak positions and the corresponding assignments for this series of DRIFTS are summarized in Table 5-1. These DRIFTS measurements on pure C_{16} and C_{16} coated particles were repeated many times and the exact same spectra were obtained each time. These results

corroborate previous studies on SAM obtained by deposition of alkanethiols on metal surfaces (Allara and Nuzzo, 1985b, Laibinis et al., 1991, Allara et al., 1991, Smith et al., 1992, and Tao, 1993).

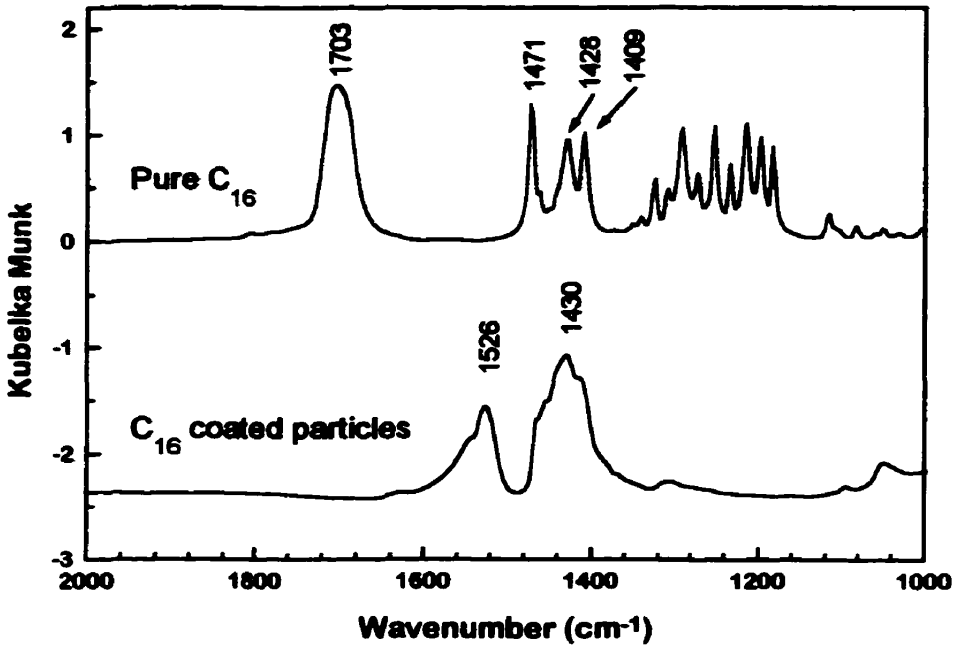

Figure 5-3: DRIFTS spectra of the low frequency region for pure C_{16} surfactant (top), and C_{16} coated particles (bottom). The pure C_{16} spectrum shows three regions: a peak at 1703 cm^{-1}, a series of peaks between 1400 and 1500 cm^{-1}, and a region between 1100 and 1350 cm^{-1}. On the C_{16} coated particle spectrum, only two peaks can be observed, at 1526 and 1430 cm^{-1}.

Allara and Nuzzo (1985b) used $HS-(CH_2)_{15}-COOH$ (C_{16}) to coat SAMs on flat Al_2O_3. Their results show the same differences between pure C_{16} and C_{16} adsorbed on Al_2O_3 for the low frequency region: loss of the peak at 1703 cm^{-1}, loss of the series between 1100 and 1350 cm^{-1}, and a new broad peak around 1608 cm^{-1}. They attributed these differences to dissociation of the acid proton to form an anionic surface carboxylate species. In their case, this indicated that the C_{16} molecules were binding to the aluminum oxide surface through a carboxylate bond. In the high frequency region, they found two peaks at 2918 and 2850 cm^{-1} for pure C_{16} and four peaks at 2966, 2926, 2880, and 2857

cm^{-1} for C_{16} on Al_2O_3. Laibinis et al. (1991) report that the CH_2 antisymmetric and symmetric stretching vibrations for polycrystalline alkyl-S chains ($C_{16}H_{33}S$ to $C_{22}H_{45}S$) are respectively 2925 and 2853 cm^{-1}. Smith et al. (1992) compared the spectra of C_{16}, C_{16} assembled on flat gold surface, and a SAM of C_{16} on gold surface covered with an overlayer of Cu. In the three cases, they found that in the high frequency region the C-H stretching peaks were at 2918 and 2850 cm^{-1}, indicative of a microscopic crystalline-like environment similar in the monolayers or in the bulk C_{16} phase. The values found in this work differ by 3 to 4 wavenumbers, which indicates that the coating has not achieved the same degree of crystallinity as theirs. Their monolayers were oriented with the thiolate bound to the gold surface and the carboxylic group sticking out. When they loaded Cu on the monolayer, they observed the loss of the peak at 1703 cm^{-1}, and two new peaks appeared at 1544 and 1430 cm^{-1}, characteristic of a Cu carboxylate. Tao (1993) studied SAMs of n-alkanoic acids on the surface of silver, copper, and aluminum. The focus of his study was that COOH, being the only reactive group, must bond with the metal surface. For monolayers formed on aluminum oxide, the C-H- antisymmetric and symmetric stretches were 2916 to 2927 and 2850 cm^{-1}, respectively. Tao found that the symmetric carboxylate vibration peaks were 1402, 1440, and 1478 cm^{-1}, respectively, for SAM on silver, copper, and aluminum. He attributed these differences to the increasing basicity of the metal surfaces ($AgO>CuO>Al_2O_3$). Tao also concluded that the more basic the metal, the stronger the metal-carboxylate bond.

In the light of these studies, the present results can now be interpreted. The loss of the peak at 1703 cm^{-1} and the two new peaks at 1527 and 1430 cm^{-1} indicate that the proton from COOH was lost and that a new surface carboxylate species was formed. Although no previous study focused on the formation of SAM on iron oxide, the positions of the two new peaks fall exactly in the range of the carboxylate peaks suggested by Tao. It is therefore evident that the C_{16} surfactant is attached to the maghemite surface through a carboxylate bond. The other conclusion that can be drawn concerns the polymethylene chain. The results suggest that the polymethylene chains have very similar microscopic environments in the bulk C_{16} phase and in the coating. The peak positions found are

consistently higher than those of SAMs on flat metal surfaces by 3 to 4 wavenumbers. These values are intermediary between a crystal-like structure and an amorphous structure. This suggests that chains are organized in a dense, well packed, semi crystalline monolayer, but that they have a certain degree of disorder. Only part of the chain near the surface is packed and in a crystalline form. The tails are free to vibrate due to the curvature. The sharp bands however suggest a crystalline nature.

Table 5-1: DRIFTS spectra results and mode assignments for pure C_{16}, C_{16} coated particles, and C_{12} coated particles.

Frequency			Mode
pure C_{16}	C_{16} coated part.	C_{12} coated part.	
2927	2927	2927	ν_a (C-H of CH_2)
2853	2853	2853	ν_s (C-H of CH_2)
1703			ν (C=O)
	1526	1526	ν_a (COO^-)
1471			-CH_2: scissors mode
	1430	1430	ν_s (COO^-)
1428			-CH_2: scissors mode
1409			-CH_2: scissors mode
1350 to 1100			CH_2-: twisting and wagging

Other DRIFTS experiments were performed on C_{12} and on C_{16} samples (Figure 5-4 and Figure 5-5). Figure 5-4 shows DRIFTS spectra for C_{12} and for C_{16} coated particles. The peak positions are the same for C_{12} and C_{16} coated carriers, indicating that both coatings have very similar microscopic structures. Figure 5-5 shows that DRIFTS can be used to detect incomplete washing by monitoring the COOH peak. A small peak of COOH indicates that some of the surfactant on the surface has not reacted with the surface, and that additional washing (e.g., total five washes) is needed.

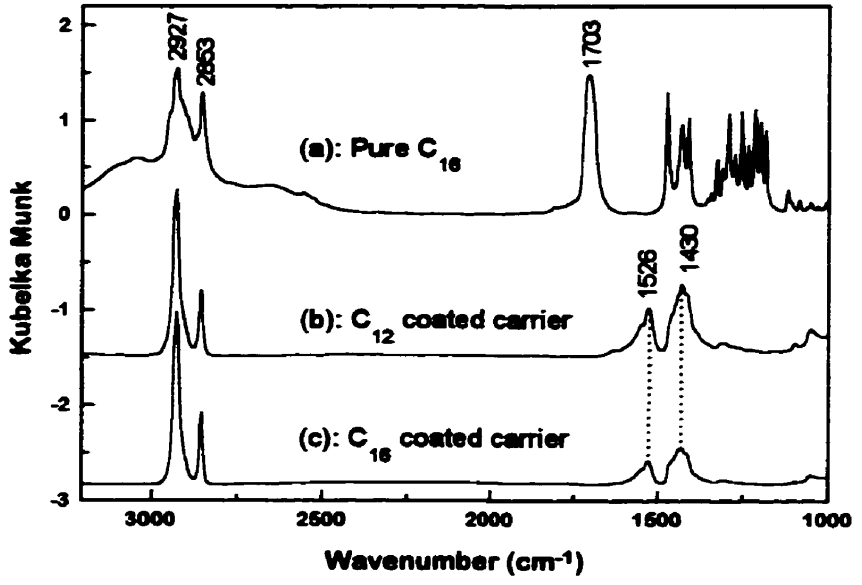

Figure 5-4: DRIFTS spectra of unbound (pure) C_{16} surfactant (a), C_{12} coated carrier (b), and C_{16} coated carrier (c). The peak positions for C_{12} and C_{16} coated carriers are exactly the same.

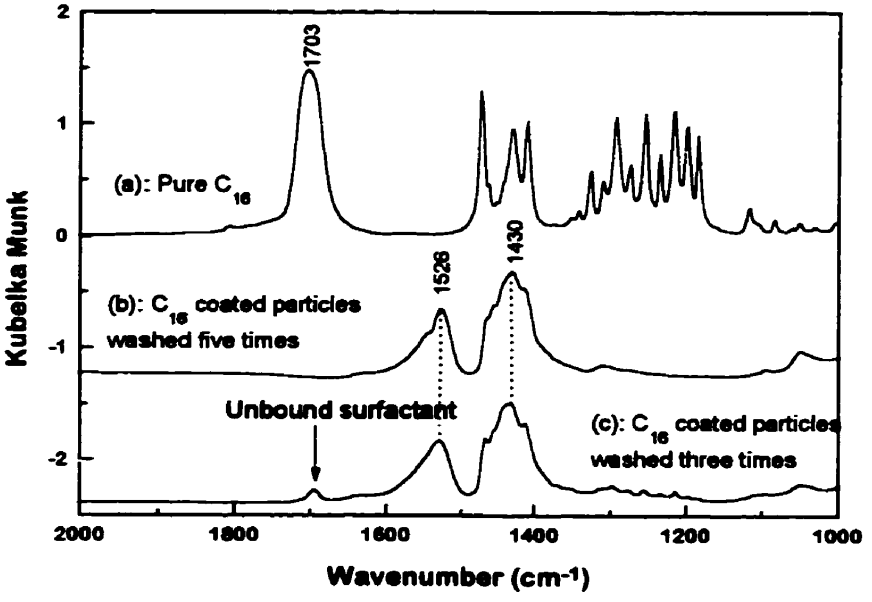

Figure 5-5: DRIFTS spectra of unbound C_{16} surfactant (a), C_{16} coated particles washed three times in EtOH (c), and C_{16} coated particles washed five times in EtOH (b). Bottom spectrum (c) shows traces of unbound surfactant due to incomplete washing that disappeared after two additional washings (b).

5.1.1.2.XPS

Figure 5-6 shows the XPS survey spectrum for C_{16} coated particles. This spectrum shows peaks for Fe (Fe2p), O (O1s), C (C1s), and S (S2p). The peaks for C, O, and S are shown in more detail in Figure 5-7 to Figure 5-11.

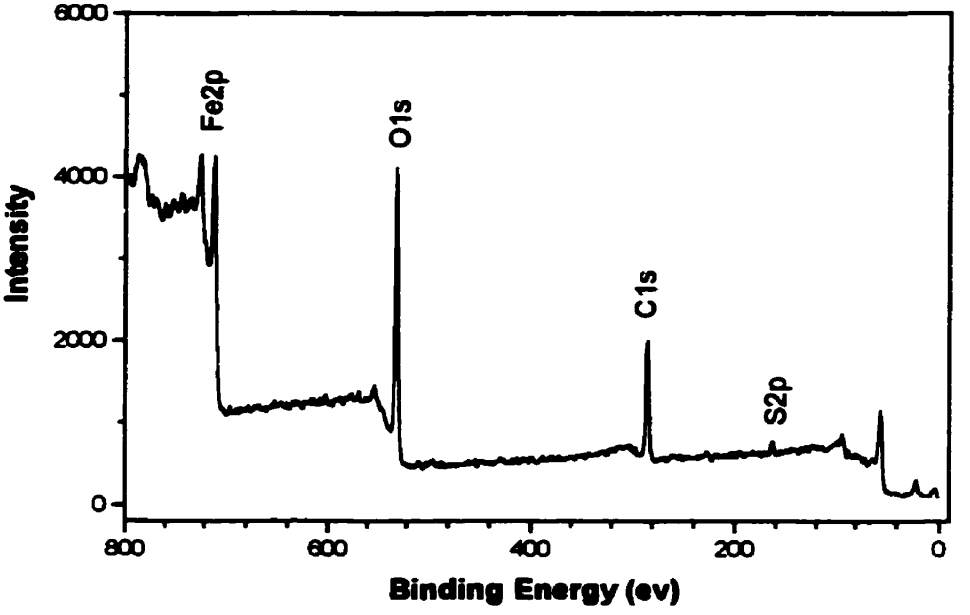

Figure 5-6: XPS survey spectrum for C_{16} coated particles.

Figure 5-7 shows two C1s peaks at 288.4 and 284.9 eV. The peak at 284.9 is consistent with carbon in a hydrocarbon chain (C-C) (Liu and Xu, 1995, Freeman et al., 1995, Bandyopadhyay et al., 1997). All of the XPS spectra presented in this thesis were corrected for charging by shifting their C1s peak to 284.9 eV. This peak position has been chosen as the reference peak for the present spectra. The small peak at 288.4 eV indicates the presence of carbon in a carboxylic group (Freeman et al., 1995, Bandyopadhyay et al., 1997), in agreement with the present IR results.

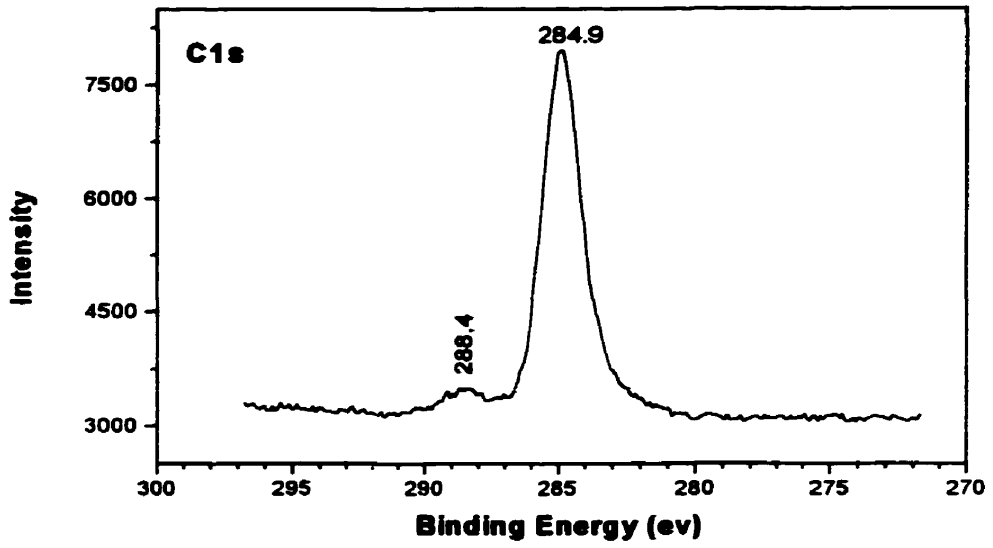

Figure 5-7: XPS carbon C1s peak for C_{16} coated particle.

Figure 5-8 shows the oxygen O1s peaks. When looking at the spectrum more closely, it can be seen that the peak is not symmetrical, and that there is a shoulder on the higher energy side of the peak. The fitted peak is shown in Figure 5-9, corresponding to two 1s components, at 529.7 and 531.4 eV. I have not found peak assignments for Fe_2O_3 but the peak at 529.7 eV is consistent with the oxygen binding energy value of 530.0 eV for Fe oxide in Fe_3O_4 reported by Briggs and Seah (1994), and is due to oxygen bond stretching in Fe_2O_3. The peak at 531.4 agrees with the values reported by Konstadinidis et al. (1992) for oxygen in metal oxides.

Figure 5-10 shows the sulfur S2p peak, and Figure 5-11 the fitted peak. This peak was fitted with a single spin-orbit pair, with S2p3/2 at 163.0 eV and a spin-orbit split of 1.15 eV. That position at 163.0 eV differs slightly from the referenced values for unreacted thiol peak around 163.6 eV (Baldwin, 1996, Laibinis et al., 1991, Liu and Xu, 1995). The reasons for that shift are unclear. There was some concern the thiol group could have been oxidized while being coated or stocked. XPS results confirm that the thio group is not oxidized because sulfate or sulfonate groups have binding energies of 168.0 and 167.4 eV, respectively (Colvin et al., 1992, Laibinis et al., 1995).

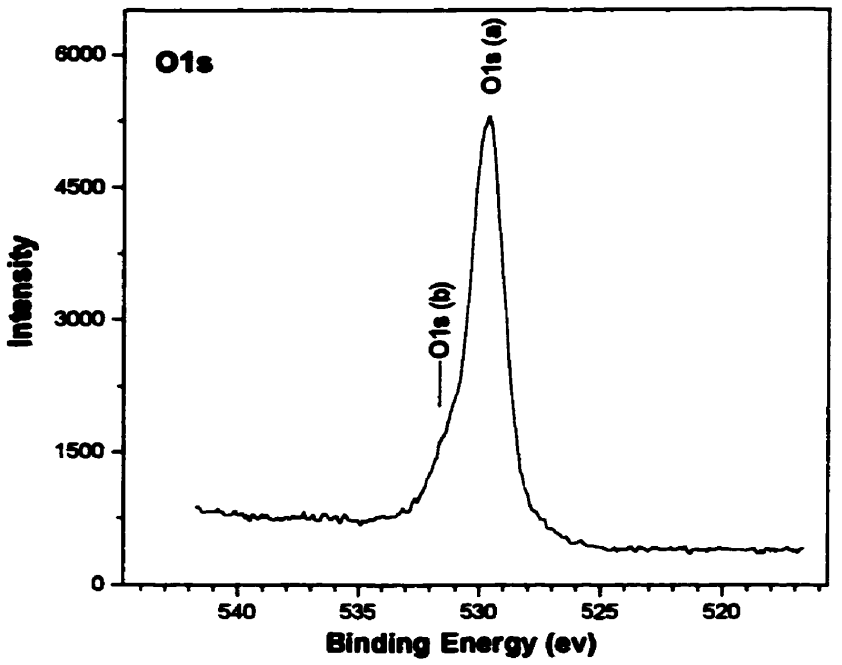

Figure 5-8: XPS oxygen O1s peaks for C_{16} coated particle.

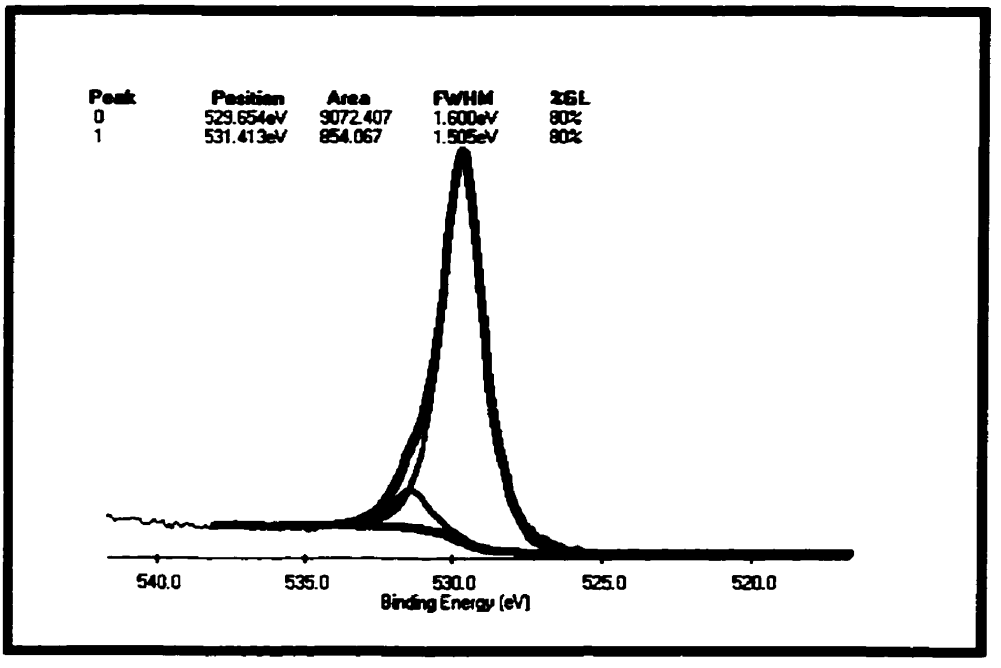

Figure 5-9: XPS O1s fitted peak for C_{16} coated particles.

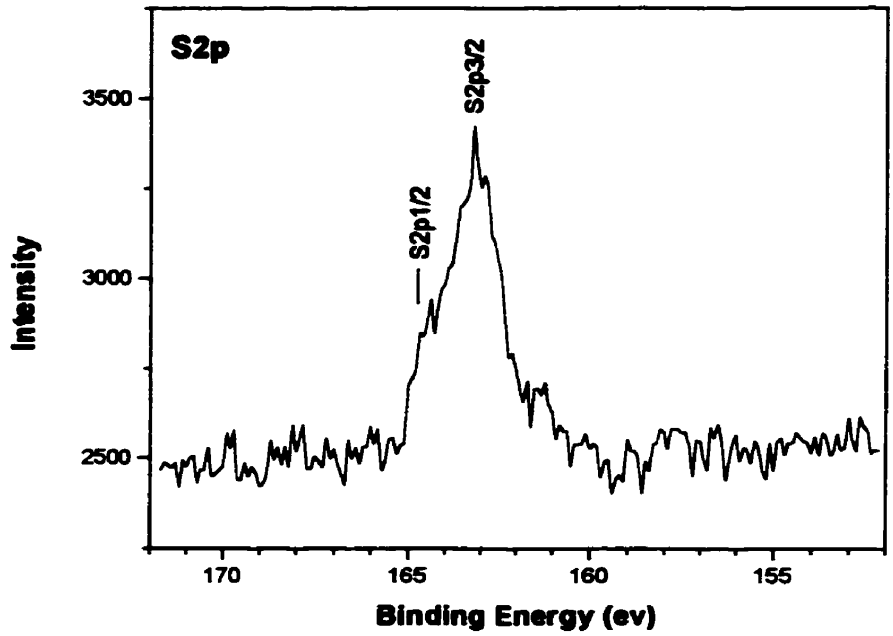

Figure 5-10: XPS sulfur S2p peaks for C_{16} coated particle.

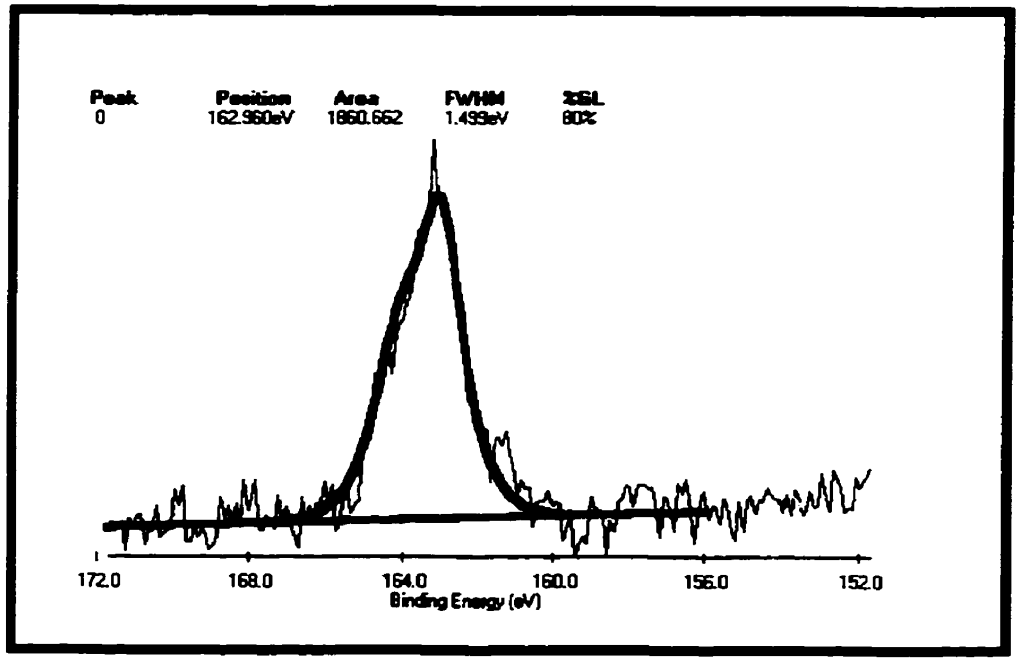

Figure 5-11: XPS S2p fitted peak for C_{16} coated particles.

5.1.2. Packing density

5.1.2.1. Wetting test

The results of the wetting test on C_{12} and C_{16} coated particles are shown in Figure 5-12. The surface tensions are 30 and 35 mN/m at the low limit (0 % floats), and 43 and 53 mN/m at the high limit (100 % floats) respectively, for C_{16} and C_{12} coated particles. The critical surface tensions (50 % floats) are 39 and 49 mN/m respectively for C_{16} and C_{12} samples.

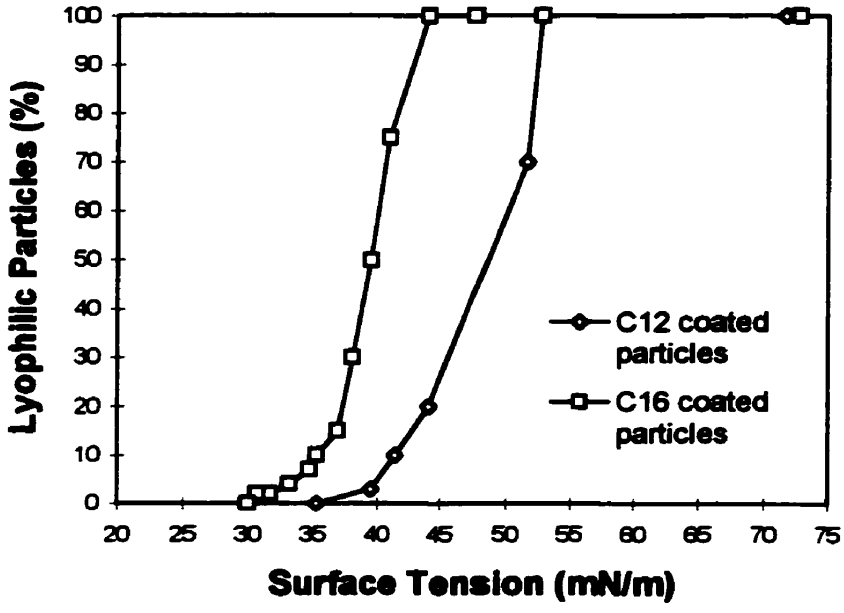

Figure 5-12: Floatability of C_{12} and C_{16} coated particles in water-methanol solution.

The results for the C_{16} coated particles are very similar to those obtained by Liu and Xu (1995). They compared the critical surface tension obtained for MHA (C_{16}) (33 mN/m) to that of normal hydrocarbon liquids (25 mN/m) and CH_3 terminated monolayers (22 mN/m). Liu and Xu concluded that the MHA coated particles are hydrophobic, but less so than for methyl terminated monolayers probably because of the polar thio or disulfide groups. Liu and Xu also noted that the difference between the high and the low

limit is indicative of the heterogeneity of the coated surface: the higher the difference between those two limits, the higher the surface heterogeneity. In the present case, as described in the procedure section, the experiment was performed in a very qualitative way. It would not be meaningful to try to exploit it quantitatively. For instance, the difference between the C_{12} and C_{16} curves seems to indicate that the C_{12} coated particles are less lyophobic, but it could be ascribed as experimental error. The experiment performed shows that the coated particles are hydrophobic, but to be able to draw more conclusions on the packing or the heterogeneity of the surface, a more quantitative experimental procedure should be designed.

5.1.2.2.Leaching test

The results of the leaching test are summarized in Table 5-2. The two pH solutions were also analyzed by AA to account for any Fe ions present. The solutions from both C_{12} and C_{16} coated particles had Fe concentrations below the detection limits (0.5 ppm). Although the amount of particles in contact with the 25 mL solution was quite low (15 mg), the leachates from bare particles contained significant amounts of Fe ions. If only as little as 2 % of the amount of Fe would have been leached out of coated particles, it would have been detected. It can be concluded that both C_{12} and C_{16} coated particles are effectively protected from leaching. This implies that the iron oxide surface is covered by a layer of surfactant that is sufficiently dense and well packed that the leachate solution cannot reach its surface. This corroborates the hydrophobicity test.

Table 5-2: Leaching test results.

pH	pH water	γ-Fe_2O_3	C_{12} coated particles	C_{16} coated particles
2.8	0	30.8 mg/l	0	0
10.55	0	19.5 mg/l	0	0

5.1.2.3. Elemental Analysis (EA)

Table 5-3 shows the percentage of carbon (C), hydrogen (H), and sulfur (S) of both C_{12} and C_{16} coated particles samples analyzed by EA. The theoretical results were compared for molar ratio of H/C and C/S. The theoretical molar ratios were calculated from the formula of the surfactants. The measured molar ratios are calculated from the following: measured H/C = [(% H)/1]/[(% C)/12].

We can see from the results in Table 5-3 that the measured H/C ratios are in good agreement with the theoretical results. However, the C/S ratio is almost 5 times too high for C_{12} and 1.5 times too low for C_{16}. There are three main reasons for such a discrepancy in the results. First, EA requires the use of standards, that should be as close as possible in composition to the sample analyzed. The standard used was the only one available, and did not have a good fit with the samples analyzed. Second, the EA has a detection limit around 5 μg. Given the mass of the sample and its estimated S %, the total S content must have been very close to the detection limit. Third, with this technique, the accuracy of measurement for S is less than for other elements. The EA given here is therefore not meaningful for S content. The H/C ratios, on the other hand, are reliable.

Table 5-3: Analysis of C_{12} and C_{16} coated sample composition by elemental analysis.

Sample	% C	% H	% S	Theoretical H/C ratio	Theoretical C/S ratio	Measured H/C ratio	Measured C/S ratio
Standard	93.56	5.63	0.38				
C12 coated	2.56	0.40	0.12	2	12	1.9	56.67
C16 coated	4.22	0.65	0.93	2	16	1.9	12.04

From % H and % C given by EA, the surface coverage by surfactant can be estimated. The EA results give the percentage of each element relative to the total mass of the sample. The percentage of organic material on the particle being small relative to the total mass of the sample, it can be estimated that the total mass of the sample is identical to the mass of the iron oxide core. The % of carbon relative to the mass of the particle can be related to the surface coverage through the specific surface area of the particle, 49 m^2/ g. By relating the grams of C per gram of particle, it is possible to

calculate the grams of carbon per surface area of particle. Hence the density of surfactant on the particle surface can be determined. The result is usually more meaningful when given as the surface occupied by each molecule, in $Å^2$.

The calculations, based on EA % C results (see box below, for C_{12}), give a figure of 46 $Å^2$ per molecule of C_{12}, and 37 $Å^2$ per molecule of C_{16} surfactant. It is useful to convert these results to mole of surfactant per gram of particles. In this case, the results are 0.17 mM C_{12}/ g particles and 0.22 mM C_{16}/ g particles. The results differ by 22 % for the two types of coating, which may not be very significant considering the uncertainty due to the non-ideal conditions for EA measurements.

These results can be compared to a theoretical maximum density calculated from the thio group surface area. The thio group surface area is reported in the literature to be 21.4 $Å^2$. A theoretical maximum surfactant density can be estimated by calculating how many thio groups can be fit on each particle. Knowing the particle surface area, this calculation is straightforward. It amounts to 0.38 mM thio group/ g particle. Knowing that the carboxylate group is larger than a thio group, the measured surfactant densities found fall in a very reasonable range compared to the theoretical maximum.

Calculation of C_{12} density on particle surface based on EA % C results

% C = 2.55

$\therefore$ 0.255 g C per g Fe

$\therefore$ (0.255/12) mol C per g Fe

$\therefore$ (0.255/12)/12 mol C_{12} (surfactant molecule) per g Fe {there are 12 atoms of C for each C_{12} molecule}

$\therefore$ (0.255/12)/12 * 6.023 x 10^{23} molecules of C_{12} per g Fe

The surface area of Fe particles is 49 m^2/g Fe = 49 10^{20} $Å^2$/g Fe

$\therefore$ there are [(0.255/12)/12 * 6.023 x 10^{23}]/(49 x 10^{20}) molecules of C_{12} per $Å^2$

$\therefore$ there are 0.0213 molecules of C_{12} per $Å^2$

$\therefore$ each molecule occupies approximately 46 $Å^2$.

5.1.3. Summary

5.1.3.1. Orientation of the surfactants at the surface of the particles

The presence of C_{12} and C_{16} coatings on the surface of maghemite was confirmed by DRIFTS, XPS, wetting test, leaching test, and EA. DRIFTS results indicated that the carboxylic function of the unbound surfactant had transformed into a carboxylate function when the surfactant is adsorbed on the particles. This was confirmed by the presence of both oxygen and carbon XPS peaks. This important observation indicates that the surfactants are bound to the surface via the carboxylic head, through a carboxylate bond with the maghemite surface. The sulfur XPS characterization indicates that S is present on the particle, most likely as thiol or disulfide. XPS characterization also proved that the thio group had not been oxidized.

5.1.3.2. Density and stability of the coating

The leaching test showed that the coatings are resistant to acid and base attack. The fact that iron is not leached out at all indicates that the coating forms an effective barrier between the leaching solution and the maghemite surface. The effectiveness of this barrier shows a dense and well packed coating. The wetting test showed the hydrophobicity of the particles, which further confirmed the coating was dense. The observed CH_2 peak positions by DRIFTS indicate that the coatings have properties similar to the bulk surfactant, which is a relatively ordered crystalline-like solid. The peak positions, however, were at frequency slightly higher than these observed for well ordered polymethylene crystals, which implies that although dense, the coatings probably contain a fair amount of disorder. Such a result is not surprising on nanosized particles.

5.1.3.3. Estimation of surfactant density on particles surface

The EA results allowed to estimate the packing density of the surfactants. The calculations gave figures of 46 $Å^2$ per molecule of C_{12}, and 37 $Å^2$ per molecule of C_{16} surfactant (or alternatively, 0.17 mM C_{12}/ g particles and 0.22 mM C_{16}/ g particles). This density falls in the range expected for a theoretical maximum density of 0.38 mM/ g per particle.

5.2. Step II: Loading of Cu and Ag on C_{12} and C_{16} coated particles

5.2.1. Theoretical maximum metal ion loading

In the previous section the surfactant density on maghemite surface was estimated for C_{12} and C_{16} coated particles (respectively, 0.17 and 0.22 mM per gram particle). The difference between C_{12} and C_{16} should not be considered significant, and from now on the assumption will be that they have the same coating density. As the EA results were not very accurate, it would not be meaningful to try to use the exact values calculated. The results do give an order of magnitude for coating density. To be conservative, it can be estimated that as a minimum, the coating density is 0.15 mM surfactant per gram of particles. From that value, the maximum theoretical metal ion loading can be calculated.

If the metal ion is coordinated at 1:1 ratio with the thiol terminated coating, it means that up to 0.15 mM metal ion can be loaded per gram particle. If the coordination is 1:2 (one metal for two thiol), the maximum loading will be 0.075 mM/ g. Table 5-4 summarizes the maximum loading capacities in mg metal/ g particle calculated for Cu and Ag by this approach.

Another theoretical calculation can be done, based on the diameter of fully hydrated Cu ions, which is 0.5 nm for Cu. With the assumption that a monolayer of hydrated Cu ions is deposited on the surface, a maximum of 6.6 mg Cu can adsorb on 1 gram of particles. The different calculation routes give figures in the same range, from 5 mg/ g to 10 mg/ g for Cu, and from 8 mg/ g to 16 mg/ g for Ag.

Table 5-4: Maximum theoretical Cu and Ag loading capacities on C_{12} and C_{16} coated particles.

Metal Ion	Surfactant Density (mM/ g particle)	Maximum loading 1:1 coordination (mg metal/ g particle)	Maximum loading 1:2 coordination (mg metal/ g particle)
Cu	0.15	9.5	4.8
Ag	0.15	16.2	8.0

5.2.2. XPS

XPS spectra were collected on three samples: C_{16} coated particles prior to loading (a), C_{16} coated particles loaded with Ag (b), and C_{12} coated particles loaded with Ag (c). Figure 5-13 shows the survey spectra for the three samples. It shows Fe2p, O1s, C1s and S2p peaks for the three samples, and a Ag3d peak in the spectra of the two Ag loaded samples. Figure 5-14 to Figure 5-20 show C1s, Ag3d, S2p, O1s, and Fe2p spectra in more detail. All the measured XPS peaks and the corresponding referenced peak assignments are summarized in Table 5-5.

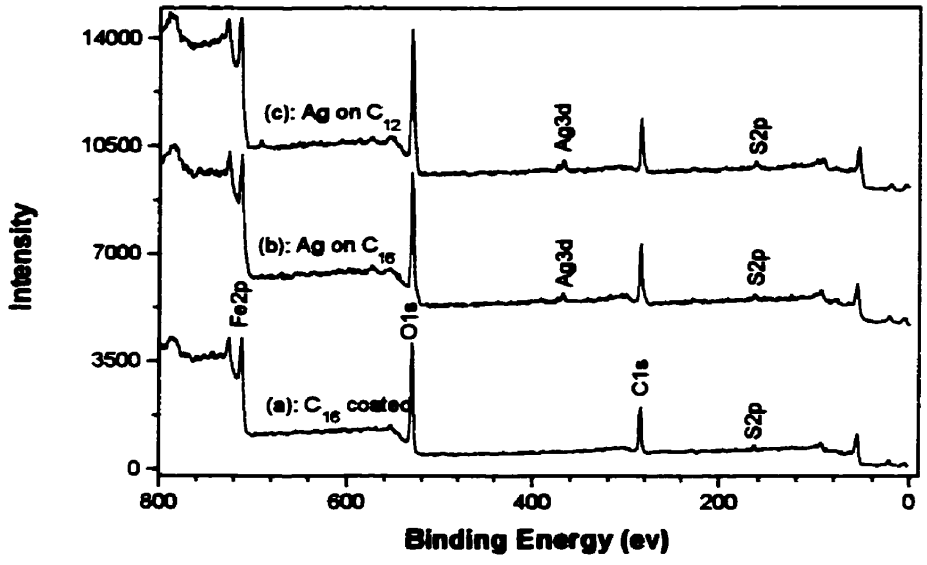

Figure 5-13: XPS survey spectra for C_{16} coated particles (a), C_{16} coated particles loaded with Ag (b), and C_{12} coated particles loaded with Ag (c).

Table 5-5: XPS measured peak positions for S2p, C1s, Ag3d, S2p, and Fe2p, and referenced peak positions and their corresponding bond types.

Element	Meas. XPS peaks	Ref. peak positions	Type of bond	Reference
Sulfur S2p	161.8	161.8	Silver thiolate (C-S-Ag)	Bandyopadhyay et al., 1997
	162.0	162.3		Laibinis et al., 1995
		162.4		Baldwin, 1996
	163.0	163.6		Laibinis et al., 1995
	163.3	163.7	Thiol C-SH	Baldwin, 1996, Liu and Xu, 1995
	163.5	163.9		Bandyopadhyay et al., 1997
		167.4	SO_3H	Laibinis et al. 1995
		168	SO_4^-	Colvin et al., 1992
Carbon C1s	284.9	285	CH_2-CH_2-alkylchain	Bandyopadhyay et al., 1997 Freeman et al., 1995
		286.9	C-SH bond	Bandyopadhyay et al., 1997
	288.4	288.6	COO^-/Cu	Freeman et al., 1995
		288.6	COO^-/Ag	Bandyopadhyay et al., 1997
		289.2	COOH	Freeman et al., 1995
Silver Ag3d	368.1	368	Ag	Briggs and Seah, 1994
	368.5			
		368	Ag-S	Khun et al., 1994
		368		Bandyopadhyay et al., 1997
	374.2	374.1	Ag spin orbit split	Bandyopadhyay et al., 1997
	374.6			
Oxygen O1s	530.0	530	Fe_3O_4	Briggs and Seah, 1994
	530.2			
	530.3			
		530.7	Carboxylate O_2^-	Konstadinidis et al., 1992
	531.3	531.8	Metal oxides	Konstadinidis et al., 1992
		533.3	Metal oxides	Konstadinidis et al., 1992
Iron Fe2p	710.7			
	710.8	710.9	Fe_2O_3	Briggs and Seah, 1994
	711.0			

The C1s peaks are shown in Figure 5-14. The C1s peak was selected as the reference peak. Each XPS measurements showed some charging on the particles, and a charging correction was necessary. All spectra were corrected for charging by shifting them to set the C1s peak at 284.9 ev. This is a standard method in XPS practice. On the three spectra, a small peak is seen at 288.4 ev. The peak position at 284.9 is consistent with previous assignments for aromatic carbon and alkyl chain carbon (Briggs and Seah, 1994, Bandyopadhyay et al., 1997). Freeman et al. (1994) performed XPS studies of a carboxylic terminated monolayer before and after adsorbing Cu on this monolayer. They assigned the peak at 289.2 ev to the C1s electrons of carbon in COOH function. They observed a shift of that peak to 288.6 after Cu loading, indicative of a Cu-carboxylate complex. These results are consistent with the peak position of 288.6 reported by Bandyopadhyay et al. (1997) for a carboxylate bond on aluminum oxide. Considering these results, the peak at 288.4 ev in Figure 5-14 is assigned to the carboxylate bond formed on maghemite.

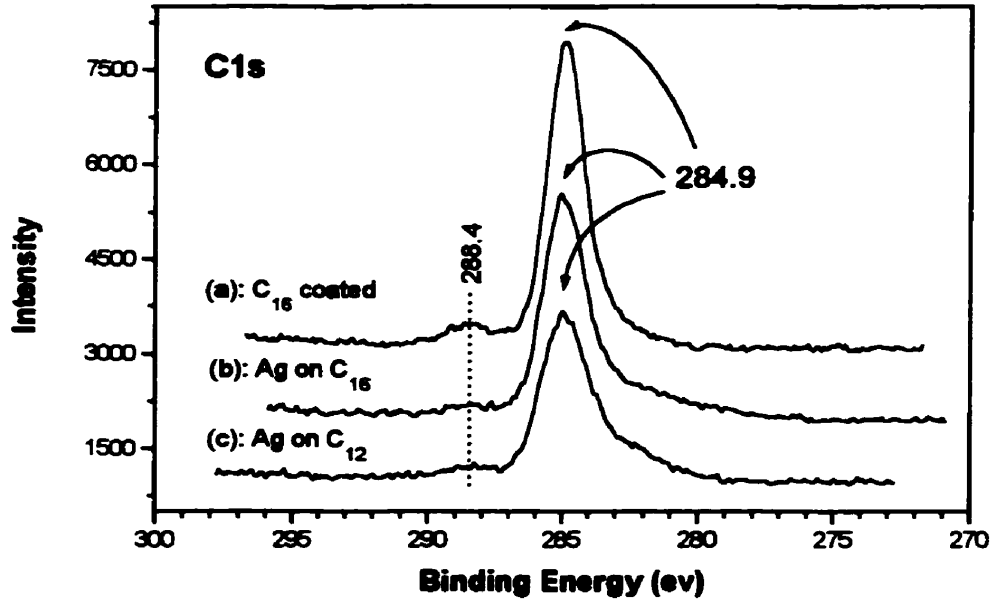

Figure 5-14: XPS C1s peak for C_{16} coated particles prior to loading (a), C_{16} coated particles loaded with Ag (b), and C_{12} coated particles loaded with Ag (c).

Figure 5-15 shows two peaks for Ag, $Ag3d_{1/2}$ and $Ag3d_{5/2}$. The positions differ by 4 ev in the case of C_{12} and C_{16} sample, and this discrepancy may be due to the signal to noise ratio that makes peak position reading less accurate. The peak positions at 368.1 and 374.2 are in very good agreement with Bandyopadhyay et al.'s assignment for colloidal Ag covalently bonded to a thiol-terminated self-assembled monolayer (Bandyopadhyay et al., 1997). This peak position is essentially the same as that of elemental silver (Briggs and Seah, 1994). This corroborates a study by Khun et al. (1994) who demonstrated that the formation of an Ag-S bond induced only a 0.15 ev reduction in the binding energy of Ag3d.

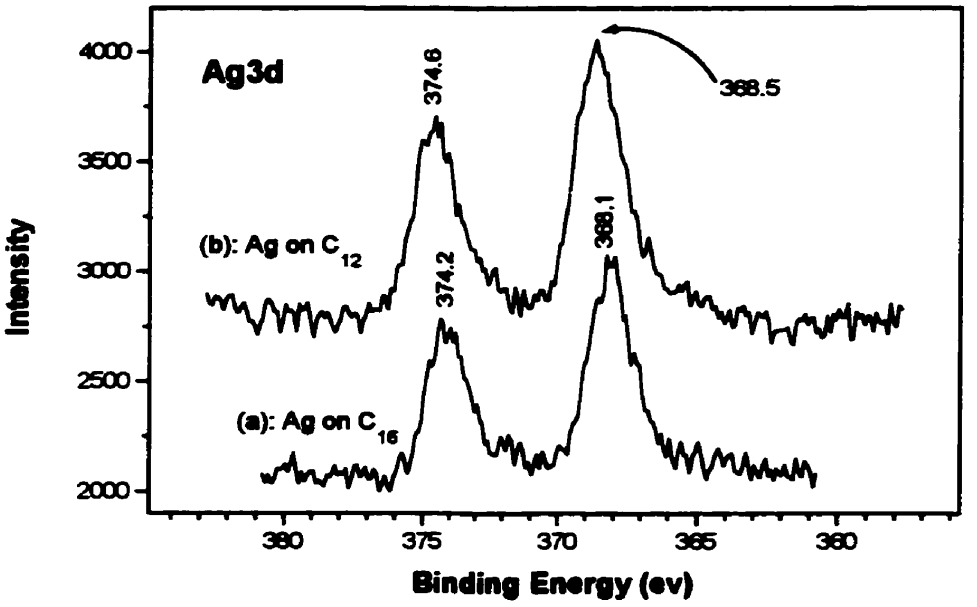

Figure 5-15: XPS $Ag3d_{1/2}$ and $Ag3d_{5/2}$ peaks for C_{16} coated particles loaded with Ag (a), and C_{12} coated particles loaded with Ag (b).

The S2p peaks are shown in Figure 5-16. The peak for C_{16} coated particles could be fitted with a single spin-orbit pair, with $S2p_{3/2}$ at 163.0 ev and a spin orbit split of 1.15 ev. The fitted peak is shown in Figure 5-17. The S2p peaks for C_{12} and C_{16} coated particles

could not be fitted with a single $p_{1/2}$-$p_{3/2}$ pair of peaks, but were adequately fitted with two pairs. Figure 5-18 shows the S2p peak fitted with two spin-orbit peaks. The major component has a $S2p_{3/2}$ peak at 163.5 ev and the minor component is found at 161.8 ev. An analogous peak fitting procedure for C_{16} coated particles loaded with Ag showed two similar peaks at 163.3 and 162.0 ev.

The peak positions at 161.8 and 162.0 ev are consistent with previous assignments for different metal thiolate (Cu, Ag, and Au) (Baldwin, 1996, Bandyopadhyay et al., 1997, and Laibinis et al., 1995). The peaks at 163.0, 163.3 and 163.5 ev indicate the presence of unreacted thiol groups. Previous studies reported peaks at 163.6, 163.7, and 163.9 ev for thiol groups (Baldwin, 1996, Bandyopadhyay et al., 1997, and Laibinis et al., 1995). The small difference may be due to variations in charging, however overall these peak positions are consistent with only thiol species, indicating that no detectable oxidation has occurred.

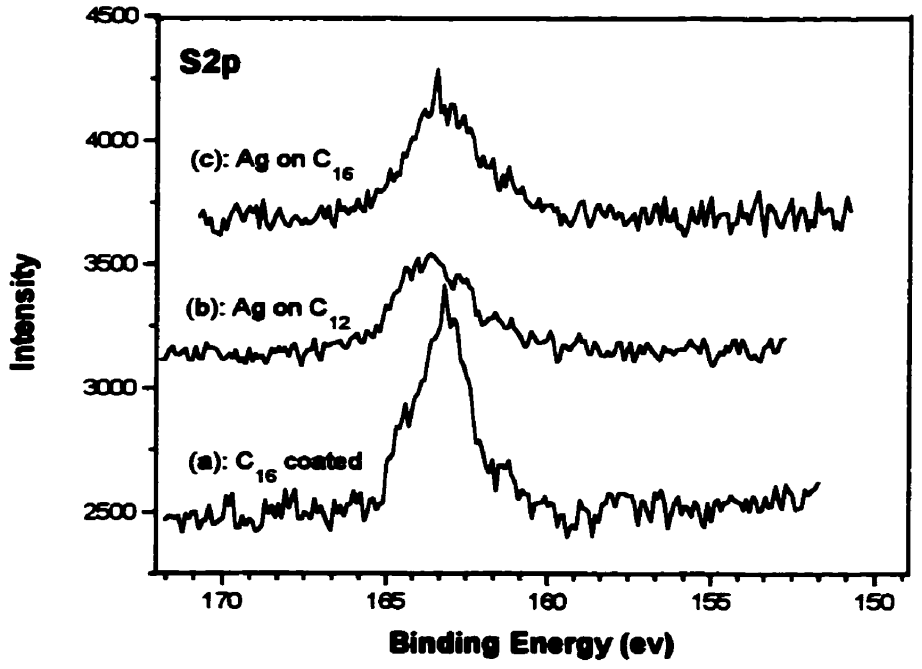

Figure 5-16: XPS S2p peaks for C_{16} coated particles prior to loading (a), C_{12} coated particles loaded with Ag (b), and C_{16} coated particles loaded with Ag (c).

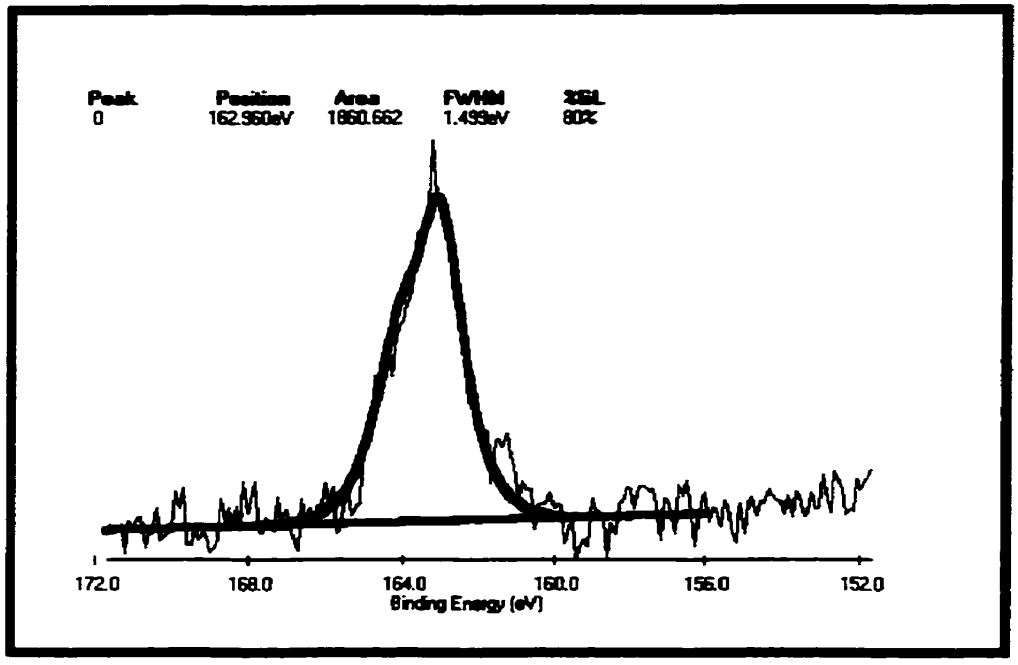

Figure 5-17: XPS S2p fitted peak for C_{16} coated particles.

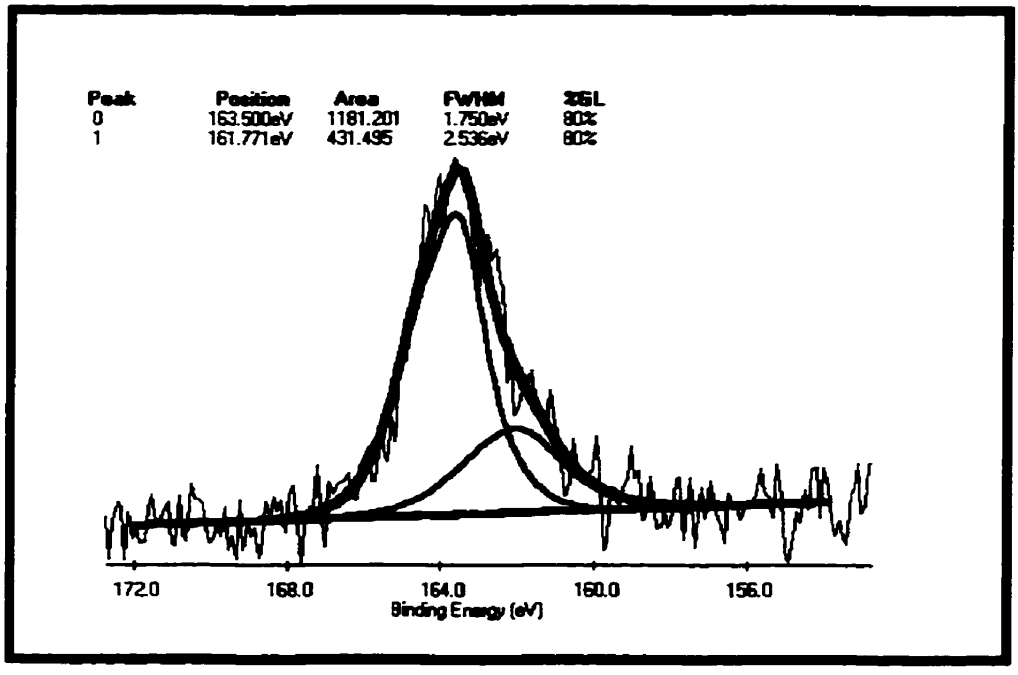

Figure 5-18: XPS S2p fitted peak for C_{12} coated particles loaded with Ag.

The O1s region is shown in Figure 5-19 for each of the samples. The peaks for the two Ag coated samples are shorter, with a larger peak width at half height. The three peak centers are located at 530.0, 530.2 and 530.3 ev, which is not significantly different. This peak position (530.0 ev) was assigned in step I to the oxygen from the iron oxide composing maghemite.

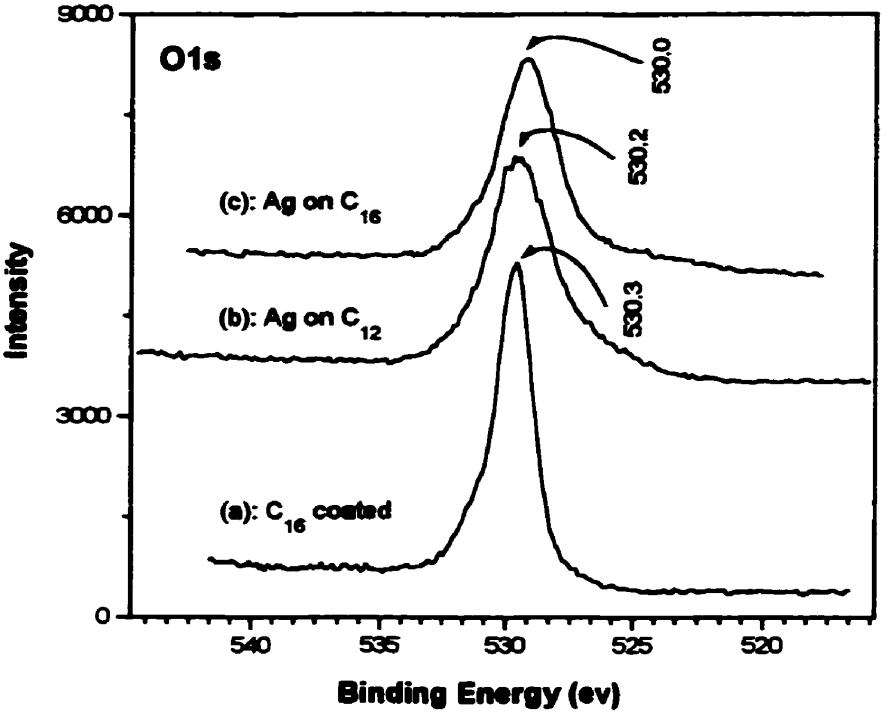

Figure 5-19: XPS O1s peaks for C_{16} coated particles prior to loading (a), C_{12} coated particles loaded with Ag (b), and C_{16} coated particles loaded with Ag (c).

Figure 5-20 shows the XPS peaks for Fe. The $Fe2p_{3/2}$ is found at 710.7, 710.8, and 711.0 ev. As expected, here also, the peaks are not significantly different in the three cases. The loading of Ag had no effect on the core iron oxide. These peak positions are in excellent agreement with the value of 710.9 reported by Briggs and Seah (1994) for Fe_2O_3.

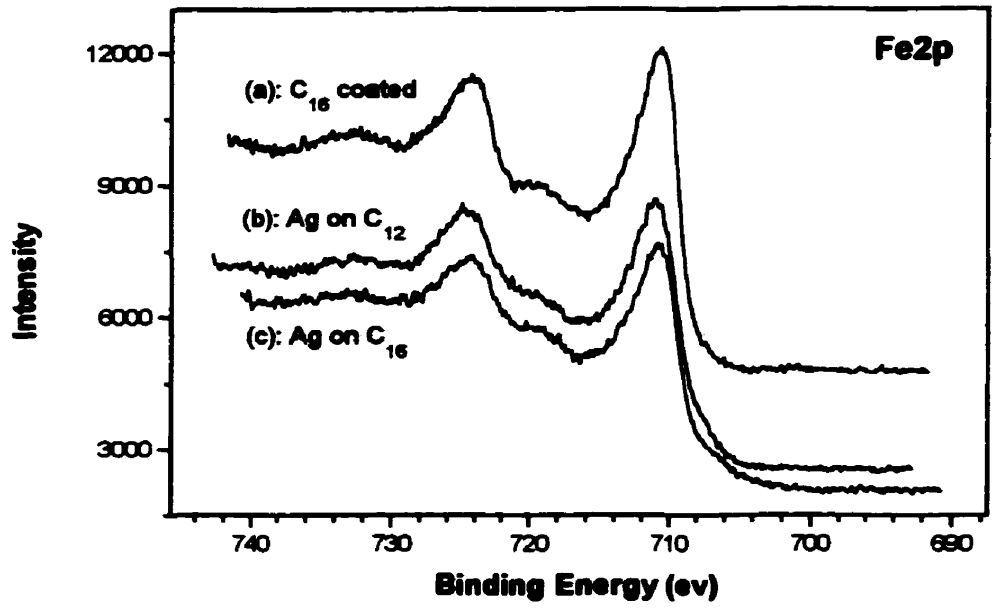

Figure 5-20: XPS Fe2p peaks for C_{16} coated particles prior to loading (a), C_{12} coated particles loaded with Ag (b), and C_{16} coated particles loaded with Ag (c).

5.2.3. DRIFTS

Some DRIFTS were also performed on the four C_{12} and C_{16} coated particles samples loaded with Cu and Ag. The presence of Cu or Ag could not be detected by DRIFTS in the mid-infrared region. However, the spectra showed that the loading procedure had not altered the coating.

5.2.4. Atomic Absorption (AA)

The concentrations of Cu and Ag in solution before and after loading were measured by atomic absorption as explained in the procedure section. The mass of Cu and Ag adsorbed on the particles were calculated, and the equivalent adsorption was converted to milligrams of metal adsorbed per gram of particles. The AA measurements, intermediate calculations and final results are shown in Table 5-6 for Ag and Table 5-7 for Cu. The adsorption of Ag amounted to 6 mg Ag/ g on C_{12} and 5.1 mg Ag/ g on C_{16} coated

particles. This corresponds to loadings of 65 and 55 % of maximum capacity, respectively. For Cu, 2.5 mg Cu/ g was adsorbed on C_{12} and 2.2 mg Cu/ g on C_{16} coated sample, corresponding to loadings of 52 and 46 %.

Table 5-6: AA results. Adsorption of Ag on C_{12} and C_{16} coated particles.

Sample Label	Initial [Ag] (ppm)	Final [Ag] (ppm)	{Initial [Ag]- Final [Ag]} (ppm)	Mass of Ag loaded/ 20 mg (mg)	Mole of Ag loaded/ 20 mg (mmol)	Mass of Ag loaded /g of particles (mg)
(C_{12})	7.4	2.6	4.8	0.12	1.1×10^{-3}	6
(C_{16})	7.4	3.3	4.1	0.1	0.92×10^{-3}	5.1

Table 5-7: AA results. Adsorption of Cu on C_{12} and C_{16} coated particles.

Sample Label	Initial [Cu] (ppm)	Final [Cu] (ppm)	{Initial [Cu]- Final [Cu]} (ppm)	Mass of Cu loaded/ 20 mg (mg)	Mole of Cu loaded/ 20 mg (mmol)	Mass of Cu loaded /g of particles (mg)
(C_{12})	3.94	1.9	2.04	0.05	$0.79\ 10^{-3}$	2.55
(C_{16})	3.94	2.15	1.8	0.044	$0.69\ 10^{-3}$	2.23

5.2.5. Discussion

XPS spectra have shown the presence of Ag on both C_{12} and C_{16} coated samples following exposure to a Ag solution. From the Ag spectra it was not possible to determine whether the Ag was simply held in the double layer as elemental Ag, or if it was covalently bound to the surface. Previous studies have shown that both elemental Ag and S-Ag exhibit very similar XPS peaks (Khun et al., 1994, Bandyopadhyay et al., 1997). However, the sulfur spectra showed a very interesting feature. Whereas the C_{16} coated sample had only one spin-orbit (S2p1/2 and S2p3/2) component, the Ag coated samples exhibited two spin-orbit components. The additional component is consistent with a silver thiolate species peak (Laibinis et al., 1995, Baldwin, 1996, and Bandyopadhyay et al., 1997). This suggests that at least part of the adsorbed Ag on the particle surface is coordinated to the surface thiol through thiolate bonding.

AA results show that both Cu and Ag are partially adsorbed from solution on the particles. The difference between the amount of Ag and Cu loaded on C_{12} and C_{16} coated particles was approximately 15 %. The amount of Ag loaded on particles was about 30 % higher than that of Cu. The actual loading of Ag from solution was around 60 % of maximum, versus 50 % for Cu. The apparent loading capacity of the particles was half the maximum theoretical capacity for a 1:2 coordination for Cu, and was approximately 70 % of that maximum for Ag. This low loading capacity may result from the experimental procedure used for metal loading. The particles tended to aggregate after drying, and it was difficult to redisperse them in solution (particularly as they are hydrophobic). Therefore, it is likely that not all of the surface of the coated particles was available for adsorbing metal ions. This conclusion is supported by the study of the effect of sonication on loading capacity.

5.3. Step III: More Cu loading tests

5.3.1. Reproducibility test

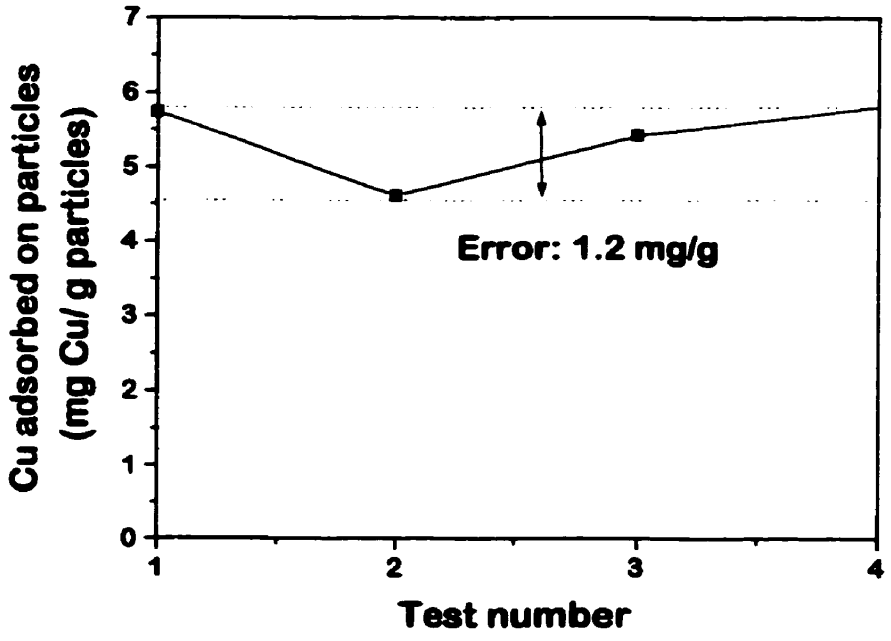

Figure 5-21: Reproducibility test for Cu loading on C_{16} coated particles.

The results of the reproducibility tests are shown in Figure 5-21. It shows a mean error of 1.2 mg Cu/ g. The average value for loading was found to be 5.1 mg Cu/ g, meaning the error is of approximately 20 %, which is considered large. It is very likely that this error is due to the loading procedure used, as will be discussed in section 5.3.3.

5.3.2. Incremental Cu loading

Figure 5-22 shows the adsorption of Cu on C_{12} coated particles as a function of Cu concentration. As Cu concentration increases, the uptake of Cu by the particles also increases. This test also investigated the effect of sonication (not shown in Figure 5-22). At 4.4 ppm Cu, three different sonication times were used (1, 4, and 8 min.). The resulting Cu uptakes were, respectively, 3.5, 3.7, and 4 mg Cu/g. This indicates that sonication is a factor, and that sufficient sonication time should be chosen to disperse the coated particles prior to loading.

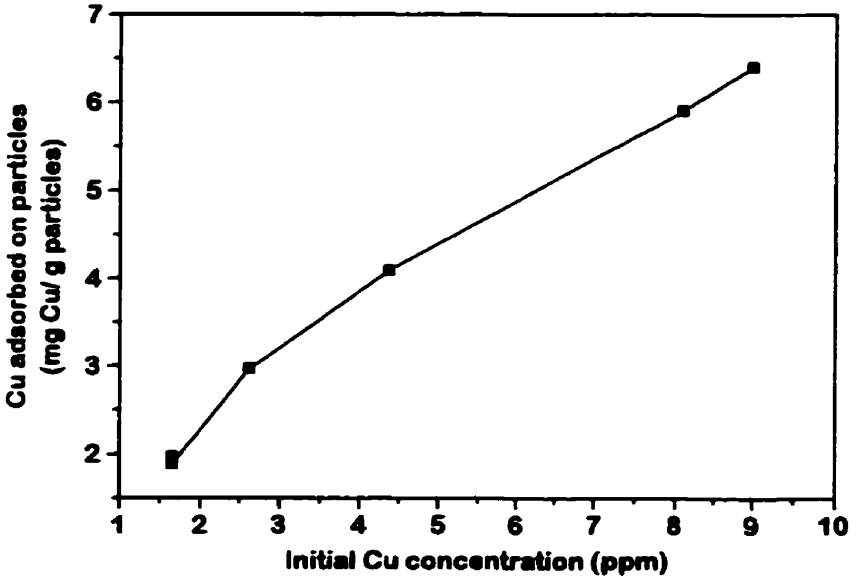

Figure 5-22: Cu loading on C_{12} coated particles as a function of Cu concentration.

5.3.3. Discussion.

The reproducibility test gives an average loading capacity of 5.1 mg Cu/ g. This value is twice as much as the value measured in step II. There appear to be two reasons for this: i) the Cu concentration used was higher, and ii) the sonication time was longer (5 min.). The error of 1.2 mg/ g is relatively high (about 20 %), which indicates that this method is not very accurate. The AA for measuring the Cu concentration before and after loading was performed very carefully, and under these conditions, should not introduce significant errors. Therefore, this large error is mainly attributed to the loading procedure itself, associated with the difficulty in dispersing the coated particles evenly. The state of dispersion of the particles has not been monitored and may vary from one experiment to the other, depending on the nature of the dried sample. This was confirmed by the effect of sonication demonstrated in the incremental Cu loading test. The ability to disperse the particles is a critical factor for subsequent metal ion adsorption.

In spite of this error, we are confident in the mean loading value of 5.1 mg/ g obtained. The incremental Cu loading showed that up to 6.5 mg Cu/ g could be loaded on the particles. A question raised by this test was whether the curve would level off shortly or if it would keep increasing until a much higher Cu concentration. Later experiments on C_{16} coated particles at 25 and 50 ppm Cu showed that the value of 6.5 mg Cu/ g was not exceeded, even at much higher Cu concentrations. The curve reaches saturation at about 6-6.5 mg Cu/ g. Other experiments will also confirm that the maximum loading capacity of the particles for Cu is around 6 mg/ g.

5.4. Step IV: Investigations of the mechanisms controlling Cu loading on the carriers

The coated particles used in all step IV experiments were batch coated particles. The procedure for batch coating was described in section 4.3.4.1.

5.4.1. Cu Loading on bare and C_{16} coated particles vs. pH

Figure -5-23 shows the adsorption of 20 ppm Cu solutions at pH 3.2, 4.4, and 5.6 on C_{16} coated and bare particles. The experiment was initially designed to show the

difference in loading capacity between bare particles and C_{16} coated particles as a function of pH. Surprisingly, the results show that Cu loading versus pH gives almost exactly the same response for bare and coated particles. This result will be discussed later in section 5.4.4. The two curves in Figure -5-23 show clearly that pH has an effect on Cu loading. At pH 3.2, almost no Cu is adsorbed. At pH 4.4, up to 5 mg Cu/ g is adsorbed, and at pH 5.6, up to 6.5 mg Cu/ g, approaching the maximum capacity of the particles. A possible explanation for the influence of pH on Cu adsorption is that the adsorption mechanism is mainly electrostatic. A series of zeta potential test was performed to study the charge of the particles as a function of pH.

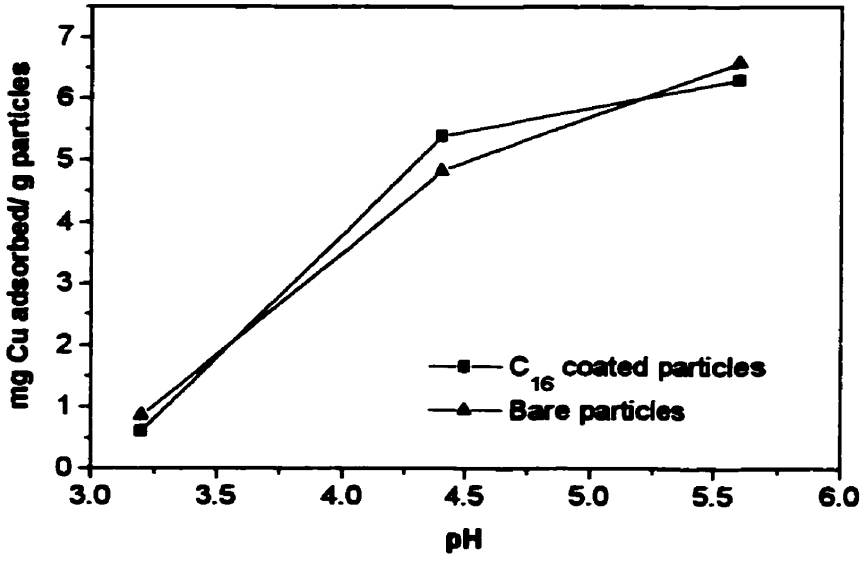

Figure -5-23: Adsorption of Cu on bare maghemite (▲) and C_{16} coated maghemite (■) from 20 ppm Cu solutions at pH 3.2, 4.4, and 5.6.

5.4.2. Zeta potential measurements

Figure 5-24 represents the zeta potential curves for bare and C_{16} coated particles. The curves show that the coating affects the particle charge. The C_{16} coated particles are more negatively charged than bare particles. The pzc for C_{16} coated particles is 3.3, and is 5 for bare particles.

Some zeta potential measurements were also performed on bare and coated particles after loading with Cu at pH 3.2 and 5.6. The results are shown in Figure 5-25. On C_{16} coated particles (solid symbols), the curves for Cu loaded at pH 3.2 and 5.6 are very similar. Both are shifted upward by about 10 mV. For bare particles, the curves for Cu loaded at pH 3.2 and 5.6 are also similar to that at pH above 7, and show a comparable shift upward of about 10 mV. They however, differ for pH below 6, with the curve for Cu at pH 5.6 almost identical to bare particles without Cu addition.

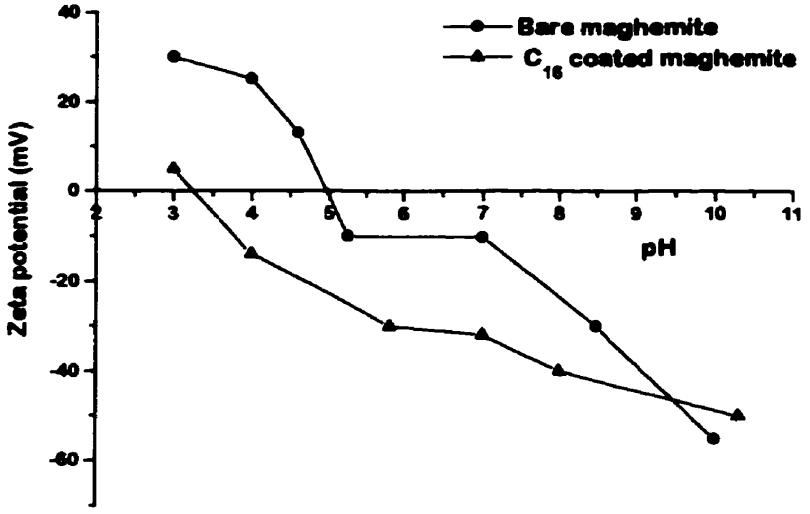

Figure 5-24: Zeta potential measurements for bare maghemite (●) and for C_{16} coated maghemite (▲).

An observable difference between the curves for Cu loaded at pH 3.2 and 5.6, because of the difference of Cu adsorbed at these pHs, was expected. A higher concentration of Cu ions adsorbed on the surface should induce a larger shift in the zeta potential curve for loaded particles. However, such a difference was not observed. Because the two curves for C_{16} coated particles at pH 3.2 and pH 5.6 are so similar, I suggest the following explanation. It may be that only a fraction of the Cu adsorbed on

the particles is really bound to the particles, the rest being simply held in the double layer. Such Cu on the surface can easily be washed away, and would not show on zeta potential measurements. The only Cu detectable by zeta potential may be the Cu bonded to the surface by covalent bonds, and that may be the small fraction that adsorbed already at pH 3.2. That fraction would be responsible for the 10 mV shift upward.

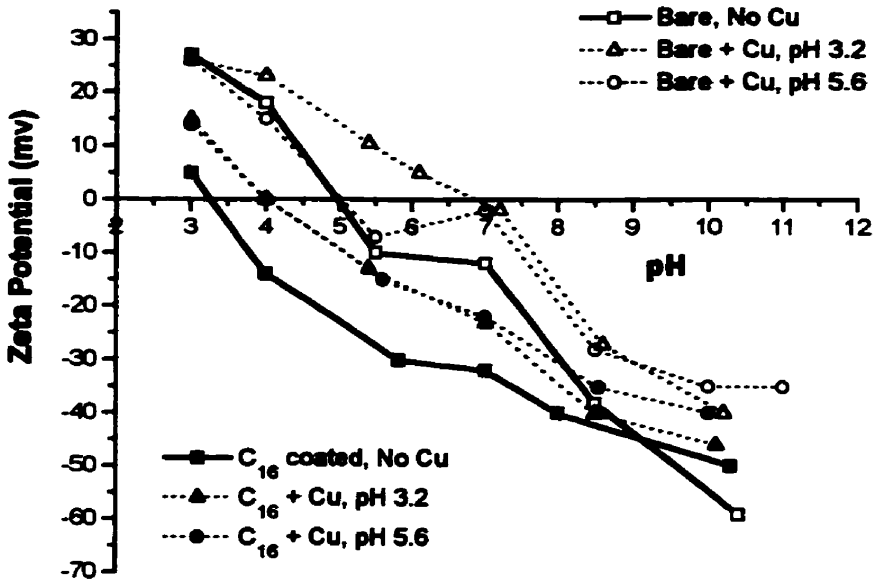

Figure 5-25: Zeta potential measurements for C_{16} coated particles before Cu addition (■), with Cu at pH 3.2 (▲), and at pH 5.6 (●), and for bare particles before Cu addition (□), with Cu at pH 3.2 (Δ), and at pH 5.6 (○).

5.4.3. Cu and Ca loading on bare and C_{16} coated particles

Figure 5-26 shows the adsorption of Cu and Ca on bare and C_{16} coated particles at pH 3, 4.5, and 6. There was no adsorption of Ca at all, either on bare, or on coated particles. The graph also shows that the maximum loading capacity is about half of that expected for Cu loading (2.5 mg/ g versus 5 or 6 mg/ g). In that set of experiment, the conditions used were different from the typical conditions used in previous loading tests: 100 mg of particles were used (versus 25 mg previously), with 50 ppm Cu and 50 ppm

Ca. It was expected that the amount of Cu loaded would be proportional to the amount of particles added, but this is not what the results indicate. A possible explanation is that when using a larger quantity of sample, it becomes even more difficult to fully disperse the particles, and only part of the total particle surface is available for reaction. Hence, the lower Cu adsorption observed.

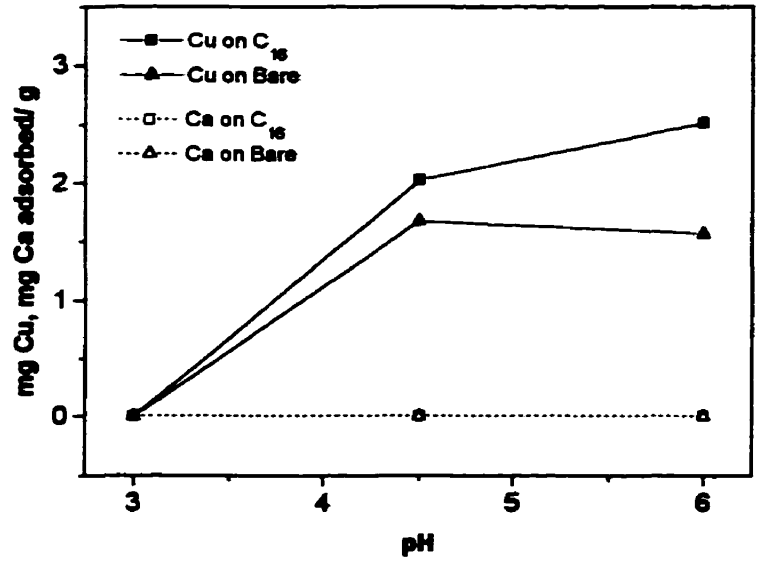

Figure 5-26: Loading of Cu on C_{16} coated particles (■) and on bare particles (▲). Loading of Ca on C_{16} coated particles (□) and on bare particles (Δ).

5.4.4. Discussion

This series of experiments was designed to investigate some of the mechanisms controlling Cu adsorption on the particles. The results obtained are somewhat puzzling. Cu loading versus pH on bare and coated particles showed that bare particles exhibited a behavior almost identical to that of the coated ones. From that observation, it was suggested that the mechanism controlling adsorption on the particles might be electrostatic interaction, through surface charges. Zeta potential measurements were performed to study the electrophoretic characteristics of both bare and coated particles. Those measurements showed that coated particles have a more negative charge, and a lower i.e.p. This difference in surface charge does not help to understand the virtually identical

loading behavior of both types of particles. The test on Ca versus Cu was designed to show a possible difference in selective adsorption (e.g., Cu over Ca) by bare and coated particles, but again, the results showed the response was similar. The series of experiments in step V was performed to check whether step IV results were reproducible.

5.5. Step V: Confirmation of step IV results

Because step IV results were puzzling, they were repeated carefully. One issue that had come up a few times in the work was the problem associated with dispersing the coated particles prior to loading. This was made difficult by the fact the coated sample had been dried overnight in an oven, and was then in the form of a "cake". For loading experiments, this aggregated sample needed to be dispersed in EtOH, a procedure that was not well controlled. To avoid the problem, the coated particles would not be dried for step V tests. The procedure used is described in the procedure section. Additionally, some blank tests were performed, to account for Cu adsorption on the plastic vials (see procedure).

5.5.1. Loading of Cu vs. Cu concentration

Figure 5-27 shows the loading of Cu on C_{16} coated sample, bare particles, and blank tests for 2, 5, 7, 10, 15, 20, 30, and 50 ppm Cu. First, we can observe that there is a significant adsorption occurring in the blank tests: Cu adsorption increased with increasing Cu concentration, and reached a maximum around 2 mg Cu/ g above 15 ppm Cu. This result will be discussed in section 5.5.3. Second, once again, bare and C_{16} coated particles have a very similar response to Cu loading. The maximum reached is approximately 4.4 mg Cu/ g for coated, and 4.7 mg Cu/ g for bare particles. Saturation loading is reached a little after 20 ppm Cu. Figure 5-28 is another way to plot the data from Figure 5-27. On this graph, Cu adsorption is plotted as percentage of Cu adsorbed versus initial Cu concentration. The dotted line on the graph allows to read the corresponding values for a given Cu concentration of 10 ppm. On this plot, it can be seen that the efficiency of the process is low for initial Cu concentrations above 10 ppm. Another noteworthy point is that the difference between the blank test and the two other samples is between 10 and 20 percent. This point will also be discussed in section 5.5.3.

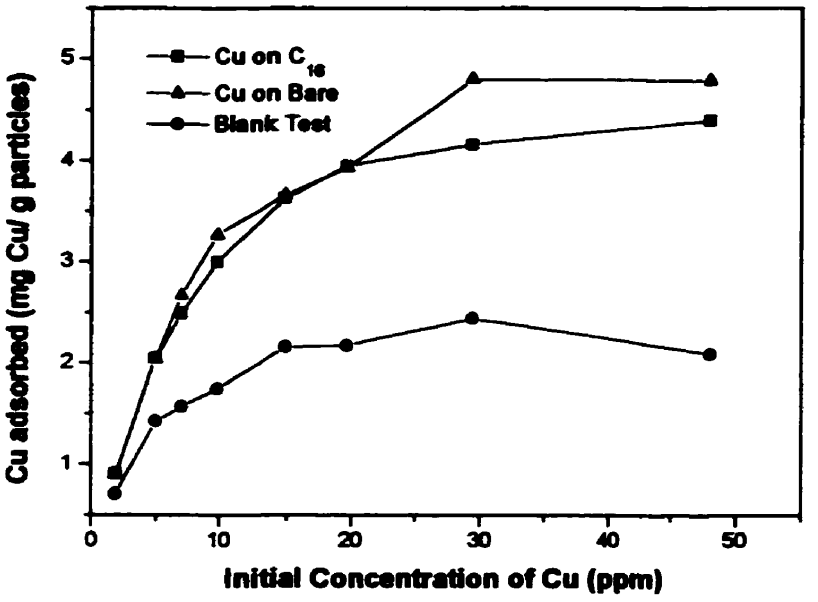

Figure 5-27: Cu loading versus Cu concentration on C_{16} coated particles (■), on bare particles (▲), and blank test (●).

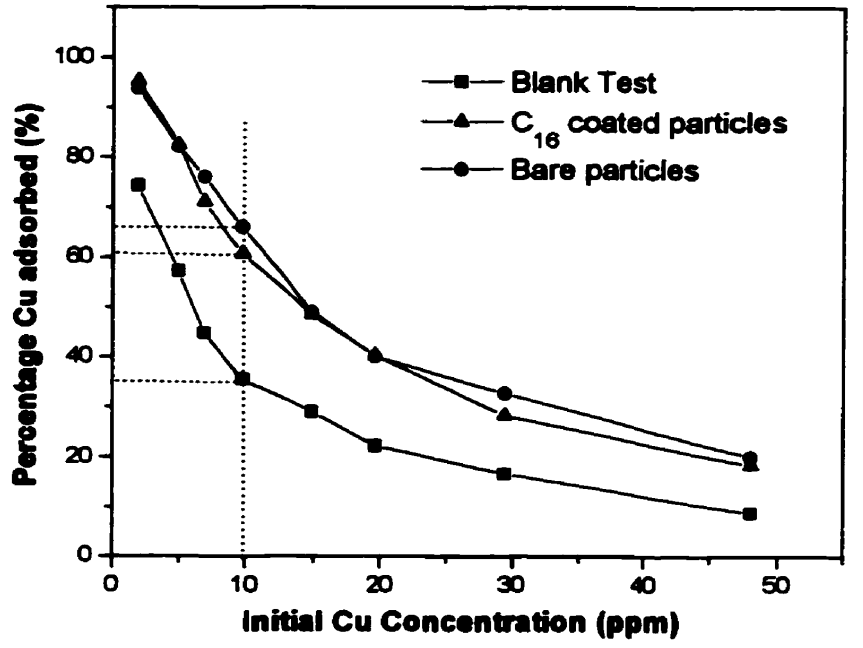

Figure 5-28: Percentage of Cu adsorbed versus initial Cu concentration for Cu adsorbed on C_{16} coated particles (▲), bare particles (●), and blank test (■).

5.5.2. Loading of Cu vs. pH

Figure 5-29 shows the loading of 30 ppm Cu on bare, C_{16} coated, and blank samples at pH 3, 3.5, 4, 4.5, 5, and 6. One repeat measurement was performed for each sample at pH 3.5, 4, and 5. A few observations can be made. First, here too, the blank test shows some Cu adsorption, and that it has the same dependence on pH as the adsorption on particles. Second, the curves for bare and coated particles are similar. Third, the repeat tests at pH 3.5, 4, and 5 show good reproducibility (all repeat points are within 0.3 mg /g except the points for bare and coated particles at pH 4). Fourth, in this series the maximum adsorption is reached at pH 4, and it does not increase at higher pH (the small decrease after pH 4 is not considered significant). Finally, in this series, the maximum adsorption reached is only 3.3 mg Cu/ g.

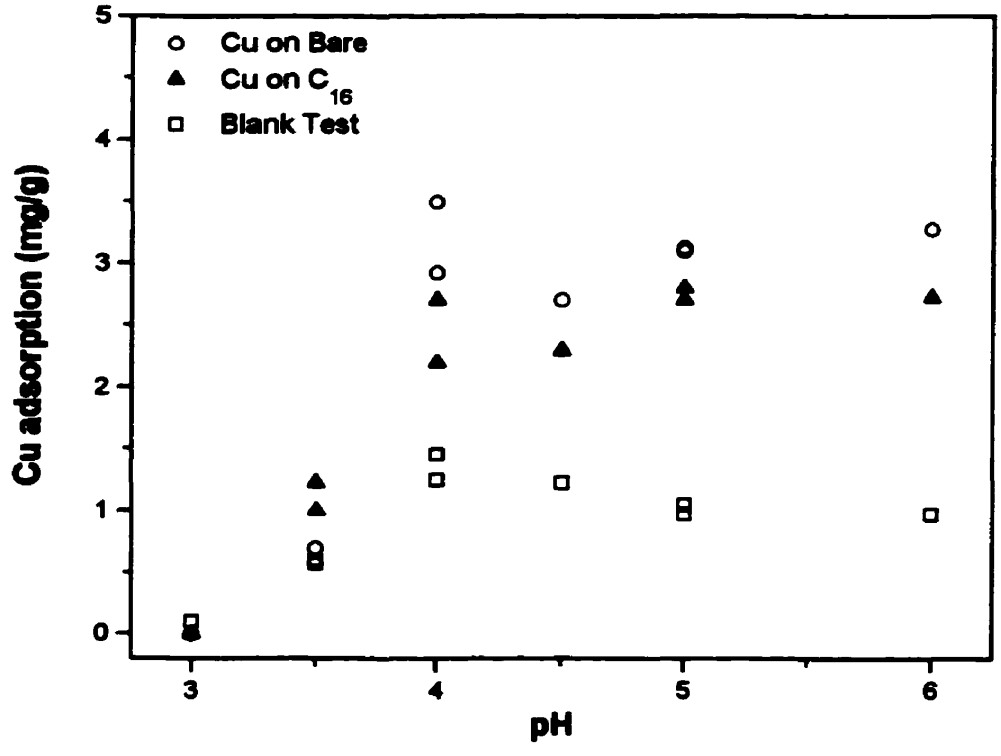

Figure 5-29: Loading of Cu (20 ppm) versus pH on bare particles (○), C_{16} coated particles (▲), and blank test (□).

5.5.3. Discussion

Overall, step V experiments confirmed those found in step IV. All loading measurements on bare and coated particles have shown that both have similar loading responses. The trend of Cu loading versus pH was confirmed: No adsorption occurs at pH 3, and adsorption occurs at pH 4 and above. Some repeat tests proved that the errors are not large, and that the results can be interpreted with confidence.

I would like to make some observations concerning the blank tests. The results in Figure 5-27 show that in a blank test adsorption can be as high as 40 % of the adsorption on particles, a very high figure. I believe these blank test measurements question the validity of the procedure for evaluating Cu adsorption on particles. The proportion of Cu "lost" on the vial compared to that of the Cu supposedly "adsorbed" on the particles is unacceptably high. The phenomenon that is the object of the measurement is almost of the same magnitude as the "noise" in the process. That final observation puts in perspective the results gathered all along the thesis concerning metal ion adsorption. The errors measured are large, and there is a large difference observed in maximum adsorption from one set of experiment to the other. There are definite and reliable trends revealed concerning metal ion uptake but absolute values are not reliable and raise questions regarding the procedure adopted. At least for the range of parameters tested here (20 to 100 mg particles, and 2 to 50 ppm metal), the methodology does not seem appropriate. In parallel work, Stéphanie Gélinas, who is doing her Ph.D (results not published yet) on the same type of magnetic carriers, has changed the procedure and is evaluating metal ion loading using potentiometric titration. This method seems to be efficient and accurate, and could be a good alternative to the procedure used here.

Chapter 6

Conclusions and Recommendations

6. Conclusions and recommendations

6.1. Summary

DRIFTS, wetting characterization, and leaching tests demonstrated that both C_{12} and C_{16} surfactants could be successfully coated on maghemite particles to form a dense, well-packed monolayer, resistant to acid and base attack. DRIFTS and XPS analyses showed that the surfactant is bound to the surface through a carboxylate bond and that the thio groups are oriented outwards from the maghemite. These results confirmed the work by Liu and Xu (1995). No significant difference was observed in the characteristics of C_{12} and C_{16} coated particles. The average surfactant density on the particles was estimated at 0.15 mM/ g particles.

Adsorption tests were performed with Cu and Ag solutions on three types of carriers: bare maghemite, C_{12} coated maghemite, and C_{16} coated maghemite. These tests indicated that metal ion uptake occurs at comparable levels on both bare and coated particles. XPS studies showed that part of the Ag adsorbed was covalently bound to the thio groups through thiolate bonding. Zeta-potential measurements, on the other hand, suggested that not all Cu adsorbed on the particles was covalently bound, but that it was mainly held in the double layer. This could account for the similar behavior of bare and coated particles. The influence of pH on metal ion uptake was similar for the three carriers. No adsorption occurred at pH 3, and adsorption occurred from pH 4 to pH 6. The maximum loading capacity was found to be approximately 6 mg Cu/ g particles.

Some questions were raised concerning the choice of the procedure for evaluating metal uptake by the carriers. The error introduced by indirect measurement using atomic adsorption was large. This error was partially attributed to adsorption of metal ions by the test tubes. For the range of parameters tested, (20 to 100 mg carriers, and 2 to 50 ppm metal), the procedure used was not accurate enough. It was suggested that a direct technique such as potentiometric titration be used in future work. It was also suggested that the coated particles should not be dried prior to adsorption experiments.

6.2. Conclusions

Molecular self-assembly proved to be an efficient method to produce dense and well-packed monolayers. These magnetic carriers were designed to be potential candidates for the treatment of metal contaminated effluents and sludges. However, the adsorption tests did not show the advantage of using such functionalized particles over the use of bare maghemite. The adsorption capacity attained was small, 6 mg Cu/ g particles, and the coating did not appear to enhance that capacity.

The preparation of selective functionalized magnetic carriers is a promising field of research. However, in the light of the review on magnetic carriers, and particularly for the treatment of metal-bearing effluents, it appears that the choice of materials in the present study was not appropriate. First, the size of the particles. The study on the SIROFLOC process (section 2.2.2.4) pointed out that for industrial application a 1-5 μm size range was desirable. Second, for industrial application the materials should be commercially available and preferably inexpensive. Both the nanosized maghemite and the surfactant are expensive. Finally, the magnetic carriers should be robust and not prone to degradation upon reuse. These types of coated magnetic carriers will likely find application in biology and pharmaceutical application, but not in metal-bearing effluent treatment.

6.3. Recommendations for future work

If the work on these functionalized carriers is pursued:

- The coated particles should not be dried prior to adsorption experiments.
- Bare and coated particles loaded with Cu and Ag should be analyzed by XPS. This a direct method to assess the existence of covalent bounds between the metal and the carrier.
- More zeta-potential experiments would be desirable. Zeta-potential measurements are not easy to perform but can yield precious information.

- **Far-IR tests could be performed on loaded samples to detect the presence of the metals on the surface. Mid-region IR could not detect the metals.**

- **Selective adsorption tests could be performed with two or more metal ions at different pHs.**

If new magnetic carriers are to be designed for metal-bearing effluent treatment:

- **A cheap, commercially available product such as magnetite (Fe_3O_4) should be used as adsorbent.**

- **Selective metal ion precipitation on magnetite could be an alternative to functionalization by surfactant, and a much cheaper option.**

- **Effective treatment of sludges or effluents could be achieved by stage recovery of metals on magnetic carriers, using different precipitation agents (e.g., carbonates, sulfates, hydroxides, silicates) for each stage, as shown in the diagram below.**

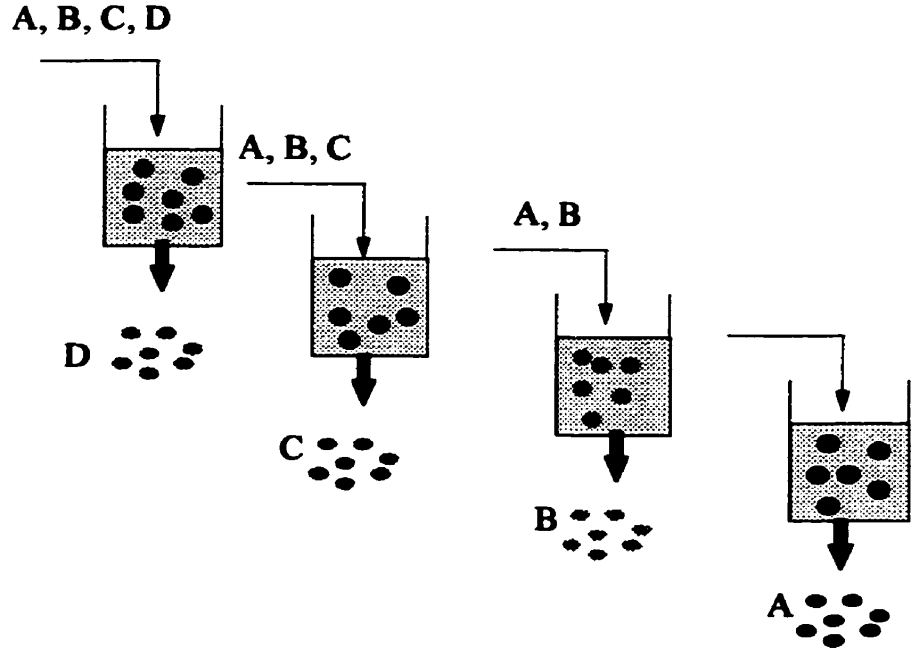

Chapter 7

References

7. References

Ahn, C. H, Allen, M. G., Trimmer, W., Jun, Y-N, and Erramilli, S.: "Fully integrated micromachined magnetic particle separator," *Journal of Microelectromechanical Systems*, Vol. 5, No. 3, Sep. **1996**, pp. 151-158.

Allara, D. L., and Nuzzo, R. G.: "Spontaneously organized molecular assemblies. 2. Quantitative infrared spectroscopic determination of equilibrium structures of solution-adsorbed *n*-Alkanoic acids on an oxidized aluminum surface," *Langmuir*, **1985a**, Vol. 1, No. 1, pp. 52-66.

Allara, D. L., and Nuzzo, R. G.: "Spontaneously organized molecular assemblies. 1," *Langmuir*, **1985b**, Vol. 1, No. 1, pp. 45-52.

Allara, D. L., Atre, S. V., Elliger, C. A., and Snyder, R. G.: "Formation of a crystalline monolayer of folded molecules by solution self-assembly of α,ϖ-alkanedioic acids on silver," *J. Am. Chem. Soc.*, Vol. 113, No. 5, pp. 1852-1855, **1991**.

Anderson, N. J., Dixon, D. R., and Swinton E. A.: "Continuous ion exchange using magnetic shell resins. II. Dealkalization - Pilot plant study," *J. Chem. Tech. Biotechnol.*, **1979**, Vol. 29, pp. 325-331.

Anderson, N. J., Kolarik, L. O., Swinton, E. A., and Weiss, D.: "Colour and turbidity removal with reusable magnetic particles - II. Coagulation with magnetic polymer composites," *Wat. Res.*, Vol. 14, **1980**, pp. 967-973.

Anderson, N. J., Bolto, B. A., Elderidge, R. J., Kolarik, L. O., and Swinton, E. A.: "Colour and turbidity removal with reusable magnetic particles - III. Immobilized metal hydroxide gels," *Wat. Res.*, Vol. 16, **1982**, pp. 1327-1334.

Anderson, N. J., and Priestley, A. J.: "Colour and turbidity removal with reusable magnetite particles - V. Process development," *Wat. Res.*, Vol. 17, No. 10, pp. 1227-1233, **1983**.

Anderson, N. J., Bolto B. A., Blesing N. V., Kolarik, L. O., Priestley, A. J., and Raper, W. G. C.: "Colour and turbidity removal with reusable magnetite particles - VI. Pilot plant operation," *Wat. Res.*, Vol. 17, No. 10, **1983**, pp. 1235-1243.

Anderson N. J., Blesing N. V., Bolto B. A., and Jackson M. B.: "The role of polyelectrolytes in a magnetic process for water clarification," *Reactive Polymers*, Vol. 7, **1987**, pp. 47-55.

Anderson N. J., Bolto, B. A., Elderidge, R. J., and Jackson, M. B.: "Polyampholytes for water treatment with magnetic particles," *Reactive Polymers*, Vol. 19, **1993**, pp. 87-95.

Bain, C. D., Troughton, E. B., Tao, Y-T., Evall, J., Whitesides. G. M., and Nuzzo, R. G.: "Formation of monolayer films by the spontaneous assembly of organic thiols from solution onto gold," *J. Am. Chem. Soc.*, **1989**, Vol. 111, No. 1, pp. 321-335.

Baldwin, Jean A.: "Surface enhanced Raman scattering of mercaptopyridine and pyrazinamide and the fabrication of a metal-ion sensor," Ph.D. Thesis, McGill University, Department of Chemistry, 1996.

Bandyopadhyay, K., Patil, V., Vijayamohanan, K., and Sastry, M.: "Adsorption of colloidal silver particles through covalent linkage to self-assembled monolayers," *Langmuir*, Vol. 13, No. 20, pp. 5244-5548, 1997.

Benjamin, M. M., Hayes, K. F., and Leckie, J. O.: "Removal of toxic metals from power-generation waste streams by adsorption and co-precipitation," *Journal WPCF*, Vol. 54, No. 11, November 1982, pp. 1472-1481.

Bolto, B. A., Dixon, D. R., and Elderidge, R. J.: "Graft polymerization on magnetic polymer substrates," *J. Appl. Poly. Sci.*, Vol. 22, 1978, pp. 1977-1982.

Bolto, B. A., Dixon, D. R., Swinton E. A., and Weiss, D. E.: "Continuous ion exchange using magnetic shell resins. I. Dealkalization - Laboratory scale," *J. Chem. Tech. Biotechnol.*, 1979, Vol. 29, pp. 325-331.

Bolto, B.A.: "Novel water treatment processes which utilize polymers," *J. Macromol. Sci. Chem.*, A14 (1), pp. 107-120, 1980.

Booker, N. A., and Brooks, R. B.: "Scale-up of the rapid sewage treatment Sirofloc™ process," *Process Safety and Environmental Protection* (Transactions of The Institution of Chemical Engineers, Part B), Vol. 72, Part B, May 1994, pp. 109-112.

Briggs, D., and Seah, M. P.: *Practical Surface Analysis. 2nd ed.*, Vol. 1, Auger and X-ray Photoelectron Spectroscopy, Wiley Publishers, reprinted 1994.

Chen, W. Y., Anderson, P. R., and Holsen, T. M.: "Recovery and recycle of metals from wastewater from a magnetite-based adsorption process," *Research Journal WPCF*, Vol. 63, No. 7, 1991, pp. 958-964.

Colvin, V.L., Goldstein, A. N., and Alivisatos, A. P.: "Semiconductors nanocrystals covalently bound to metals surfaces with self-assembled monolayers," *J. Am. Chem. Soc.*, Vol. 114, pp. 5221-5230, 1992.

Dixon, D. R.: "Magnetic adsorbents: Properties and applications," *J. Chem. Tech. Biotechnol.*, 1980, Vol. 30, pp. 572-578.

Feasby, D. G., Tremblay, G. A., and Weatherell, C. J.: "A decade of technology improvement to the challenge of acid mine drainage - A Canadian perspective," in *Proceedings of the Fourth International Conference on Acid Rock Drainage*, Vancouver, Canada, June 1997, Vol. 1, pp. i-ix.

Ferraro, J. R., and rein, A. J.: "Application of diffuse reflectance spectroscopy in the far-infrared region," in *Fourier Transfrom Infrared Spectroscopy*, Vol. 4, Academic Press, 1985.

Freeman, T. L., Evans, S. D., and Ulman, A.: " XPS studies of self-assembled multilayers films," *Langmuir*, Vol. 11, No. 11, pp. 4411-4417, 1995.

Fuller, M. P., and Griffiths, P. R.: "Diffuse reflectance measurements by infrared Fourier transform spectrometry," *Analytical Chemistry*, Vol. 50, No. 13, Nov. 1978, pp. 1906-1910.

Fuller, M. P., Nicolet FT-IR Technical Note: "Diffuse reflectance infrared analysis: A brief review of theory and applications," *Nicolet FT-IR Technical Note - TN-0933.*

Fuerstenau, D. W. and Williams, M. C.: "A simple flotation method for rapidly assessing the hydrophobicity of coal particles," *International Journal of Mineral Processing*, 20, pp. 153-157, 1987.

Gregory, R., Maloney, R. J., and Stockley M.: "Water treatment using magnetite: A study of a Sirofloc pilot plant," *Journal of the Institution of Water and Environmental Management*, 1988, 2, October, pp. 532-544.

Harries, John: "Estimating the liability for acid mine/rock drainage in Australia," in *Proceedings of the Fourth International Conference on Acid Rock Drainage*, Vancouver, Canada, June 1997, Vol. 4, p.1907.

Herbert et al.: "A science-based, watershed strategy to support effective remediation of abandoned mine lands," in *Proceedings of the Fourth International Conference on Acid Rock Drainage*, Vancouver, Canada, June 1997, Vol. 4, p. 1870.

Hwang, J. Y.: *U.S. Patent 4*,834,898, 1989.

Hwang, J. Y.: *U.S. Patent 4*,906,382, 1990.

Home, G. P., Stockley, M., and Shaw, G.: "The Sirofloc process at Redmires water-treatment works," *Journal of the Institution of Water and Environmental Management*, 1992, 6, February, pp. 10-18.

Israelachvili, J., N.: *Intermolecular and Surface Forces*, 2nd Edition, Academic Press, 1991.

Kelly, E., and Spottiswood, D.: *Introduction to mineral Processing*, John Wiley & Sons, New York, pp. 95-112, 1982.

Khun, M., and Rodriguez, J. A.: *J. Phys Chem.*, Vol. 98, No. 46, pp. 12059-12066, 1994.

Kolarik, L. O.: "Colour and turbidity removal with reusable magnetite particles - IV. Alkali activated magnetite- A new solid, reusable coagulant-adsorbent," *Wat. Res.*, Vol. 17, 1983, pp. 141-147.

Konstadinidis, K., Thakkar, B., Chakraborty, A., Potts, L. W., Tannenbaum, R., Tirrell, M., and Evans, J. F.: *Langmuir*, Vol. 8, No. 5, pp. 1307-1317, 1992.

Kopp, J.: "Superconducting magnetic separators," *Magnetic and Electrical Separation*, 3 (1), pp. 17-32, 1991.

Laibinis, P. E., Whitesides, G. M., Allara, D. L., Tao, Y-T., Parikh, A. N., and Nuzzo, R. G.: "Comparison of the structures and the wetting properties of self-assembled monolayers of *n*-Alkanethiols on the coinage metals surfaces, Cu, Ag, Au," *J. Am. Chem. Soc.*, 1991, Vol. 113, No. 19, pp. 7152-7167.

de Bruyn, P. L., and Agar, G. E.: Surface chemistry of flotation, in *Froth Flotation 50th Anniversary Volume*, AIME, pp. 91-138, 1962.

de Latour, C.: "Seeding principles of high gradient magnetic separation," *Journal of American Water Works Association*, 68, August 1976, pp. 443-446.

Liu, Q.: "An innovative approach in magnetic carrier technology," *Ph.D. Thesis*, McGill University, Mining and Metallurgical Department, August 1996.

Liu, Q. and Friedlander, F. J.: "Fine particle processing by magnetic carrier methods," *Minerals Engineering*, Vol. 7, No. 4, pp. 449-463, 1994.

Liu, Q. and Xu, Z.: "Self-assembled monolayer coating on nanosized magnetic particles using 16-mercaptohexadecanoic acid," *Langmuir*, Vol. 11, No. 12, 1995.

Liu, Q. and Xu, Z.: "Functionalization and applications of nanosized γ-Fe_2O_3 particles," *J. Appl. Phys.*, Vol. 79, No. 8, April 1996, pp. 4702-4704.

Mathieu, G.: "Historical evolution of magnetic separation," *Proc. Ann. Meet. Can. Min. Proc.*, pp. 339-364, 1988.

Moffat, G., Williams, R. A., Webb, C., and Stirling, R.: "Selective separation in environmental and industrial processes using magnetic carrier technology," *Minerals Engineering*, Vol. 7, No. 8, 1994, pp. 1039-1056.

Olinger, J. M, and Griffiths, P. R.: "Effects of sample dilution and particle size/morphology on diffuse reflection spectra of carbohydrate systems in the near- and mid-infrared. Part II: Durum wheat," *Applied Spectroscopy*, Vol. 47, No. 6, 1993, pp. 695-701.

Parsonage, P.: "Selective magnetic coating for mineral separation," *Trans. Inst. Min. Metall. (Sect. C: Mineral Process. Extr. Metall.)*, 93, March 1984, pp. C37-C44.

Parsonage, P.: "Coating and carrier methods for enhancing magnetic and flotation methods," in *Colloid Chemistry in Mineral Processing*, J. S. Laskowski, and J. Ralston eds., Elsevier, Amsterdam, 1992.

Rao, S. R., Xu, Z., and Finch, J. A.: Flotation fundamentals, *Professional Development Seminar, McGill University, Mining and Metallurgical Department*, 1996.

Smith, E. L., Alves, C. A., Anderegg, J. W., Porter, M. D., and Siperko, L. M.: *Langmuir*, Vol. 8, No. 111, pp. 2707-2714, 1992.

Standing Committee on Natural Resources: Streamlining Environmental Regulation for Mining: Final Report, November 1996.

Svoboda, J.: *Magnetic methods for the treatment of minerals*, Elsevier, 1987.

Tao, Y-T.: "Structural comparison of self-assembled monolayers of n-alkanoic acids on the surfaces of silver, copper, and aluminum," *J. Am. Chem. Soc.*, Vol. 115, No. 10, pp. 4350-4358, 1993.

Terashima Y., Ozaki, H., and Sekine, M.: "Removal of dissolved heavy metals by chemical coagulation, magnetic seeding, and high gradient magnetic separation magnetic filtration," *Wat. Res.*, Vol. 20, No. 5, 1986, pp. 537-545.

Ulman, A., and Elman, J. F.: "X-ray Photoelectron spectroscopy of organic thin films," in *Characterization of Organic thin films*, Abraham Ulman and Lee E. Fitzpatrick eds., Materials Characterization Series, Butterwoth-Heineman publisher, pp. 213-225, 1995.

Urbain, O. M., and Steman, W. R.: "Magnetic flocculation for removing suspended matter from whey, distillery and east plant wastes, straw board-mill wastes etc.," *US Patent 2, 232, 294*, (Feb. 18, 1941).

van Velsen, A. F. M., van der Vos, G., Boersma, R., and de Reuver, J. L.: "High gradient magnetic separation for wastewater treatment," *Wat. Sci. Tech.*, Vol. 24, No. 10, pp. 195-203, 1991.

Wasny, Garrett: "Heart of Gold," *World trade*, 10 (6), pp. 48-51, June 1997.

Wells, I. S. and Rowson, N. A.: Applications of rare earth magnets in mineral processing, *Magnetic and Electrical Separation*, 3(2), pp. 105-112, 1992.

Chapter 8

Appendices

The reactions of synthesis for C_{12} are:

$$2Br(CH_2)_{11}COOH + 2H_2N-CS-NH_2 \text{ (thiourea)} \xrightarrow{\text{reflux } 70°C,\ 24\ h}$$

$$2\,[COO-(CH_2)_{12}-S-C(NH_2)=NH_2^{+}BR^{-}] \xrightarrow{NaOH,\ N_2,\ 2\ days}$$

$$2COOH-(CH_2)_{12}-SH+H_2NC=NH-NH-CN$$

For the synthesis of C_{16}, a preliminary reaction is necessary, to transform the alcohol in bromide:

$$OH(CH_2)_{15}COOH \xrightarrow{HBr(48\%),\ CH_3COOH,\ \text{reflux two days}} Br(CH_2)_{15}COOH$$

The following reactions were similar to those for C_{12} synthesis. The final products were dried overnight under vacuum, and tested for purity using H_1 nuclear magnetic resonance (^{H}NMR).

A slightly different synthesis route to prepare C_{16} is decribed by Coyle et al. in *Chemistry of Materials*, Vol. 1, No. 6, 1989, p. 608.

Synthesis of 12-mercaptododecanoic acid ($HOOC(CH_2)_{11}SH$)

⇒ 3.0 g of 12-bromododecanoic acid (10.74 mmol) are dissolved in 100 mL 95 % EtOH in a 250 mL round bottom flask,

⇒ Thiourea (0.818 g, 10.74 mmol) is added,

⇒ The mixture is refluxed with stirring overnight,

⇒ Cool the reaction to room temperature and transfer to a 3-neck 250 mL round bottom flask and cap mouths of flask with rubber stoppers,

⇒ Saturate reaction vessel with N_2 (gas) and cool to ~ 0° C in an ice bath,

⇒ A 32 mL aliquot of a cold, degassed 2 N NaOH solution (64 mmol NaOH) is added,

⇒ Reflux mixture for 3 hr. under positive N_2 atmosphere,

⇒ Cool mixture to room temperature,

⇒ Pour the resulting white suspension, while stirring, in a 1 L beaker containing 60 mL 2N HCl, 200 mL H_2O, and 300 mL ether,

⇒ Acidify the aqueous phase to pH 2 with 2 N HCl if necessary,

⇒ If a white insoluble precipitate is present, filter it off,

⇒ **Pour the mixture in a 1 L separatory funnel, and separate off the ether layer. Keep the ether layer,**

⇒ **Extract the aqueous phase further with 3 x 100 mL ether,**

⇒ **Wash the combined ether extractions with 3 x 200 mL water followed by 1 x 200 mL of saturated NaCl solution,**

⇒ **The ether fraction is then dried over anhydrous sodium sulfate, filtered by vacuum, and the ether removed by rotary evaporation,**

⇒ **Recrystallize the resulting white solid from hot n-hexane,**

⇒ **Run ^{1}H NMR and DSC to check purity and melting point.**

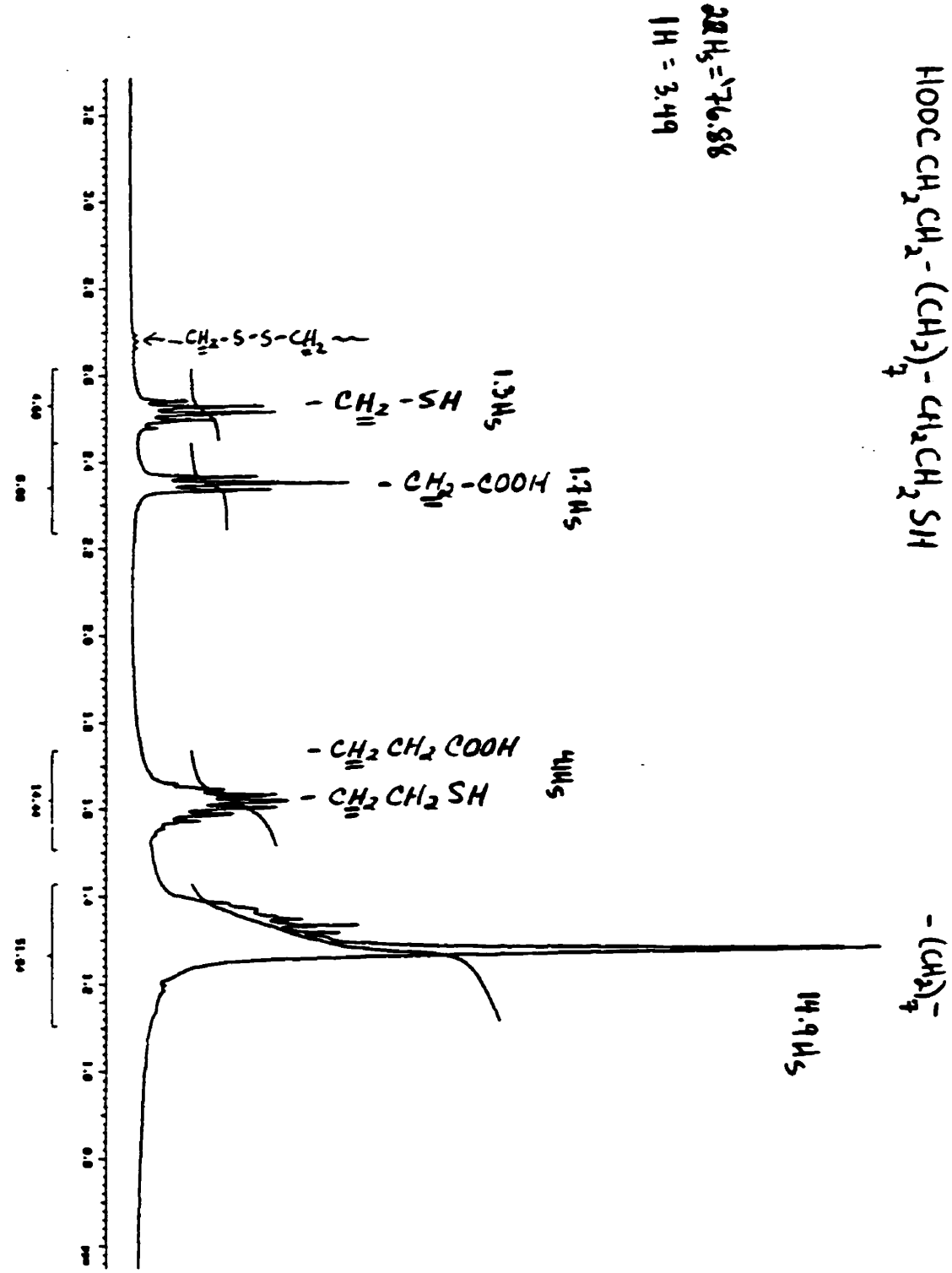
solvent = $CDCl_3$
$HOOC\,CH_2CH_2-(CH_2)_4-CH_2CH_2SH$
$2H_S = 176.86$
$\therefore 1H = 3.449$
$-CH_2-S-S-CH_2-$
$-CH_2-SH$ 1.3 H_S
$-CH_2-COOH$ 1.7 H_S
$-CH_2CH_2COOH$
$-CH_2CH_2SH$ 4 H_S
$-(CH_2)_4-$
14.9 H_S

Appendix 5: NMR spectrum for C_{16}

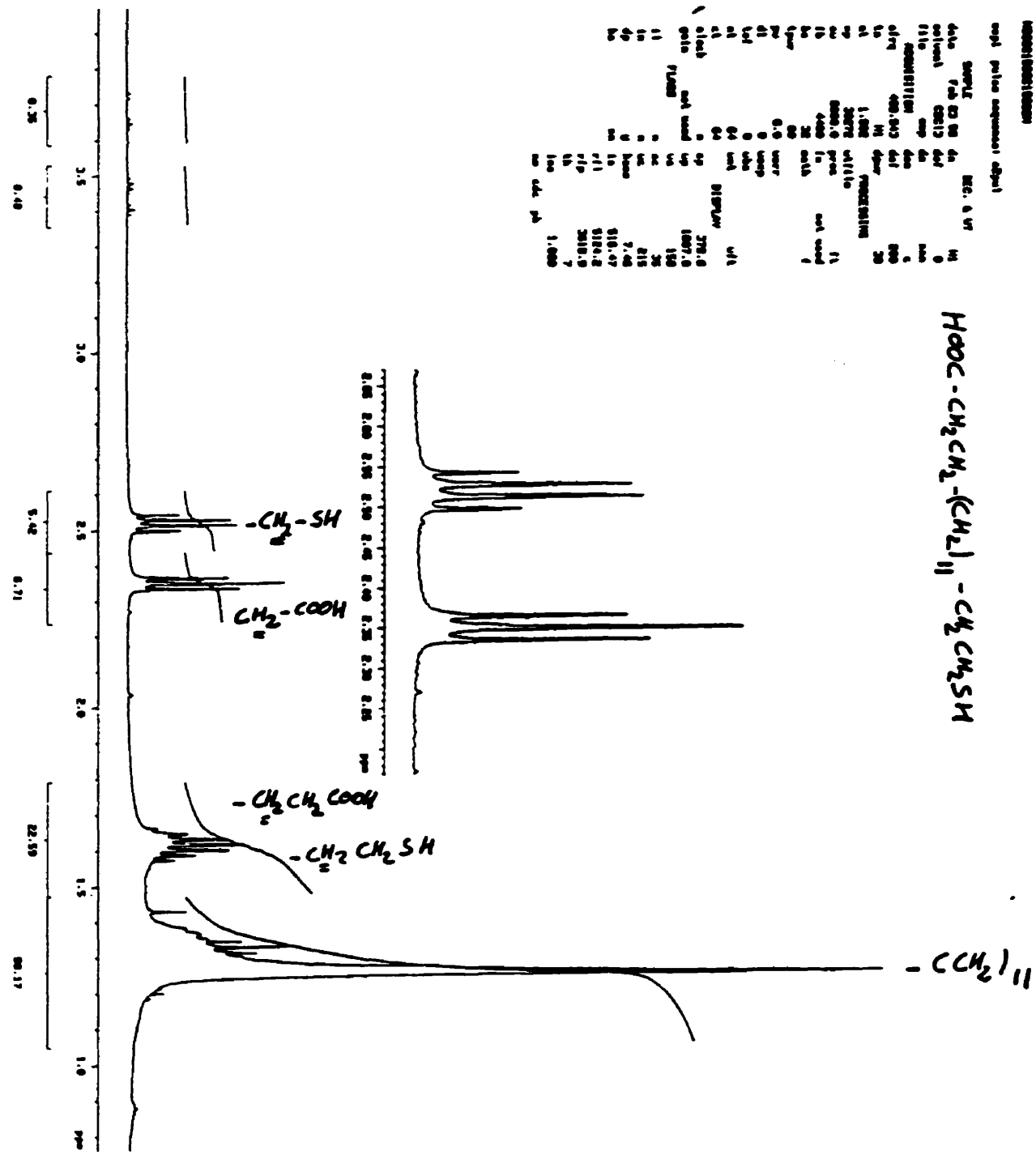

Appendix 6: Surface tension of a water-methanol mixture. Nine points were found from the literature. The curve results from fitting.